"When the going gets tough, the tough get going."
Joseph P. Kennedy

University of Alberta

Experiment Design for Nonlinear System Identification

by

Yijia Zhu

A thesis submitted to the Faculty of Graduate Studies and Research
in partial fulfillment of the requirements for the degree of

Master of Science
in
Process Control

Chemical and Materials Engineering

Spring 2011
Edmonton, Alberta

Examining Committee

Dr. Biao Huang (Supervisor)

Dr. Hongbo Zeng (Chair)

Dr. Vinay Prasad

Dr. Qing Zhao

To my beloved Dad and Mom, who help me design my character and life as optimal as possible

Abstract

Optimal experiment design has been considered as an effective tool to improve model reliability and accuracy in nonlinear system identification in the past few decades. This thesis is concerned with the following challenges which have not been previously addressed: poor initial guess problem of the nominal model in nonlinear system identification; operating points selection to improve LPV model identification accuracy; joint experimental design concerning optimal operating points and input perturbation design simultaneously.

To reduce the influence of poor initial guess of a model, the proposed constrained receding-horizon design (CRHD) incorporates steady-state constraints into the design framework. The other aspect addressed is experiment design for LPV model identification. An adaptive optimal operating point design approach is developed requiring no a-priori knowledge about the true nonlinear system. Joint experiment design involving more than one experiment design factor is also considered. This problem is solved by designing the operating points and input perturbation simultaneously.

Acknowledgements

Life is like a 'one-chance' experiment with one destiny only. On the journey to one of the milestones which is my M.Sc degree, I am always grateful that so many people around me provided me with the 'on-line' guidance and encouragement toward the 'convergence' of my dream.

Among these people who gave me the guidance, I would like to thank Dr. Biao Huang for his outstanding supervision and patience during my two years of research work. His insightful advices had always improved my problem-solving skills; his honesty toward academics and research had always shaped my work ethic. The two years learning experience working with him has become an invaluable asset. I would also like to express my appreciation to Dr. Jong Min Lee for his understanding and encouragement during my time at the University of Alberta. Special thank also goes to Dr. Phillip Choi with whom I worked and enjoyed the experience as a TA.

I would also like to show appreciation to my colleagues, especially Ruben Gonzalez, Yu Yang, Yu Zhao, Xingguang Shao and Fan Yang, who provided me with unconditional aid in my research work. I also sincerely thank my beloved friends who grant me the unselfish friendship that I will treasure for the rest of my life, especially Soo Jing Yoo, Siyi Luo, Lu Zheng, Wayne Gong, Liting Fan, Miriam Parakkal and Jun Wang.

I would also like to acknowledge the Financial support from Natural Sciences and Engineering Research Council of Canada (NSERC).

Lastly, I would like to express my endless gratitude and deepest love to my family. I thank my open-minded parents and lovely sister for their encouragement and support to allow me be an independent and strong person; I also thank my grandfather and grandmothers for their understanding that I could not take care and spend time with them during the time I pursue my dream.

Contents

List of Figures

List of Symbols

φ	Experiment condition obtained from experimental design
M	Fisher information matrix
θ	Parameter to be estimated
Z	Sensitivity matrix
Σ	Covariance matrix of output y
w_t	State noise at time instant t
v_t	Output noise at time instant t
I	Identity matrix
g	Constraint function
p	Operating point
ϕ	Base function in the orthonormal basis function
β	Parameter contained in the
α_i	Weighting function corresponding to i^{th} base function
G	System function
$\mathbb{D}_i$	Data set obtained at i^{th} local region
$\mathbb{D}_{i,i+1}$	Data set obtained at transition between i^{th} and $(i+1)^{th}$ local region
$\bar{p}^*_{(k)}$	Optimal operating point based on the current global model
$\bar{P}$	Operating point vector
σ_i	Validity width of the i^{th} local model
ε	Prediction error
V_j	Criterion function at time $t = j$

Chapter 1

Introduction

1.1 Motivation

Most industrial processes are nonlinear which are often modeled based on first principles such as energy conservation, mass conservation and chemical stoichiometry. These models contain unknown or uncertain parameters that need to be estimated. The objective of an optimal experiment design is to improve model estimation accuracy by optimizing over the experimental conditions. For an industrial process, the experimental conditions usually include what to sense (parameters selection), what inputs to use (input or testing signal design), when to sense (sampling time design), how to operate (operating points design), etc [6]. Many methodologies have been developed since the 1970s including ED(expectation of determination)/EID (expectation of the inverse of determinant)-optimal design [36, 37], minimax experiment design [26, 38], and adaptive experiment design [33]. In practice, the adaptive experiment design is more commonly used for applications toward various nonlinear processes due to its convenience compared with the other two methods. This design assumes that a nominal process model exists. The efficiency of adaptive experiment design is influenced significantly by the chosen initial model. This creates a practical dilemma in nonlinear system identification. How to improve experimental condition as well as parameter estimation under the poor initial condition is one of the areas that we are concerned with in this thesis.

In addition to first principle models, nonlinear systems can also be modeled as Linear Parameter Varying (LPV) models. Due to its simple structure and capacity to describe nonlinear behavior, the LPV model is a promising tool for nonlinear system identification. Considerable amount of work has been recently devoted to LPV model identification [35, 2, 39, 42]. LPV model contains a time-varying scheduling variable which is often called the operating or working point. For most LPV identification approaches, the model's accuracy can be significantly affected by operating points selection. In other words, for different selection of operating points, different LPV models could be obtained, some of which may deviate significantly from the true nonlin-

ear system. In most literature concerned with the LPV identification problem, operating points are considered fixed and known. Therefore, selection of operating points for a given nonlinear system to improve model accuracy is considered as a cardinal problem and has not been well investigated [34]. Targeting a solution to this problem, an adaptive operating point design (AOPD) algorithm is developed in this thesis.

By optimally selecting operating points, the accuracy of LPV models can be improved as mentioned above. However, for most nonlinear systems, the optimal experimental design involves more than one experimental factor. For this reason, a joint experimental design considering two factors is developed, which simultaneously optimizes operating point and input perturbation.

Thus, the thesis is concerned with the three problems of experimental design. To give a general perspective about the problems we deal with, the following sections will briefly illustrate the preliminaries and background before we go to the detail algorithms of the three problems. The thesis contributions and outline will be given at the end of this chapter.

1.2 Receding-horizon Experiment design

The optimal experiment design is defined as

$$\varphi^* = arg\min_{\varphi\in\Phi} f(M(\hat{\theta},\varphi)) \tag{1.1}$$

where φ is the experiment design, Φ is the space of the feasible experiment designs, M is the Fisher information matrix and $f = det(\cdot)^{-1}$, and $\hat{\theta}$ is the current parameter estimate. This φ can stand for any design variable such as sampling rate, input or operating point. In this section we mainly focus on input perturbation design. The Fisher information matrix M is defined as [40]

$$M = Z^T\Sigma^{-1}Z \tag{1.2}$$

where Z is sensitivity matrix defined as follows,

$$Z = \begin{bmatrix} \frac{\partial y}{\partial\theta_1}|_{t_1} & \frac{\partial y}{\partial\theta_2}|_{t_1} & \cdots & \frac{\partial y}{\partial\theta_p}|_{t_1} \\ \frac{\partial y}{\partial\theta_1}|_{t_2} & \ddots & & \vdots \\ \vdots & & \ddots & \vdots \\ \frac{\partial y}{\partial\theta_1}|_{t_h} & \cdots & \cdots & \frac{\partial y}{\partial\theta_p}|_{t_h} \end{bmatrix} \tag{1.3}$$

where t_1 and t_h denote the starting and ending time of the experiment respectively, and Σ is the covariance matrix of output y. Each entry in the j^{th} row and i^{th} column denotes the sensitivity with respect to the ith parameter θ_i at time instant t_j ($j = 1, \ldots, h$).

Among various approaches for experimental design, the adaptive design has gained the most popularity in practice due to its easy implementation and

samller computational load. There are different ways to implement adaptive design. In this thesis we utilize the receding-horizon experiment design which was originally formalized by [14]. In the receding-horizon design, the optimal input U_k^* is obtained according to the following equation.

$$U_k^* = [u_{k|k}^* \; u_{k+1|k}^* \; \cdots \; u_{k+h-1|k}^* \;] = \arg\min_{U_k \in \mathbb{U}} f(M(\hat{\theta}_k, U_k)) \tag{1.4}$$

where U_k^* is the optimal input vector containing $u_{k|k}^*,\ u_{k+1|k}^*,\ \cdots,\ u_{k+h-1|k}^*$ calculated at the k^{th} sampling instant, h is the optimization horizon, $\mathbb{U}$ is the feasible set which U_k^* can be chosen from, f and M are explained above in (1.1) and (1.2), and $\hat{\theta}_k$ is the parameter estimate at sampling instant k.

The procedure for receding horizon design is performed as follows: solve the optimal design problem over a time horizon $[k,\ k+h-1]$ according to an objective function such as (1.1) using the current estimate $\hat{\theta}_k$ to get $u_{k|k}^*$ to $u_{k+h-1|k}^*$; implement $u_k = u_{k|k}^*$ and obtain the sampled output y_{k+1} at time instant t_{k+1}; this new measurement y_{k+1} will be used to update the current estimate from $\hat{\theta}_k$ to $\hat{\theta}_{k+1}$; repeat the optimal design procedure with this new estimate $\hat{\theta}_{k+1}$. The process is shown in Figure 1.1.

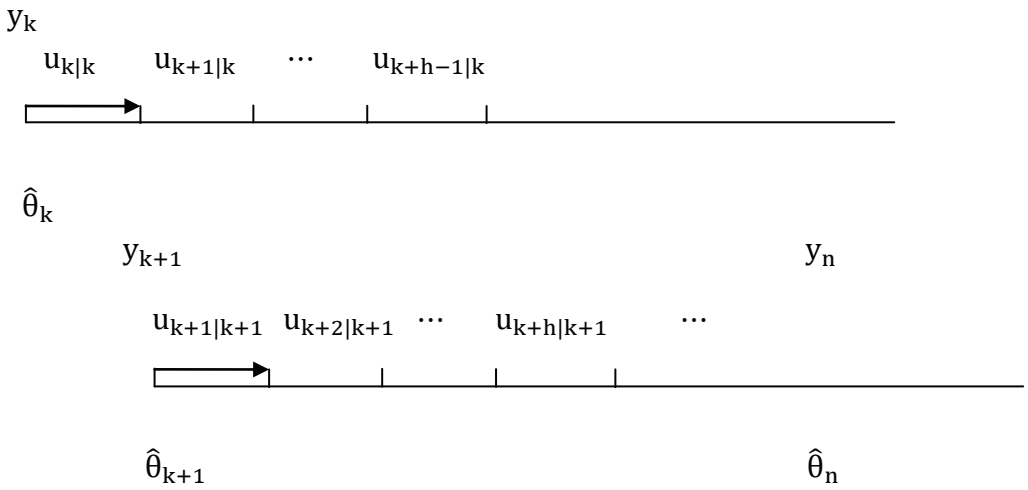

Figure 1.1: Receding horizon design

1.3 LPV Model Identification

The LPV model is often described as an Orthonormal Basis Function (OBF) as follows [35],

$$y = \sum_{i=1}^{n} \alpha_i(p, \beta_i)\phi_i(p)u \tag{1.5}$$

where p is the operating point and α_i is a function of p with parameter vector β_i acting as the ith weighting factor, $i = 1, \ldots, n$.

There are basically two groups of methods for LPV identification. One is the local approach which uses the data collected from experiments at the n operating points from $\bar{p}_1$ to $\bar{p}_n$. The parameter set β_i is estimated by interpolating between operating points $\bar{p}_i$, $i = 1, \ldots, n$. For the local approach, the LPV model can be interpreted as

$$G(p, q) = \sum_{i=1}^{n} \alpha_i(p, \beta_i) G_i(p, q) \tag{1.6}$$

where G is the model function, q is the shift operator, $G_i(p, q)$ is the ith local model G_i and n is the number of local models. The other method is the global approach. To utilize this approach, a single experiment needs to be performed along an operating trajectory composed of a large number of operating points. Though with the capacity to represent the nonlinearity well, the global approach can be hazardous and unrealistic in practice since it requires extensive testing along all varying operating points.

To address this problem, Xu et al. (2009) [39] developed a hybrid LPV identification method. In this combined method, local models are identified using data set at some typical operating points; then the global LPV model is identified by interpolating all the local models G_i using all data. This hybrid LPV identification method combines the advantages of both local approach and global approach. In chapter 3 and 4, this hybrid method will be adopted.

1.4 Contributions

The main contributions of this thesis can be categorized into three aspects which are elaborated in Chapter 2, Chapter 3 and Chapter 4 respectively. In Chapter 2, the proposed constrained receding-horizon design (CRHD) addresses the poor initial guess problem which is common and important in nonlinear system identification; in Chapter 3, the proposed optimal operating point design for LPV model identification solves a cardinal problem which has not been well investigated by other existing work [34]; in Chapter 4, a simultaneous design strategy targets at improving the model accuracy based on the operating points design proposed in Chapter 3. The main contributions of the thesis are listed below:

1. Further developed optimal experimental design and parameter estimation for nonlinear systems under a receding-horizon framework.

2. Integrated constraints (derived from a priori knowledge about the steady state) into the parameter estimation process. This addresses the issue of a poor initial guess which can have a significant effect on nonlinear system identification.

3. Proved that the proposed constrained receding-horizon design (CRHD) is superior to the unconstrained receding-horizon design (URHD) in terms of parameter uncertainty and estimation convergence.

4. Designed optimal operating points and improved the model accuracy. Since this optimal design requires no a-priori knowledge about the true nonlinear system, it is a practical approach for LPV model identification.

5. Simultaneously designed the operating points and input perturbation based on the hybrid identification framework of Xu et al. (2009) [39] and Zhu and Xu (2008) [42]. This joint experiment design can enhance the reliability of LPV models obtained from single factor design such as operating point-only design.

1.5 Thesis Outline

The rest of this thesis is concerned with solving three important problems in experiment design. Chapter 2 develops a novel constrained receding-horizon design (CRHD) combining optimal experiment design and constrained parameter estimation. This method proves to be effective and practical in solving the poor initial condition problem in nonlinear system identification, both by simulation examples and mathematical derivations. Chapter 3 formulates the online optimal operating point selection for LPV models. This framework is based on a hybrid identification method using experimental data obtained both from local regions and transition periods. Chapter 4 investigates the joint experimental design problem by simultaneously designing the operating points and input perturbation. This simultaneous design is applied to two chemical engineering simulation examples, the continuous stirred tank reactor (CSTR) and the solid oxide fuel cell (SOFC). As a complicated and highly nonlinear model, the dynamics and key mechanism of the SOFC model is illustrated at the beginning of the chapter. This thesis will conclude in Chapter 5 with discussions and some perspectives for future research.

Chapter 2

Constrained Receding-horizon Experiment Design and Parameter Estimation in the Presence of Poor Initial Conditions

[1] An optimal experiment design assumes the existence of an initial or nominal process model. The efficiency of this procedure depends on how the initial model is chosen. This creates a practical dilemma as estimating the model is precisely what the experiment tries to achieve. This chapter develops a novel approach to experiment design for identification of nonlinear systems, with the purpose of reducing the influence of poor initial values. The experiment design and the parameter estimation are conducted iteratively under a receding-horizon framework. By taking steady state prior knowledge into account, constraints on the parameters can be derived. Such constraints help reduce influence of poor initial models. The proposed algorithm is illustrated through examples to demonstrate its efficiency.

2.1 Introduction

Optimal experiment design aims at determining optimal experiment conditions to achieve a specific set of objectives. Experiment design is a broad subject which includes aspects such as input design, operating point design, and sampling time design. Though a significant amount of literature on optimal experiment design for linear systems has been published since the 1970s

1. This chapter has been been accepted for publication in AIChE Journal as "Zhu and Huang (2010). Constrained receding-horizon experiment design and parameter estimation in the presence of poor initial conditions. AIChE Journal. 2010. ".

[9, 41], the optimal experiment design concerning nonlinear systems has remained largely unexplored.

One significant challenge for nonlinear experiment design as well as parameters identification is that the sensitivity functions used to search for optimal conditions depend on the unknown model parameters. Three existing methods have been proposed to address this challenge: minimax experiment design, ED (expectation of determinant)/EID (expectation of the inverse of determinant)-optimal design, and adaptive experiment design.

Minimax experiment design attempts to achieve robust experiment by minimizing the largest possible modeling error. This approach needs no prior information about parameter distributions. There are two recent representative publications on this topic. Rojas et al. (2007)[26] developed a method of optimizing the worst case of modeling error over the parameter set, while a convex optimization algorithm is implemented on a linear system. In conjunction, Welsh and Rojas (2009)[38] proposed an algorithm to solve a robust optimal experiment design problem by *scenario approach*. To construct convex or semi-definite convex problems, both techniques formulate the identification problem in frequency domain, but neither of the methods can be used for identification in nonlinear system. Moreover, the optimality objective function for nonlinear identification is generally difficult to be formulated as a convex or semi-definite convex problem.

Another group of methods (especially popular in bioscience fields) are experiment designs by optimizing over the expected determinant of a Fisher information matrix. Pronzato and Walter (1985)[22], and Walter and Pronzato (1985)[36] proposed ED-optimal design and EID-optimal design as follows:

(Pronzato and Walter(1985)[22]): An experiment design φ_{ED} is called ED-optimal if

$$\varphi_{ED} = arg \min_{\varphi \in \Phi} E_{\hat{\theta}}[f(M(\hat{\theta}, \varphi))] \tag{2.1}$$

(Walter and Pronzato (1985)[36]): An experiment design φ_{EID} is called EID-optimal if

$$\varphi_{EID} = arg \max_{\varphi \in \Phi} E_{\hat{\theta}}[1/f(M(\hat{\theta}, \varphi))] \tag{2.2}$$

where φ is the experiment design, $\hat{\theta}$ is the estimate of parameter, E is the expectation operation, $M(\hat{\theta}, \varphi)$ is the Fisher information matrix and $f = det(\cdot)^{-1}$.

Both of these two designs require prior knowledge of unknown parameter distributions [37]. Since in practice the prior parameter distributions and the expected value cannot be easily obtained, these methods can only apply to models with well-posed distributions.

Another solution is the adaptive design which is widely used in engineering literature [33]. The adaptive design starts from a nominal model guess $\hat{\theta}_0$, by which the design criterion $f(M(\hat{\theta}_0, \varphi))$ is optimized. Then the experiment is conducted for the next one or several samples and the model parameter is identified. Afterward, the procedure iterates between experiment design

and parameter estimation. In linear systems where unbiased or asymptotic unbiased estimation can be guaranteed, the adaptive design works well and eventually yields the optimal experimental condition for estimation. However, this method will likely fail in the case of nonlinear system identification under poor initial guess of the parameters. The poor initial guess problem is not uncommon especially when we have little prior knowledge about the true process in practice and is particularly harmful to the adaptive design. Poor initial conditions induce the problems in the following aspects:

The experiment design φ^* depends on the optimality criterion:

$$\varphi^* = arg \min_{\varphi \in \Phi} f(M(\hat{\theta}_0, \varphi)) \tag{2.3}$$

Under an initial guess $\hat{\theta}_0$ that is far away from the real parameter, a design φ is far from the optimal or may even be very deviated from where a normal input signal should be; therefore, improper experiment conditions will be designed that may make the estimated parameter deviate further away from the optimal in subsequent iterations. This is particularly problematic for nonlinear systems.

Adaptive parameter estimation for nonlinear system cannot guarantee the convergence. In fact, the parameter estimator, typically an extended Kalman filter, is a local asymptotic observer only when some conditions being met such as the initial guess is near the true value or the system itself has weak nonlinearity [32]. Therefore, when the initial guess of the model parameters is poor, the parameter estimation through the extended Kalman filter may diverge quickly.

While there are numerous works on adaptive experiment design, to the best of authors' knowledge, none of them target solving poor initial condition problem. This problem is the principal concern of this work.

The remainder of the paper is organized as follows: Section 2 discusses preliminaries. In section 3, a new method is presented to solve the receding-horizon experiment design problem with poor initial conditions. To demonstrate the merits of the proposed method, two nonlinear examples are presented in section 4. Section 5 provides the conclusion.

2.2 Preliminaries

2.2.1 Sensitivity analysis

The sensitivity analysis method has been well developed over the last several decades [3]; in system identification, it is often used as a tool to assess estimability of parameters. Such estimability is described as the ability to compute parameters accurately given data and experimental conditions [40, 14]. Increasing parameter sensitivity corresponds to better estimability. In optimal experiment design where we seek to obtain the most informative data, sensitivity analysis is particularly a valuable tool. Consider the system described

by the following state space model:

$$\dot{x}(t) = f(x(t), u(t), \theta) \tag{2.4}$$
$$y(t) = h(x(t), u(t), \theta) \tag{2.5}$$

where x is the state, f is state function of the state itself, input u and parameter θ; y is the output, h is the output function. For illustrative purposes, we assume this system has p parameters, one state, one output, and $y(t) = x(t)$. The sensitivity is given by the following definition:

A sensitivity matrix can be computed as follows [40, 7],

$$Z = \begin{bmatrix} \frac{\partial y}{\partial \theta_1}|_{t_1} & \frac{\partial y}{\partial \theta_2}|_{t_1} & \cdots & \frac{\partial y}{\partial \theta_p}|_{t_1} \\ \frac{\partial y}{\partial \theta_1}|_{t_2} & \ddots & & \vdots \\ \vdots & & \ddots & \vdots \\ \frac{\partial y}{\partial \theta_1}|_{t_N} & \cdots & \cdots & \frac{\partial y}{\partial \theta_p}|_{t_N} \end{bmatrix} \tag{2.6}$$

where t_1 to t_N denote the start and end time of the experiment respectively.

As an example, consider a model with parameter nonlinearity [14]

$$\dot{x}_t = -\frac{x_t}{\theta_1 \theta_2} + \frac{u_t}{\theta_2} \tag{2.7}$$
$$y_t = x_t \tag{2.8}$$

The sensitivity matrix is calculated as[14]

$$\frac{\partial}{\partial \theta}(\frac{dx}{dt}) = \frac{\partial f}{\partial \theta} + \frac{\partial f}{\partial x}\frac{\partial x}{\partial \theta} \tag{2.9}$$

Rearrange (2.9),

$$\frac{d}{dt}(\frac{\partial x}{\partial \theta}) = \frac{\partial f}{\partial \theta} + \frac{\partial f}{\partial x}\frac{\partial x}{\partial \theta} \tag{2.10}$$

(2.10) is a differential equation from which the sensitivity ($\frac{\partial y}{\partial \theta} = \frac{\partial x}{\partial \theta}$ in this case) is calculated. Specifically,

$$\frac{d}{dt}(\frac{\partial x}{\partial \theta_1}) = \frac{x}{\theta_1^2 \theta_2} - \frac{1}{\theta_1 \theta_2}(\frac{\partial x}{\partial \theta_1}) \tag{2.11}$$
$$\frac{d}{dt}(\frac{\partial x}{\partial \theta_2}) = \frac{x}{\theta_1 \theta_2^2} - \frac{1}{\theta_1 \theta_2}(\frac{\partial x}{\partial \theta_2}) - \frac{u}{\theta_2^2} \tag{2.12}$$

(2.11) shows that when calculating the sensitivity matrix for models with parameters nonlinearity, parameters themselves are needed and so is the input. For illustrative purposes, Figure 2.1 shows that different nominal values of $\theta^{(0)}$ can lead to quite different sensitivities with respect to some parameters (θ_1 in this case), which may induce significant problems within the experiment design.

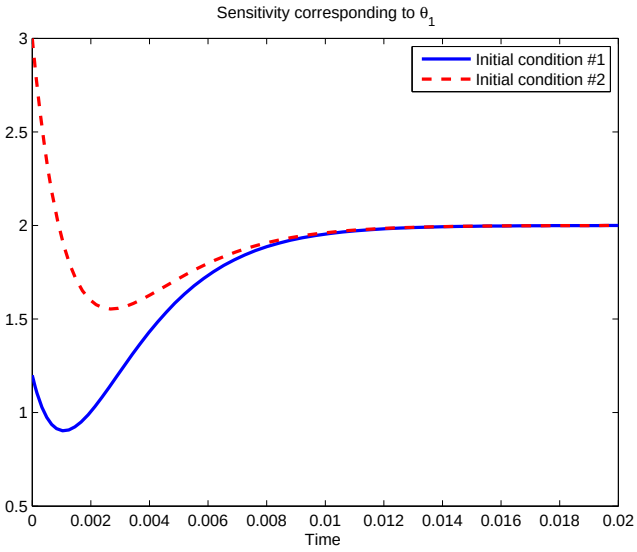

Figure 2.1: Sensitivities corresponding to different nominal values of parameters(Blue solid line: initial values $E(\hat{\theta}_1^{(0)}) = 1.2$, $E(\hat{\theta}_2^{(0)})= 0.0015$; Red dash line: initial values $E(\hat{\theta}_1^{(0)}) = 3$, $E(\hat{\theta}_2^{(0)})= 0.006$.

2.2.2 Information matrix

From (2.3), we know that the optimality criterion depends on the Fisher information matrix (FIM). A commonly used optimality criterion is

$$f(M(\hat{\theta}_0, \varphi)) = -log(det(M(\hat{\theta}_0, \varphi))) \tag{2.13}$$

whose property has been discussed by Goodwin and Payne (1977)[9]. The relation between the sensitivity matrix and the Fisher information matrix M is[40]

$$M = Z^T \Sigma^{-1} Z \tag{2.14}$$

where Z is sensitivity matrix defined in (2.6), and Σ is the covariance matrix of output y. In the case of covariance scaled response, (2.14) can be reduced to

$$M = Z^T Z \tag{2.15}$$

The advantage of the determinant criterion is its independence of the scaling of the parameters. This optimality criterion also minimizes the generalized covariance of the parameters estimate. The Cramér-Rao inequality is given by

$$P \equiv Cov(\hat{\theta}) \geq M^{-1} \tag{2.16}$$

This inequality states that the inverse of the Fisher information matrix acts as a lower bound for covariance of parameter estimate. When equality is satisfied, the estimator is said to be efficient.

For a class of unbiased estimators, the minimum variance estimator is statistically efficient. For nonlinear models, unbiased estimation has been widely known to be theoretically unapproachable. Song and Grizzle(1995)[32] showed that extended Kalman filter(EKF), as a classical nonlinear approximation filter, can be an asymptotic unbiased estimator, although certain conditions such as a proper initial guess or a weak nonlinearity is required in order to achieve convergence. Practically, EKF works well in most nonlinear models[31]. In this work, we follow the principle that "maximizing the Fisher information matrix corresponds to minimizing covariance of estimates", as stated in most of the experiment design methodologies. Therefore the optimality criterion in (2.13) is used for minimizing the covariance of $\hat{\theta}$.

2.3 Receding-horizon Experiment Design for Nonlinear System with Poor Initial Conditions

Due to the impact of poor initial conditions on nonlinear system identification, it is desirable to derive a method which is robust both in experiment design and parameter estimation. From a practical point of view, among the three methods—minimax design, ED(EID)-optimal, and adaptive design— adaptive design is easiest to implement due to relatively small computation load and suitability for nonlinear systems. As discussed in the introduction, the main problem with the adaptive design for nonlinear systems is the poor initial values. We will develop a method that provides a solution for dealing with poor initial conditions when applying the adaptive design. The flow diagram of the proposed experiment design is shown first in Figure 2.2 while the details will be elaborated shortly.

2.3.1 Constructing constraints for parameters

The first step of the proposed design is to impose a constraint according to certain steady-state information. In some cases, steady states can be known a priori while in other cases, a simple step test can help determine the steady states. When a steady state is found, it will impose certain constraints on the model parameters. Depending on the characteristics of the individual system, there are two ways to derive the parameter constraints based on the knowledge of steady states. The first method involves directly substituting steady states into the state equation and then equating it to zero. Suppose we have nonlinear state space equation as follows,

$$\dot{x}_t = f(\theta, x_t, u_t) + Nw_t \tag{2.17}$$

$$y_t = x_t + Rv_t \tag{2.18}$$

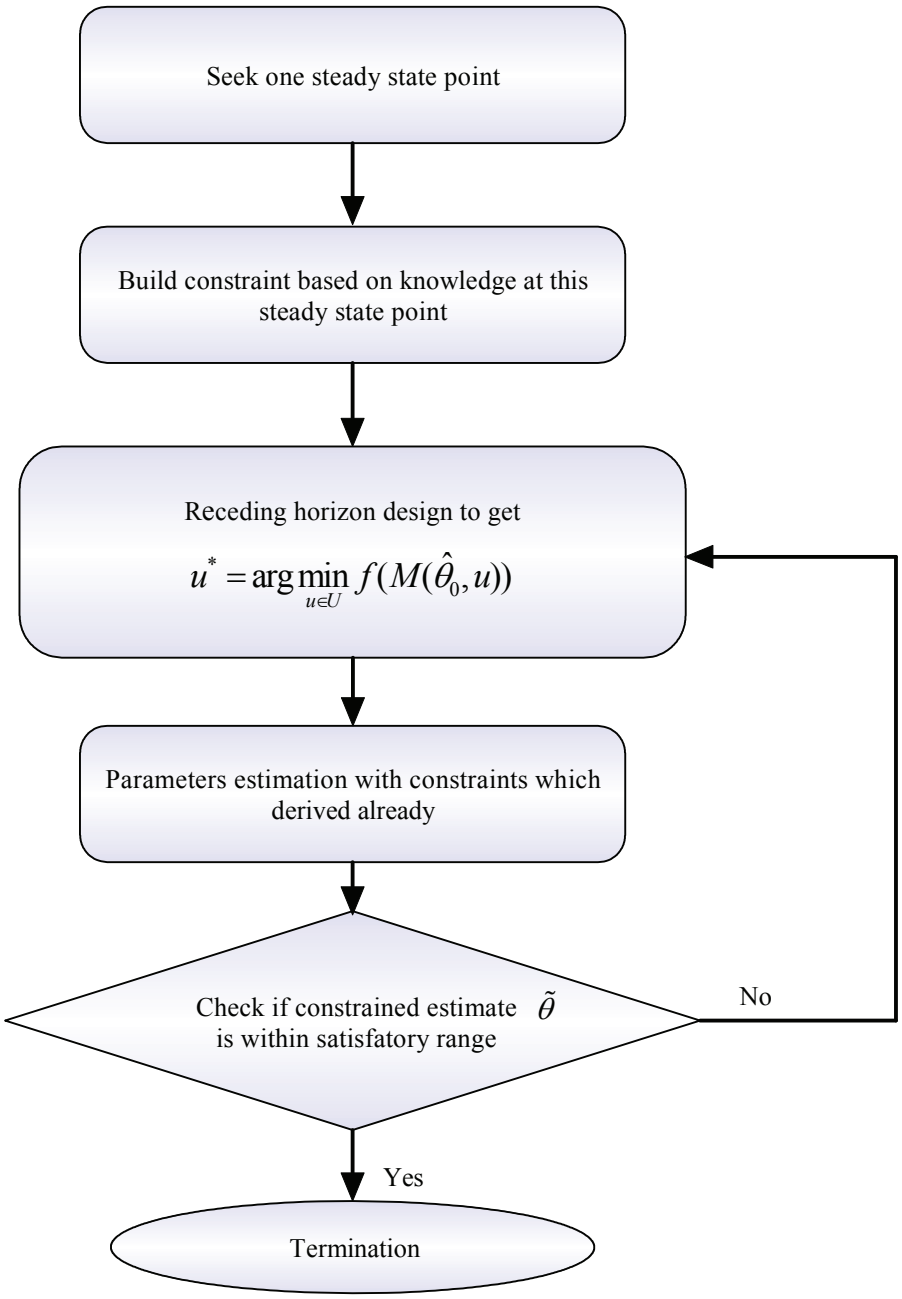

Figure 2.2: Flow diagram for proposed experiment design

where $w_t \sim \mathcal{N}(0, I_{n_x})$, $v_t \sim \mathcal{N}(0, I_{n_y})$, $\mathcal{N}$ stands for Gaussian distribution, n_x and n_y are dimensions of x and y respectively, N and R are constant matrices of appropriate dimensions. The steady state is denoted as (x_s, u_s). Substituting this steady state point into (2.17) gives

$$\dot{x} = f(\theta, x_s, u_s) \tag{2.19}$$

Since $\dot{x} = 0$ at steady state, the following constraint is established,

$$g(\theta) = f(\theta, x_s, u_s) = 0 \tag{2.20}$$

Another approach for specifying constraints is to approximate this nonlinear model at steady state by using a local linear model; these models can be identified by a linear identification algorithm around a steady state point. For illustration purpose, the electronic circuit system as shown in (2.7) is used to derive the parameter constraints. With perturbations around a steady state, perform continuous-time system identification [20], and then the following model is identified:

$$\dot{x}_t = -\frac{x_t}{0.001783} + \frac{u_t}{1.1998} \tag{2.21}$$

$$y_t = x_t \tag{2.22}$$

A constraint can therefore be set up as

$$\theta_1 \theta_2 = 0.001783 \tag{2.23}$$

Note that due to unavoidable estimation error in identification, this constraint is an approximate one.

Obviously additional steady states can be found from step response tests. Notice that more constraints are incorporated, the narrower range of parameter estimate can be. For simplification, we adopt only one constraint derived from one steady state in the examples. For additional steady state conditions, the proposed algorithm can also be applied in the same manner.

2.3.2 Receding horizon design

Stigter et al. (2006)[33] proposed an adaptive approach for experiment design with a receding horizon idea. Jayasankar et al. (2010) [13] later formalized the design and called it as a receding horizon experiment design. In receding horizon design, the optimization is performed to obtain U_k^* according to the following equation.

$$U_k^* = [u_{k|k}^* \; u_{k+1|k}^* \; \cdots \; u_{k+h-1|k}^* \,] = \arg\min_{U_k \in \mathbb{U}} f(M(\hat{\theta}_k, U_k)) \tag{2.24}$$

where U_k^* is the optimal input vector containing $u_{k|k}^*,\ u_{k+1|k}^*,\ \cdots,\ u_{k+h-1|k}^*$ calculated at the k^{th} time instant, h is the optimization horizon, $\mathbb{U}$ is the

feasible set which U_k^* can be chosen from, f and M are explained in (2.13) and (2.14) respectively, and $\hat{\theta}_k$ is the parameter estimate at time instant k.

The procedure of receding horizon design is performed as follows: solve the optimal design problem according to an objective function such as (2.3) with the current estimate $\hat{\theta}_k$ over a time horizon $[k, k+h-1]$ to get $u_{k|k}^*$ till $u_{k+h-1|k}^*$; implement $u_k = u_{k|k}^*$ and obtain the sampled output y_{k+1} at time instant t_{k+1}; this new measurement y_{k+1} will be used to update the current estimate from $\hat{\theta}_k$ to $\hat{\theta}_{k+1}$, and repeat the optimal design procedure with this new estimate $\hat{\theta}_{k+1}$. The process is shown below in Figure 1.1 and will be adopted in this chapter.

2.3.3 EKF with state constraint

The Extended Kalman filter (EKF) is a classical state estimator for nonlinear systems. Parameters can also be estimated if we consider parameters as augmented states. As discussed before, reducing $Cov(\hat{\theta})$ is equivalent to increasing the information in the data. Poor initial conditions can lead to poor experiment design as discussed before; therefore, it is natural to impose constraints on the state estimations when using EKF so that the experiment design and parameter estimation will not be unduly influenced by poor initial parameters. Contributions on constrained estimation can be found in Simon and Chia (2002) [31], Simon (2006) [29] and Simon (2009) [30]. In this work, EKF with equality constraints is adopted.

For illustration, suppose that we have a nonlinear system with one continuous state and one discrete measurement

$$\dot{x} = f(\theta, x, u) \tag{2.25}$$

$$y_k = h(x_k) \tag{2.26}$$

In the following, parameters are considered as augmented states. We use $\mathbf{x}$ to signify the state vector which includes parameters θ:

$$\mathbf{x} = \begin{bmatrix} x \\ \theta \end{bmatrix} \tag{2.27}$$

The unconstrained continuous-discrete EKF is shown in 2.1 [5], where $\hat{x}$ denotes unconstrained state estimate.

Consider that the model described by (2.25) and (2.26) has the following linear constraint:

$$D\mathbf{x}_k = d_k \tag{2.28}$$

where D is $s \times n_x$ dimensional matrix, and s stands for the number of constraints, n_x stands for the number of states being constrained, and d_k is $s \times 1$ vector. Thus the problem formulation admits inclusion of multiple constraints. More constraints are incorporated, the narrower region of parameters, and more possible to converge to the true set of parameters.

Table 2.1: Continuous-Discrete Extended Kalman Filter

Model	$\dot{\mathbf{x}}(t) = f(\mathbf{x}(t), u(t), t) + G(t)w(t), w(t)\ N(0, Q(t))$ $y_k = h(\mathbf{x}_k) + v_k, v_k\ N(0, R_k)$
Gain	$K_k = P_k^- H_k^T(\hat{\mathbf{x}}_k^-)[H_k(\hat{\mathbf{x}}_k^-)P_k^- H_k^T(\hat{\mathbf{x}}_k^-) + R_k]^{-1}$ $H_k(\hat{\mathbf{x}}_k^-) \equiv \frac{\partial h}{\partial \mathbf{x}}\|_{\hat{\mathbf{x}}_k^-}$
Update	$\hat{\mathbf{x}}_k^+ = \hat{\mathbf{x}}_k^- + K_k[y_k - h(\hat{\mathbf{x}}_k^-)]$ $P_k^+ = [I - K_k H_k(\hat{\mathbf{x}}_k^-)]P_k^-$
Propagation	$\dot{\hat{\mathbf{x}}}(t) = f(\hat{\mathbf{x}}(t), u(t), t)$ $\dot{P}(t) = F(\hat{\mathbf{x}}(t), t)P(t) + P(t)F^T(\hat{\mathbf{x}}(t), t) + G(t)Q(t)G^T(t)$ $F(\hat{\mathbf{x}}(t), t) \equiv \frac{\partial f}{\partial \mathbf{x}}\|_{\hat{\mathbf{x}}(t)}$

Based on basic equations shown in Table 2.1, Simon and Chia (2002) [31] derived the EKF with equality constraint as

$$\tilde{\mathbf{x}}_0 = \hat{\mathbf{x}}_0 \tag{2.29}$$

$$\tilde{\mathbf{x}}_k = \hat{\mathbf{x}}_k - W^{-1}D^T(DW^{-1}D^T)^{-1}(D\hat{\mathbf{x}}_k - d_k) \tag{2.30}$$

following the projection method, where W is any symmetric positive definite weighting matrix. In (2.29) and (2.30), we have used $\tilde{x}$ to denote constrained state estimate. Throughout the remainder of this chapter, a " $\hat{}$ " denotes an unconstrained estimate and a " $\tilde{}$ " denotes a constrained estimate while a " $*$ " denotes an optimal. Usually, W is set as identity matrix I or P^{-1}, where P is the inverse of the covariance matrix for the unconstrained estimate $\hat{\mathbf{x}}$ obtained from Table 2.1.

In most nonlinear systems, the constraint is also nonlinear as in (2.20). As an approximation, (2.20) can be linearized around the current estimate $\tilde{\mathbf{x}}_k$ as

$$g(\tilde{\mathbf{x}}_k) + g'(\tilde{\mathbf{x}}_k)(\mathbf{x}_{k+1} - \tilde{\mathbf{x}}_k) \approx 0 \tag{2.31}$$

Then a linear constraint having the form of (2.28) is obtained

$$g'(\tilde{\mathbf{x}}_k)\mathbf{x}_{k+1} \approx d_{k+1} - g(\tilde{\mathbf{x}}_k) + g'(\tilde{\mathbf{x}}_k)\tilde{\mathbf{x}}_k \tag{2.32}$$

where $g'(\tilde{\mathbf{x}}_k)$ is equivalent to D and $d_{k+1} - g(\tilde{\mathbf{x}}_k) + g'(\tilde{\mathbf{x}}_k)\tilde{\mathbf{x}}_k$ equivalent to d in (2.28). Then according to (2.29) and (2.30), the constrained estimate becomes

$$\tilde{\mathbf{x}}_0 = \hat{\mathbf{x}}_0 \tag{2.33}$$

$$\begin{aligned}\tilde{\mathbf{x}}_{k+1} = {} & \hat{\mathbf{x}}_{k+1} - W^{-1}g'(\tilde{\mathbf{x}}_k)^T(g'(\tilde{\mathbf{x}}_k)W^{-1}g'(\tilde{\mathbf{x}}_k)^T)^{-1}(g'(\tilde{\mathbf{x}}_k)\hat{\mathbf{x}}_{k+1} \\ & -d_{k+1} + g(\tilde{\mathbf{x}}_k) - g'(\tilde{\mathbf{x}}_k)\tilde{\mathbf{x}}_k)\end{aligned} \tag{2.34}$$

Note that both Unscented Kalman Filter (UKF) and Moving Horizon Estimation (MHE) can be applied under this constrained framework for parameter estimation. Their state estimation recursion is analogous to that of constrained EKF [30].

Both adaptive experiment design and constrained estimation have their own advantages respectively. Adaptive experiment design has low computation cost and is easy to implement. Constraint estimation can improve the performance of estimation [31]. However, neither one of them individually can address the nonlinear estimation problem under poor initial conditions. In terms of constrained state estimation itself, there is one major difference between Simon and Chia (2002)'s method [31] and the proposed method. For the constrained EKF in the proposed method, each current $\tilde{\mathbf{x}}_k$ is involved in the kth step of recursive estimation, while in Simon and Chia (2002)'s method [31] this $\tilde{\mathbf{x}}_k$ is obtained by projecting the unconstrained estimate $\hat{\mathbf{x}}_k$ into the constraint space, but is not involved in the iterative framework of EKF for the next state estimate.

With (2.33) and (2.34) being available, we use estimate $\tilde{\mathbf{x}}$ instead of $\hat{\mathbf{x}}$ in calculating optimality criterion and this gives us the optimal input $\tilde{u}^*$ for the constrained optimal design. The following Proposition shows that the constrained design achieves better estimation performance than that of unconstrained design in terms variance of estimation.

Denote the parameter estimation under constraint optimal design as $\tilde{\theta}(\tilde{u}^*)$ and the parameter estimation under unconstrained optimal design as $\hat{\theta}(\hat{u}^*)$. Then the following inequality holds:

$$Cov(\hat{\theta}(\hat{u}^*)) > Cov(\tilde{\theta}(\tilde{u}^*)) \tag{2.35}$$

Proof. For any input u, the error between the constrained state estimate $\tilde{\mathbf{x}}$, unconstrained state estimate $\hat{\mathbf{x}}$ and the true state value $\mathbf{x}$ has the following relation [31]:

$$Cov(\mathbf{x} - \tilde{\mathbf{x}}) < Cov(\mathbf{x} - \hat{\mathbf{x}}) \tag{2.36}$$

where the inequality in the form of "$A < B$" indicates that the square matrix $B - A$ is positive definite. According to $\mathbf{x}$ defined in (2.27), partition

$$\begin{aligned} A &= Cov(\mathbf{x} - \hat{\mathbf{x}}) - Cov(\mathbf{x} - \tilde{\mathbf{x}}) && (2.37)\\ &= \begin{bmatrix} A_{11} & A_{12} \\ A_{21} & A_{22} \end{bmatrix} && (2.38) \end{aligned}$$

then

$$\begin{aligned} A_{11} &= Cov(x - \hat{x}) - Cov(x - \tilde{x}) && (2.39)\\ A_{22} &= Cov(\theta - \hat{\theta}) - Cov(\theta - \tilde{\theta}) && (2.40)\\ A_{12} &= A_{21}^T && (2.41)\\ &= E[(x - \hat{x})(\theta - \hat{\theta})^T] - E[(x - \tilde{x})(\theta - \tilde{\theta})^T] && (2.42) \end{aligned}$$

The following equations hold

$$\begin{aligned} Cov(\theta - \hat{\theta}) &= Cov(\hat{\theta}) && (2.43)\\ Cov(\theta - \tilde{\theta}) &= Cov(\tilde{\theta}) && (2.44) \end{aligned}$$

Since A is positive definite, A_{22} is positive definite too, i.e. $A_{22} > 0$. In view of (2.43) and (2.44), this means $\forall u$,

$$Cov(\hat{\theta}(u)) > Cov(\tilde{\theta}(u)) \tag{2.45}$$

where $\hat{\theta}(u)$ (or $\tilde{\theta}(u)$) elaborates that $\hat{\theta}$ (or $\tilde{\theta}$) is an estimate according to the input u. Therefore, the following two inequalities should hold

$$Cov(\hat{\theta}(\hat{u}^*)) > Cov(\tilde{\theta}(\hat{u}^*)) \tag{2.46}$$
$$Cov(\hat{\theta}(\tilde{u}^*)) > Cov(\tilde{\theta}(\tilde{u}^*)) \tag{2.47}$$

where each term represents a different experiment design scheme explained as follows:
$Cov(\hat{\theta}(\hat{u}^*))$: covariance of unconstrained estimate $\hat{\theta}$ with the optimal input $\hat{u}^*$ based on unconstrained design;
$Cov(\tilde{\theta}(\hat{u}^*))$: covariance of constrained estimate $\tilde{\theta}$ with the optimal input $\hat{u}^*$ based on unconstrained design;
$Cov(\hat{\theta}(\tilde{u}^*))$: covariance of unconstrained estimate $\hat{\theta}$ with the optimal input $\tilde{u}^*$ based on constrained design;
$Cov(\tilde{\theta}(\tilde{u}^*))$: covariance of constrained estimate $\tilde{\theta}$ with the optimal input $\tilde{u}^*$ based on constrained design.

Among these four covariances, only $Cov(\hat{\theta}(\hat{u}^*))$ and $Cov(\tilde{\theta}(\tilde{u}^*))$ are the covariance of the adaptive optimal design schemes without and with constraints respectively . By optimal design, the following inequalities should hold:

$$Cov(\hat{\theta}(\tilde{u}^*)) > Cov(\hat{\theta}(\hat{u}^*)) \tag{2.48}$$
$$Cov(\tilde{\theta}(\hat{u}^*)) > Cov(\tilde{\theta}(\tilde{u}^*)) \tag{2.49}$$

From (2.46) and (2.49), we obtain the following result

$$Cov(\hat{\theta}(\hat{u}^*)) > Cov(\tilde{\theta}(\tilde{u}^*)) \tag{2.50}$$

□

2.3.4 Effect of constraints on convergence

In Proposition 4, we show that the estimation covariance with the optimal input $\tilde{u}^*$ obtained from the proposed constrained receding-horizon design (CRHD) is superior to the one with input $\hat{u}^*$ obtained from unconstrained receding-horizon design (URHD) where the constraint is referred to the constraint on the parameters. In this section, we shall discuss performance in terms of convergence.

Lemma 1 [32] in the appendices provides a condition for the existence of M iterations after which the estimation can asymptotically converge to the true value in unconstrained case. For constrained case, the number M can be proven to be smaller than that in unconstrained case. In other words,

imposing constraints will improve the convergency property. This is shown in Proposition 5 along with its proof in the Appendices.

Remark 1: The poor initial guess can cause problems in parameter estimation including large variance and slow convergence speed. Most of the experiment design algorithms including D-optimality aim at reducing the covariance (variance) of the parameter only. Imposing constraints obviously restricts space of the parameters searching and thus reduces the risk of divergence. As shown in the Proposition 4 in the previous subsection and Proposition 5 in the Appendices, imposing constrains not only improves convergence but also reduces estimation variance [25, 32].

2.3.5 Uncertainty in constraint

However, there will also be downside of introducing constraint if the constraint is not accurate. Constraint can be corrupted with some uncertainties due to, for example, identification error. This uncertainty in the constraint will lead to an asymptotic bias in the estimation. Take the electrical circuit system in (2.7) as example. The constraint as shown in (2.23) which is obtained from identification contains error since the ideal value for the product of θ_1 and θ_2 should be 0.0018. Therefore, if this inaccurate constraint is imposed throughout the whole experiment design and estimation procedure, the convergence of the parameters estimation to the true values will not be possible owing to the inaccurate constraint. To circumvent this problem one natural option is to release the constraint after certain number of iterations. However, too few steps of estimation with the constraint will not serve the purpose of reducing the effect of poor initial value either. Thus, there is a tradeoff in choosing a proper iteration number between improving the convergence and reducing the estimation bias. The Proposition 5 in Appendices has shown that there exists an integer M that constitutes a lower bound on the number of iterations, after which the iteration will converge. This provides a theoretical justification to release constraints after certain steps of iterations.

Remark 2: In practice, to determine when to release the constraints is not difficult. For example, after the estimated parameters have converged within some tolerance, the constraints can be removed and continue for a few more iterations of estimation until further convergence to eliminate possible bias due to inaccurate constraints.

2.4 Examples

In this section, two examples are discussed, one with parameter nonlinearity only, the other with nonlinearity in both parameters and input. The second example demonstrates the reduction in variance by constrained estimation. From both examples, we can see the advantage of the proposed method in dealing with the poor initial value problem.

2.4.1 The electrical circuit system

The circuit system represented by (2.7) and (2.8) is a fast dynamic system with nonlinearity in parameters [14] only. As illustrated in the previous sections, poor initial guess may lead to estimation problems. In this simulation, a poor initial guess is chosen with $E(\hat{\theta}_1^{(0)}) = 3$, $E(\hat{\theta}_2^{(0)}) = 0.006$, while the true value is $\theta_1 = 1.2$, $\theta_2 = 0.0015$.

The efficiencies of the multi-level Pseudo-Random Sequences (MLPRS), Unconstrained Receding-horizon Design (URHD) as well as the proposed Constrained Receding-horizon Design (CRHD) are compared in this example. The efficiency discussed in the following contains two aspects: efficiency of identification and design cost. We will show the identification result under poor initial conditions through the following aspects: the error between the final estimate and the true value, the convergence rate, the standard deviation of each parameter estimate and the optimality objective function value achieved.

2.4.2 Comparison of simulation results using different design algorithms

Multi-level Pseudo-Random Sequences (MLPRS) is considered as a common input to stimulate a nonlinear system. In this example, we perturb the system by a 3-level MLPRS with the values from 2 to 4. The standard deviations for the estimation results in this chapter are obtained from 30 simulations.

The receding horizon design has been illustrated in section 3. The horizon length is set as $N = 4$.

From Figure 2.3 and Figure 2.4, one can see that the proposed Constrained Receding-horizon Design (CRHD) outperforms Unconstrained Receding-horizon Design (URHD) and multi-level Pseudo-Random Sequences (MLPRS) in terms of convergence to the true values in the presence of poor initialized conditions. Since θ_2 has larger sensitivity than θ_1, the constrained estimation is more 'effective' in θ_2. For the case of unconstrained design, $\hat{\theta}_2$ does not converge. Moreover, one can see from Figure 2.5 that the constrained design can achieve much smaller objective function value than that of unconstrained design.

2.4.3 CSTR with jacket dynamics

In this example, a continuously-stirred tank reactor (CSTR) is used to demonstrate the proposed method when applied to nonlinear chemical processes. The first-order, exothermic reaction $A \to B$ without recycle is described as follows:

$$\dot{c}_A = \frac{q}{V}(c_A^f - c_A) - k_0 \exp(-(\frac{E}{R})/T)c_A \tag{2.51}$$

$$\dot{T} = \frac{q}{V}(T^f - T) + \frac{\triangle H}{\rho C_p} k_0 \exp(-(\frac{E}{R})/T)c_A + \frac{UA}{\rho V C_p}(T_c - T) \tag{2.52}$$

There are totally eight parameters with two states. The description and nominal value of each parameter are shown in Table 2.2 [10].

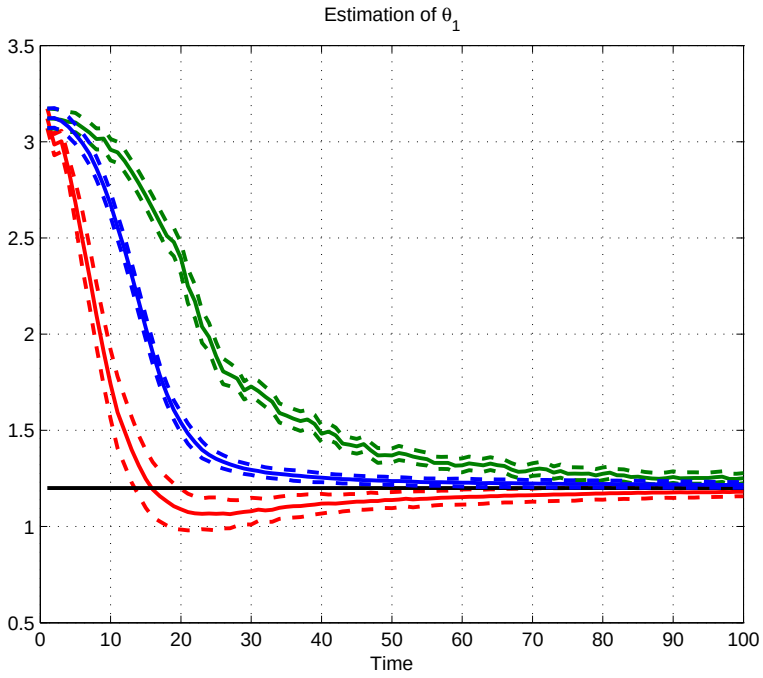

Figure 2.3: Estimate for parameter θ_1 with deviation (N=4) (Green: estimation with 3-level PRS; Blue: unconstraint estimation; Red: constraint estimation; Dotted: standard deviation; Straight black: true value of θ_1)

Table 2.2: Parameters in CSTR

Parameter	Symbol	Value
Density of A-B Mixture (kg/m^3)	ρ	1000
Pre-exponential factor (1/sec)	k_0	7.2×10^{10}
Volumetric Flowrate (m^3/sec)	q	100
Volume of CSTR (m^3)	V	100
Heat capacity of A-B Mixture ($J/kg \cdot K$)	C_p	0.239
Heat of reaction for A-¿B (J/mol)	$\triangle H$	5×10^4
U - Overall Heat Transfer Coefficient ($W/m^2 \cdot K$) A - Area this value is specific for the U calculation (m^2)	UA	5×10^4
Feed Concentration (mol/m^3)	c_a^f	1
Feed Temperature (K)	T^f	350
E - Activation energy in the Arrhenius Equation (J/mol) R - Universal Gas Constant = 8.31451 ($J/mol \cdot K$)	$\frac{E}{R}$	8750

The two states are concentration of component A, c_A, and temperature T. The temperature of cooling jacket T_c is considered as an input.

Among the large number of parameters shown in Table 2.2, some are easier to estimate than the others. According to the analysis obtained by Chu et al. (2007) [4], the fluid density ρ and the pre-exponential factor k_0 have

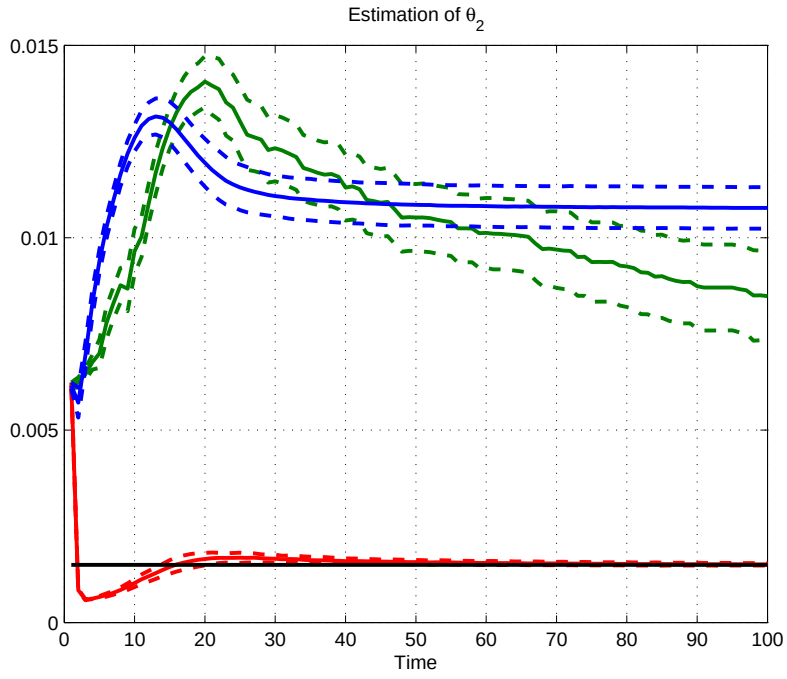

Figure 2.4: Estimate for parameter θ_2 with deviation (N=4) (Green: estimation with 3-level PRS; Blue: unconstraint estimation; Red: constraint estimation; Dotted: standard deviation; Straight black: true value of θ_2)

larger sensitivities while activation energy E/R has smaller sensitivity. In the following simulations, both easier-to-estimate and harder-to-estimate sets of parameters are tested using the proposed method.

From a preliminary steady state test, this CSTR can be determined to have one steady state point at $c_A = 0.9519$ and $T = 312.7$ when the cooling jacket $T_c = 290$. Substituting this steady state point into (2.52), the constraint equation for each pair of parameters is obtained. To deal with the uncertainty in the constraint, one can release the constraint after some number of iterations as stated in the previous section.

Estimation of ρ and k_0

We start the initial guess of these two easier-to-estimate parameters from relatively poor condition: $E(\rho) = 1000, \sigma(\rho) = 50$, $E(k_0) = 7.3 \times 10^{10}, \sigma(k_0) = 1 \times 10^9$ where σ is standard deviation.

The parameters estimation result is shown in Figure 2.6 and 2.7. From Figure 2.6 and 2.7 one can observe the notable difference between constrained design (constraint is implemented throughout the whole estimation) and unconstrained design in terms of the estimation error and the variance of parameters. This result is consistent with previous simulation example.

As stated before, the steady state information in this example obtained

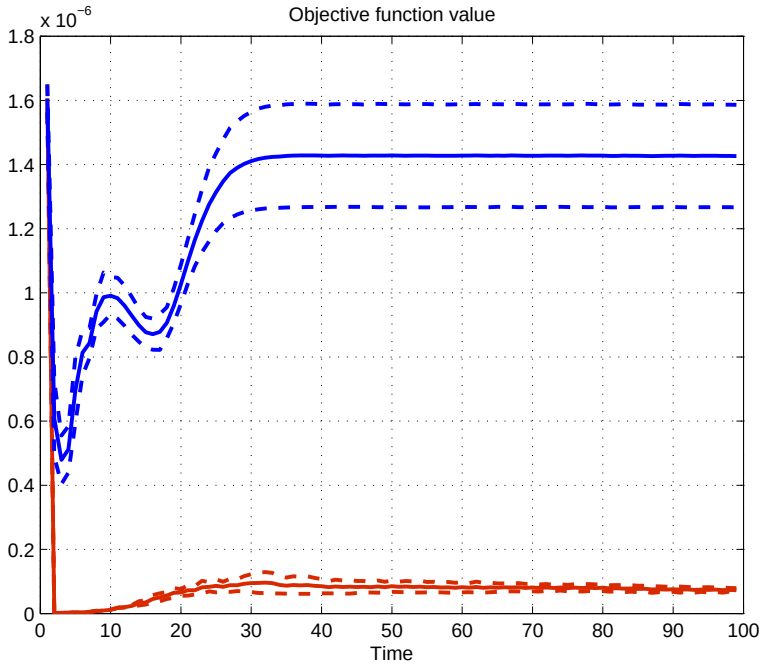

Figure 2.5: Optimality objective function value (Upper blue: unconstrained design; Bottom red: constrained design; Dotted: standard deviation)

from step test may not be accurate. In ideal case, the following equation holds.

$$g(\theta^0, x_s^0, u_s^0) = 0 \tag{2.53}$$

where (x_s^0, u_s^0) is the ideal steady state point. However, without knowing (x_s^0, u_s^0), $(\hat{x}_s, \hat{u}_s^0)$ will be used in the constraint equation. Therefore, the following equation is obtained.

$$\hat{g}(\theta, \hat{x}_s, \hat{u}_s) = 0 \tag{2.54}$$

Indeed, the error has been introduced into the constraint because of the inaccurate steady state information. Substitute $(\hat{x}_s, \hat{u}_s^0)$ into the constraint equation with true parameters, the following equation holds.

$$g(\theta^0, \hat{x}_s, \hat{u}_s) = -96.4364 \neq 0 \tag{2.55}$$

From (2.55) one can see that there is an error in the constraint equation. This reflects in Figure 2.8 that the bias appears when the constraint is imposed throughout the estimation procedure ($K = 200$). This is consistent with the analysis in section 3. Results of releasing the imprecise constraint after different iterations K are shown in Figure 2.8 from which one can find that a value of M within the range from 30 to 50.

Since states and parameters are estimated simultaneously, we can also verify the estimate of the states c_A and T to see whether the proposed method shows any advantage.

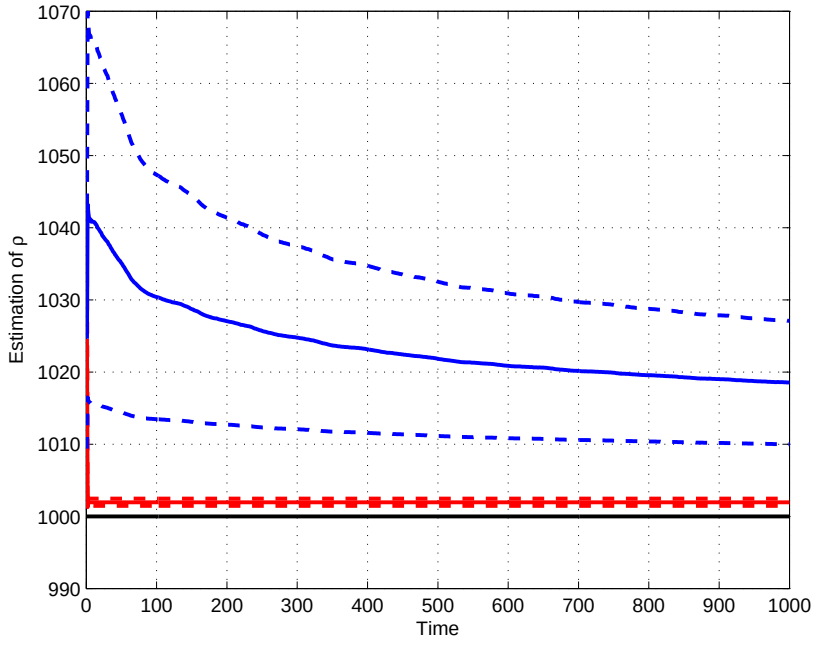

Figure 2.6: Estimate for ρ with deviation (Upper blue: unconstraint estimation; Bottom red: constraint estimation; Dotted: standard deviation; Straight black: true value of ρ)

As shown in Figure 2.9, the state estimation by constrained design is closest to the true state.

Estimation of ρ and E/R

Compared to the first set of parameters, this is a set of harder-to-estimate parameters. The initial guesses for the pair of parameters ρ and E/R are chosen as follows: $E(\rho) = 1025$, $E(E/R) = 8755$. For this set of parameters, constraint is released after 150 iterations. The estimation results are shown in Figure 2.10 and 2.11.

From Figure 2.10 and 2.11, we can see that both estimated parameters converge to the true values by constrained design but fail to converge with unconstrained design. Moreover, from Figure 2.12, one can see that the constrained design estimate is closer to the true value comparing to unconstrained design.

2.5 Conclusion

A constrained receding-horizon approach for nonlinear dynamic experiment design and parameters estimation was presented, with the purpose of solving problems brought out by poor initial condition. The proposed method

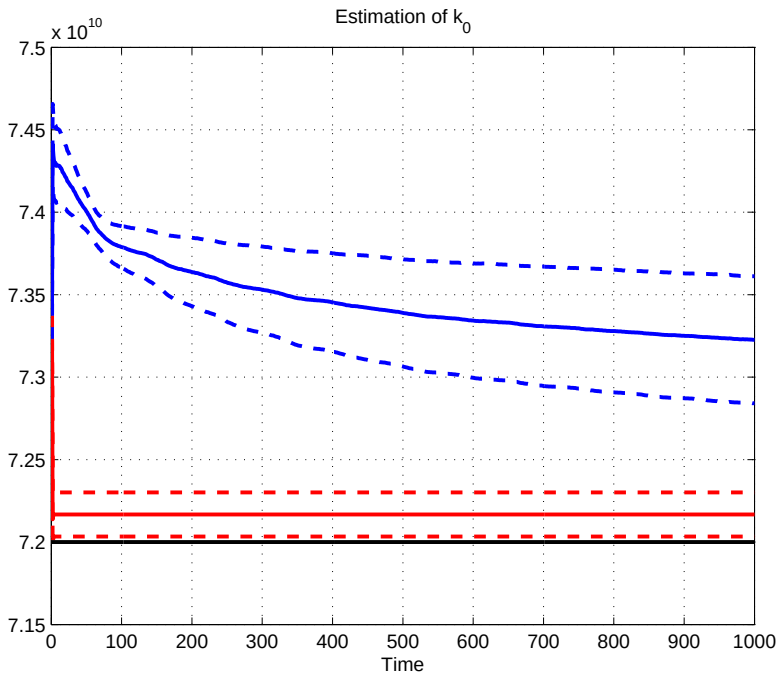

Figure 2.7: Estimate for k_0 with deviation (Upper blue: unconstraint estimation; Bottom red: constraint estimation; Dotted: standard deviation; Straight black: true value of k_0)

incorporated experiment design based on sensitivity analysis and constrained parameter estimation. It is shown that the steady-state condition can be used to form the constraint. It is suggested that when the constraint is not exact, the constraint should be used only for a few iterations in the beginning of the experiment design and parameter estimation and then release after certain steps.

Integration of adaptive experiment design and parameter estimation with constraint proves to be efficient and superior to the unconstrained design. Two simulation examples are used to demonstrate the advantage achieved by the proposed method.

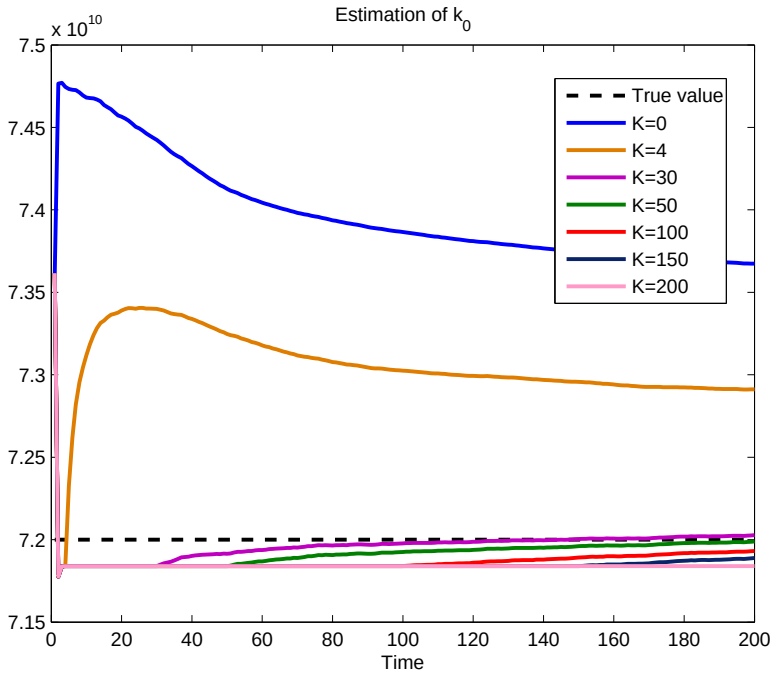

Figure 2.8: Estimation for parameter k_0 under different K (the number of time steps when constraints implemented)

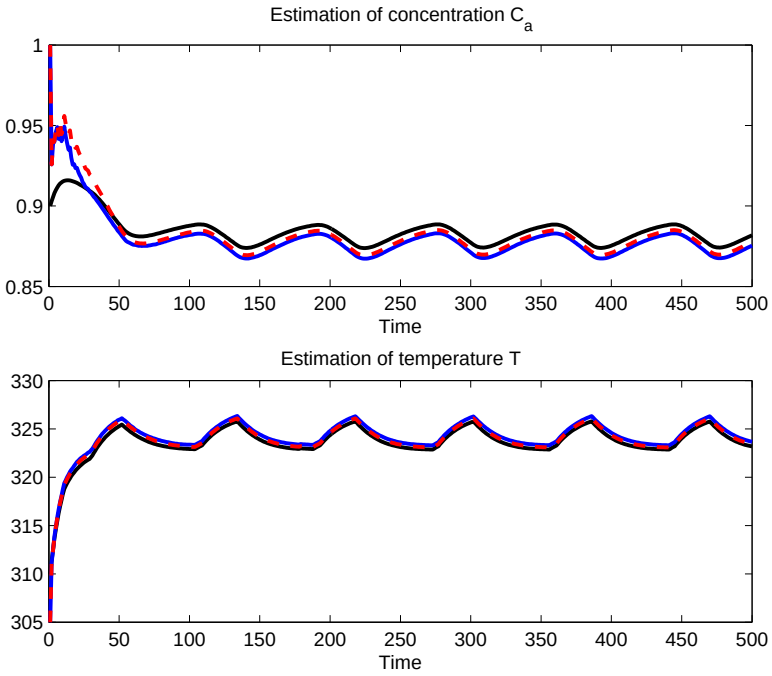

Figure 2.9: Estimate for c_A(top) and T(bottom) (Black: true state value; Blue: unconstrained design; Red dashed: constrained design)

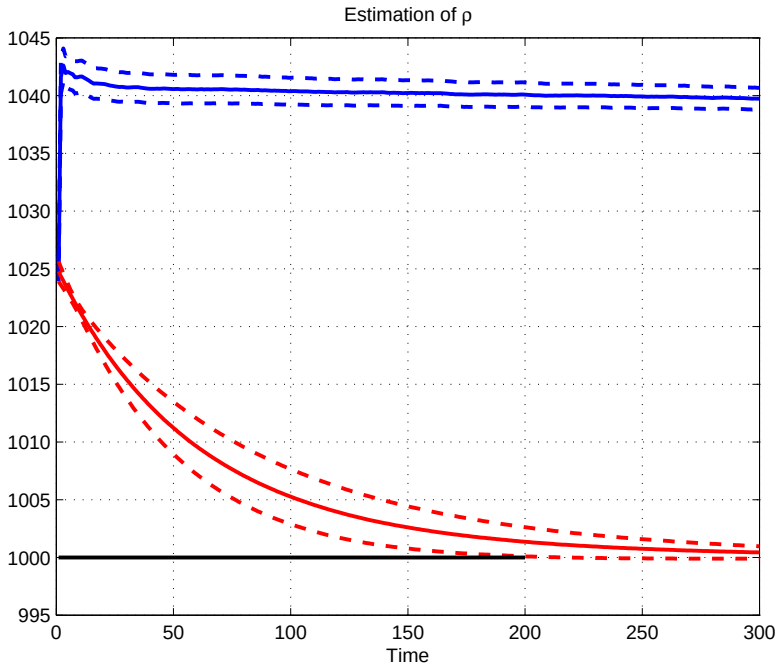

Figure 2.10: Estimate for ρ with deviation ((Upper blue: unconstraint estimation; Bottom red: constraint estimation; Dotted: standard deviation; Straight black: true value of ρ)

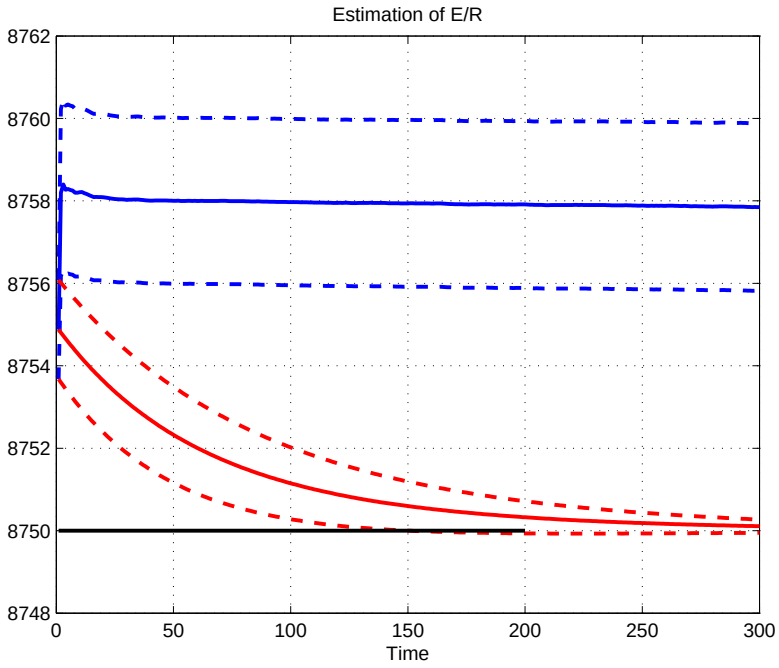

Figure 2.11: Estimate for E/R with deviation (Upper blue: unconstraint estimation; Bottom red: constraint estimation; Dotted: standard deviation; Straight black: true value of E/R)

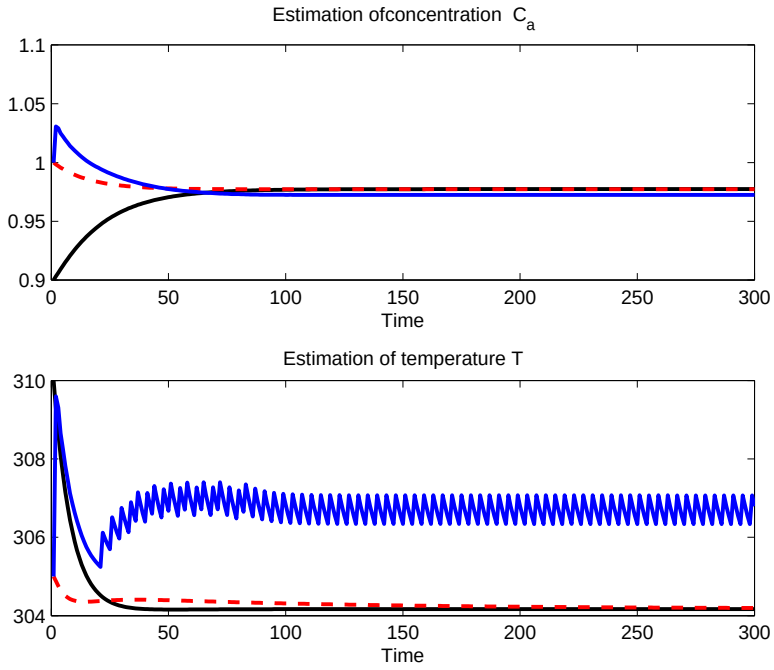

Figure 2.12: Estimation of state (Black: true value of state; Blue: unconstrained design; Red dashed: constrained design; Upper subplot: estimate of C_a; Bottom subplot: estimate of T)

Chapter 3

Adaptive Optimal Operating Points Design for LPV Identification

In this chapter, a class of Linear Parameter Varying (LPV) models for nonlinear system identification is considered. Based on a hybrid LPV identification method and optimal experiment design, an adaptive optimal operating point design approach is developed. First, experiment is performed based on the current operating points, and then the global LPV model is identified by interpolating the current local models. Next, the new optimal operating point is selected in an adaptive manner based on the identified global model. Requiring no a-priori knowledge about the true nonlinear system, the adaptive optimal operating point design is able to improve estimation performance compared to non-optimal design. Two examples show the improvement over the experiments with randomly picked operating points.

3.1 Introduction

While nonlinearity is common for industrial processes, identifying a nonlinear process can be an arduous task. The intuitive approach is to consider a model with simple structure having flexible parameters which can capture the nonlinear process behavior. The Linear Parameter Varying (LPV) model offers the possibility of modeling complex nonlinear systems with good accuracy and low computational cost. This appealing modeling framework has attracted much attention and a considerable number of algorithms have been recently developed. The LPV model contains a time-varying scheduling variable $p(t)$ which is often called the operating or working point [27]. The operating point of a dynamic system can be given by an input variable, a state, an output, or an independent variable. For example, in a Continuous Stirred-Tank Reactor (CSTR), the operating point can be the cooling fluid flow rate which is often considered as an input or an independent variable; for a car engine

model given by [1], the operating point can be the engine speed, throttle angle, engine temperature, and surrounding atmospheric conditions. The structure of LPV model can be described as a basis function, which is given as follows [35]:

$$y = \sum_{i=1}^{n} \alpha_i(p, \beta_i)\phi_i(p)u \tag{3.1}$$

where p is the operating point and α_i is a function of p with parameter vector β_i acting as the i^{th} weighting factor, $i = 1, \ldots, n$.

Depending on which operating period the data is acquired and used, the algorithms for identification of a LPV model can be categorized into two mainstream classes [35]:

- Local approach: In (3.1), $\phi_i(p)$ is identified using the data collected through experiments at these n operating points, i.e. from $p = \bar{p}_1$ to $p = \bar{p}_n$. Then the parameter set β_i is estimated by interpolating between the n operating points $\bar{p}_i$, therefore obtaining weighting factors α_i, $i = 1, \ldots, n$. In this case, an LPV model can be interpreted as

$$G(p, q) = \sum_{i=1}^{n} \alpha_i(p, \beta_i)G_i(p, q) \tag{3.2}$$

  where G is the model function, q is the shift operator, $G_i(p, q)$ is the ith local model G_i, and n is the number of local models.

- Global approach: Perform a single experiment along an operating trajectory which covers a large number of operating points. Use this collected input-output data set to identify α_i directly ($i = 1, \ldots, n$). In this approach, ϕ_i needs not to be the local model [35].

Both approaches have their own advantages and disadvantages. The local approach requires less testing but may not be sufficient to capture the global nonlinear behavior. In contrast, the global approach will not heavily rely on a few operating points and will represent the nonlinearity well; however, it requires extensive testing along varying operating points which can be hazardous when applied to industrial processes. One solution which combines advantages of these two methods is developed by Xu et al. (2009) [39]. In this combined method, local models are identified using data set at some selected operating points; and then the global LPV model is identified by interpolating local models G_i using total data. Although this method shows attractive features both in identification and control, it makes an assumption that those typical operating points are sufficiently informative and no discussion is made about how to select those operating points. It should be noted that how to specify the operating point can affect modeling accuracy. However, in most literature about LPV identification, operating points are considered fixed and known before identification is performed. Choosing operating points for a given physical

system to improve model accuracy is considered as a cardinal problem but has not been well investigated [34].

Recently, Khalate et al. (2009) [16] developed an algorithm to determine the optimal operating points based on a local approach. The system they try to identify is described as follows:

$$y(t) = \phi^T(t)\alpha_0(p) + v(t) \tag{3.3}$$

where $\phi(t) = [-y(t-1),\ -y(t-2), \ldots, u(t-1),\ u(t-2)]^T$ is a regression vector and y is the output data set, and α_0 is the parameter vector changing with respect to p which is parameterized as

$$\alpha_0(p) = \lambda_0 + \lambda_1 p + \ldots + \lambda_m p^m \tag{3.4}$$

and $v(t)$ is the noise with zero mean and bounded variance. Given an initial set of fixed operating points $\mathcal{P} = \{\bar{p}_1,\ \bar{p}_2,\ \ldots,\ \bar{p}_n\}$, they used local input and output data (ϕ and y) at each of the operating points to estimate the parameter vector (denoted as $\hat{\alpha}(\bar{p}_i)$); with these $\hat{\alpha}(\bar{p}_i)$ values and the corresponding operating points in $\mathcal{P}$, the parameters $\{\lambda_i\}$ in Equation (3.4) were determined by interpolation. For one initial set of fixed operating points $\mathcal{P} = \{\bar{p}_1,\ \bar{p}_2,\ \ldots,\ \bar{p}_n\}$, a set of parameters $\{\lambda_i\}$ can be obtained. Different selection of operating points set yield different parameters set $\{\lambda_i\}$ in the parameter vector α. By choosing operating points set $\mathcal{P}$, they tried to minimize the error between the interpolated parameter vector α and the true parameter vector α_0. Assume that after one selection of operating points set $\mathcal{P}$, the parameter α is described as:

$$\tilde{\alpha}_{\mathcal{P}}(p) = \tilde{\lambda}_0 + \tilde{\lambda}_1 p + \ldots + \tilde{\lambda}_{n-1} p^{n-1} \tag{3.5}$$

where the m value in (3.4) is chosen as $(n-1)$. The objective function they used to determine the optimal operating points set is

$$J_{\mathcal{P}} = \int_{\bar{p}_{min}}^{\bar{p}_{max}} \|\tilde{\alpha}_{\mathcal{P}}(p) - \alpha_0(p)\|^2 dp \tag{3.6}$$

where "$\|$" denotes the Euclidean norm of $\tilde{\alpha}_{\mathcal{P}}(p) - \alpha_0(p)$, and $\mathbb{P} = [\bar{p}_{min},\ \bar{p}_{max}]$ is the range of p.

As a first attempt toward optimal operating points design, this algorithm is built by making several assumptions to simplify the complex optimal LPV experiment design problem [16]. The first assumption is that the true nonlinear process is an explicit function of the varying operating points. Another assumption is the first principle model α_0 is known. Although these assumptions help derive a solution to the optimal operating point design problem, they are unrealistic or difficult to realize in practice.

In this work, we propose an optimal adaptive operating point design algorithm which can be applied to systems with nonlinear behavior that can be approximated by LPV models. No specific a-priori knowledge about the true

process or first principle model is required. This chapter is organized as follows: Section 3.2 introduces the hybrid method combining local approach and global approach for LPV identification. Section 3.3 describes the optimal adaptive operating point design algorithm which is composed of LPV identification and optimal experiment design followed by a simple example for illustration. In Section 3.4, the applicability of the proposed method is shown and discussed through two examples.

3.2 Hybrid Method for LPV Identification

The hybrid method combining the local and global approaches requires experimentation to be conducted both in local operating points and in the transition period [39]. Before the identification experiment is performed, the initial operating points as well as transition regions (or operating trajectory) should be specified. The LPV model can be formulated as follows:

$$y(t) = \sum_{i=1}^{n} \alpha_i(p, \beta_i) G_i(p, q) u(t) + v(t) \tag{3.7}$$

where $v(t)$ is the noise with zero mean and bounded variance. Once the input-output data is obtained, the local models G_i can be identified; this is considered to be the first step of hybrid identification for LPV models. The local model G_i in Equation (3.2) is usually described by an ARX model, which is valid given that input perturbation are small [19].

Once the local models G_i are determined based on the nominal operating points, the weighting function α_i can be estimated. There are a number of ways to model the weighting function. A simple model is a piece-wise linear function; however, it does not capture the transition nonlinearity. Other more frequently-used methods include polynomial functions and cubic splines. The cubic splines function can be represented in the form [39]:

$$\alpha_i(p) = \beta_{i,1} + \beta_{i,2} p + \sum_{j=2}^{s-1} \beta_{i,j+1} |p - k_j|^3 \tag{3.8}$$

where $k_1, k_2, ..., k_s$ are a set of knots which satisfy

$$p_{min} = k_1 < k_2 < ... < k_s = p_{max} \tag{3.9}$$

These knots can be randomly distributed throughout the range of operating point. Similar to polynomial functions, the cubic splines function is linear with respect to the parameter set $\beta_{i,j}$. When substituting (3.8) into (3.7), one can see that the output is also linear with respect to the parameter set $\beta_{i,j}$. This model structure enables linear least squares estimation, effectively reducing the computational cost. Once the experimental test along the operating

trajectory is done, off-line estimation can be performed using the entire data. The parameter set $\beta_{i,j}$ to be estimated can be denoted as

$$B = [\beta_1^T, \beta_2^T, \ldots, \beta_n^T]^T \tag{3.10}$$

where β_i corresponds to the i^{th} local model. The objective function for estimation can then be formulated as

$$\hat{B} = arg\min_B \frac{1}{N}\sum_{t=1}^{N}[e(t)]^2 \tag{3.11}$$

where N is the total number of data points including local regimes and transitions, and $e(t)$ is the output error between measurement and prediction which is described as

$$e(t) = y(t) - \sum_{i=1}^{n}\hat{\alpha}_i(p, \hat{\beta}_i)\hat{G}_i(p, q)u(t) \tag{3.12}$$

3.3 Optimal adaptive operating point design

The hybrid identification method requires local models to be identified before a global model is interpolated. As discussed before, it offers advantage in the computation cost; however, it can also cause problem. Since there is no a-priori knowledge available about the nonlinear model structure, operating point design relies solely on the estimated LPV model. On the other hand, LPV model identification also depends on the operating trajectory where the experiment is carried out. The LPV model will only be correctly identified if experiment is done along an appropriate operating trajectory. To solve this problem, an Adaptive Operating Point Design (AOPD) algorithm is developed which allows the determination of a single operating point for each new experimental test, and requires no knowledge about the true process. The framework for the proposed AOPD procedure is shown in Figure 3.1 with the details being elaborated afterward.

According to Figure 3.1, the procedure of this operating point design problem consists of the following steps:

Step 1: Start from two nominal operating points which are typically the minimum and the maximum value within the operating range.

Step 2: While traveling through one operating point to the other, perform experimental along the operating trajectory thus collecting local data $\mathbb{D}_i$ and transition data $\mathbb{D}_{i,i+1}$.

Step 3: Identify local models $\hat{G}_i$ using local data set $\mathbb{D}_i$.

Step 4: Estimate parameters β_i involved in the weighting factor α_i using the entire data set to form a global model.

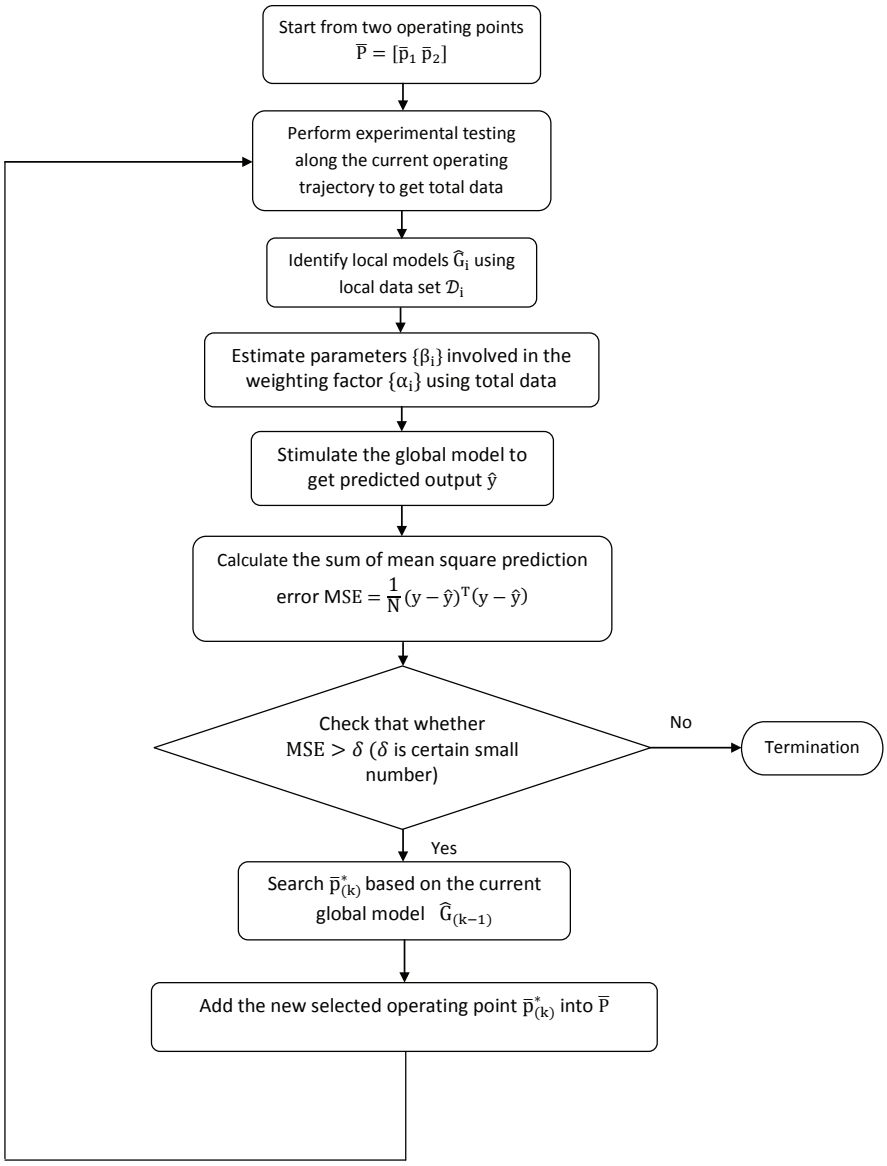

Figure 3.1: The framework for adaptive operating point design procedure

Step 5: Simulate the global model to predict output $\hat{y}$.

Step 6: Calculate the sum of mean square prediction error $MSE = \frac{1}{N}(y - \hat{y})^T(y - \hat{y})$.

Step 7: Check that whether the mean squares error is smaller than a certain

tolerance δ, i.e. $MSE < \delta$.

Step 8: If $MSE < \delta$ terminate the design procedure with the current optimal operating point vector $\bar{P}_{(k-1)}$; otherwise, search the optimal operating point $\bar{p}^*_{(k)}$ is based on the current global model $\hat{G}_{(k-1)}$, where k represents the k^{th} experiment .

Step 9: Append the new $\bar{p}^*_{(k)}$ into the operating point vector $\bar{P}_{(k)}$. Go to step 2.

3.3.1 The process to determine the optimal operating point $\bar{p}^*$

The optimal operating point $\bar{p}^*$ is determined as follows:

$$\bar{p}^* = arg \min_{\bar{p} \in \mathbb{P}} J(\bar{p}, B) \tag{3.13}$$

where $\mathbb{P}$ is the operating point space, B is the parameter set in the weighting function defined in (3.10), and J is the objective function. The widely-used objective function for LPV identification problem is MSE.

$$J = \frac{1}{N}(y - \hat{y})^T (y - \hat{y}) \tag{3.14}$$

However, this common objective function cannot be applied since it requires actual experiment data after trying a new operation point. This forms another dilemma. To circumvent this problem, we solve the following optimization problem according to the global model estimated:

$$\bar{p}^*_{(k)} = arg \min_{\bar{p}_{(k)} \in \mathbb{P}_{(k-1)}} J_{(k)}(\bar{p}_{(k)}, \bar{P}_{(k-1)}, B(k)) \tag{3.15}$$

where $J_{(k)}$ is the objective function in the k^{th} optimization step, $\bar{p}_{(k)} \in \mathbb{P}_{(k)}$ is the operating point to be searched, $\bar{P}_{(k-1)}$ is the $(k-1)^{th}$ operating points vector based on which $\bar{p}^*_{(k)}$ will be added, and $B_{(k)}$ is the parameter set in the weighting function defined in Equation (3.10) at the kth iteration. The objective function can be expressed as

$$J_{(k)} = \max\{J_{k,j} | j = 1, \ldots, n_{k-1} - 1\} \tag{3.16}$$

with

$$J_{k,j} = \int_{\bar{p}_{k-1,j}}^{\bar{p}_{k-1,j+1}} \|G(\bar{p}_{(k)}, B_{(k)}, q) - G(p, B_{(k)}, q)\|^2 dp \tag{3.17}$$

where $j = 1, \ldots, n_{k-1} - 1$ is the index of transition sections after the latest operating point is added, n_{k-1} is the number of operating points in the $(k-1)^{th}$ run of the experiment. $\bar{P}_{k-1} = [\bar{p}_{k-1,1}, \ldots, \bar{p}_{k-1,j}, \ldots, \bar{p}_{k-1,n_{k-1}}]$ denotes as the

$(k-1)^{th}$ operating point vector. The optimal operating point $\bar{p}^*_{(k)}$ is determined by the following procedure: calculate $\|G(\bar{p}_{(k)}, B_{(k)}, q) - G(p, B_{(k)}, q)\|^2$ at certain $\bar{p}_{(k)}$ and p, where p is a varying operating point; integrate this square of 2-norm individually over p for each transition section from $\bar{p}_{k-1,j}$ to $\bar{p}_{k-1,j+1}$, $j = 1, \ldots, n_{k-1} - 1$; next, after comparing the $n_{k-1} - 1$ values of integration, choose the maximum $J_{k,j}$ as $J_{(k)}$ (if $k = 1$, $J_{(k)} = J_{k,j}$); then, the optimal $\bar{p}$ which minimizes this $J_{k,j}$ is defined as the optimal operating point $\bar{p}^*_{(k)}$ in the k^{th} run of the design. Repeat this procedure until the mean square error between the measurement and prediction is reduced within a certain small tolerance.

3.3.2 An illustrational example

For illustration, a pure gain system is taken as an example before proceeding to the two dynamic systems in the next section. Suppose this static gain has the following form which is an explicit function of operating point p,

$$K(p) = -1 + 0.6e^{-sin(0.06p)} \tag{3.18}$$

where $p \in [60\ 150]$. Following the description of the optimal adaptive operating point design procedure discussed above, four new optimal operating points are found. First, based on the initial set of operating points $\bar{P}_0 = [60.00\ 150.00]$, the first new optimal operating point $\bar{p}^*_{(1)}$ is determined as 100.27, with the objective function $J_{(1)} = 25.02$. Once the first new optimal operating point $\bar{p}^*_{(1)}$ is obtained, the current operating trajectory has three fixed local operating points [60.00 100.27 150.00] and two sections of transitions between these operating points. For each of these two sections of transitions, calculate the objective function $J_{1,1} = 2.55$ and $J_{1,2} = 2.53$ as shown in (3.17). The larger one of these two objective function values ($J_{1,1}$) is defined as the objective function value for $J_{(2)}$, which is achieved at $\bar{p}^*_{(2)} = 67.54$. So the second new operating point is found at 67.54. This design procedure is carried on until four new optimal operating points are determined and the last objective function value is less than a pre-selected threshold of 1.

The vector of optimal operating points is

$$\bar{P}^*_{(4)} = [60.00\ 67.54\ 88.61\ 100.27\ 147.18\ 150.00] \tag{3.19}$$

Figure 3.2 shows objective functions $J_{(k)}$ when $k = 1$, $k = 2$, $k = 3$ and $k = 4$. The $\bar{p}^*_{(k)}$ in each of these runs of experiments are marked with stems and circles in the four subplots.

Since the static gain K is an explicit function of the operating point p only, the changing of k with p can be represented in a 2-dimensional figure as shown in Figure 3.3 where the four new optimal operating points can be visualized.

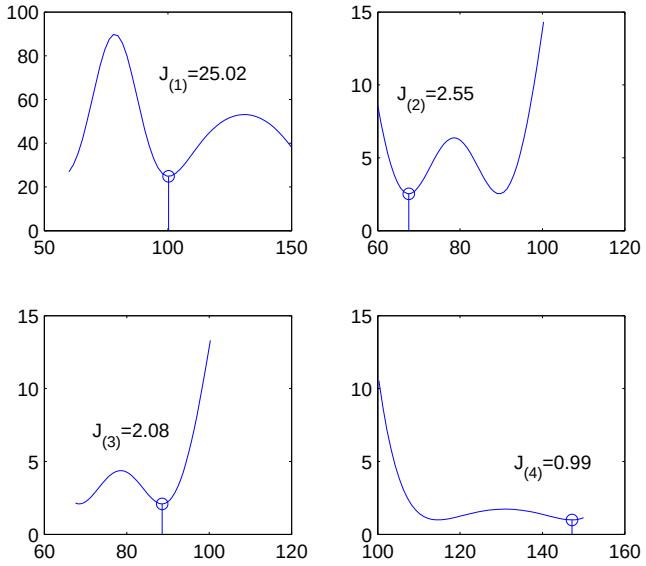

Figure 3.2: The operating point searching process (objective function vs. operating point interval)

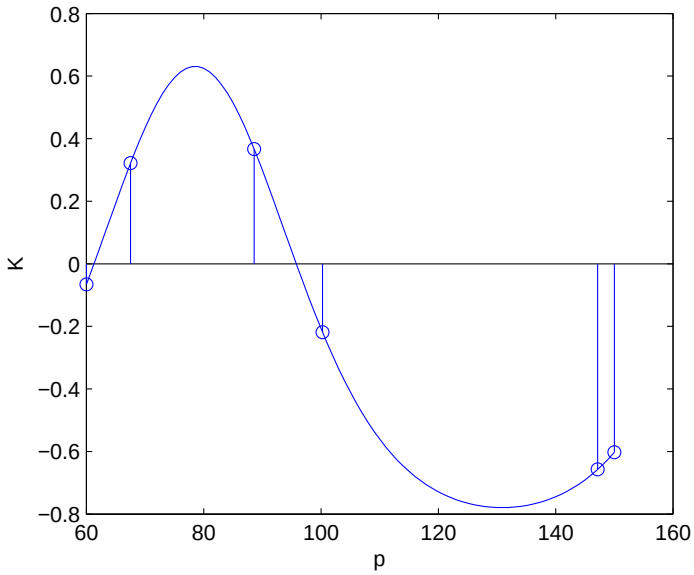

Figure 3.3: The gain K vs operating point

3.4 Simulation

3.4.1 Continuous stirred tank reactor (CSTR) model

The continuous stirred tank reactor (CSTR) has been considered as a benchmark process for nonlinear process modeling. The dynamics of an irreversible,

exothermic reaction A→B taking place in a constant-volume reactor, which is cooled by a single coolant stream, is shown as follows [39, 28],

$$\dot{C}_A(t) = \frac{q(t)}{V}(C_{A0}(t) - C_A(t)) - k_0 C_A(t)\exp(-(\frac{E}{RT(t)})) \quad (3.20)$$

$$\dot{T}(t) = \frac{q(t)}{V}(T_0(t) - T(t)) + \frac{\triangle H k_0 C_A(t)}{\rho C_p}\exp(-(\frac{E}{RT(t)})) + \frac{\rho_c C_{pc}}{\rho C_p V} q_c(t)\{1 - \exp(\frac{-hA}{q_c(t)\rho C_p})\}(T_{c0}(t) - T(t)) \quad (3.21)$$

The description and nominal value for each parameter in Equation (3.20) and Equation (3.21) are shown in Table 3.1 [15].

Table 3.1: Parameters and their nominal values in CSTR model

parameters	nominal values
production concentration of component A, C_A	1st state
temperature of the reactor, T	2nd state
feed concentration of component A, C_{A0}	1 mol/L
feed temperature, T_0	350.0 K
specific heats, C_p, C_{pc}	1 $cal/(gk)$
liquid density, ρ, ρ_c	1×10^3 g/L
heat of reaction, $-\triangle H$	-2×10^5 cal/mol
activation energy term, E/R	1×10^4 K
reaction rate constant, k_0	7.2×10^{10} min^{-1}
heat transfer term, hA	7×10^5 $cal/(min\ K)$
reactor volume, V	100 L
inlet coolant temperature, T_{c0}	350.0 K
process flow rate, q	100 L/min
coolant flow rate, q_c	input

As shown in Table 3.1, the two states are the concentration of component A, C_A and the temperature of the reactor, T, while C_A is selected as output. The coolant flow rate q_c is selected as a manipulated variable as well as an operating point which varies in the range [97 109]. Note that for a given operating point, steady states are unknown until the local dynamics have been tested.

Following the design framework in Figure 3.1, the optimal operating point design starts from testing along the operating point trajectory which consists of the minimum operating point 97 L/min, the maximum value 109 L/min and the transition between these two values. For all experiments along the local operating points as well as the transition from one local point to another, the measurements are corrupted by noise having a standard deviation of 10% of the measurement. We use generalized binary noise (GBN) [42] for the simulated input perturbation. For each of the local and transition experiments, 500 sample points were taken. Figure 3.4 shows the GBN input signal q_c as a function of time. Fixing the mean square error tolerance δ to be 0.005,

the optimal design ends with three newly-added operating points; the set of operating points is

$$\bar{P}^*_{(4)} = [97\ 100.1141\ 103.0733\ 105.9893\ 109] \tag{3.22}$$

where the middle three are the new selected optimal operating points.

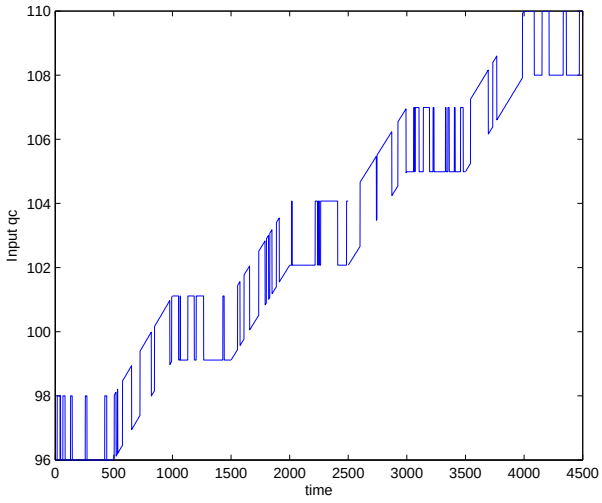

Figure 3.4: The input q_c as a function of time

Figure 3.5 shows that the objective functions changes with varying p when the number of elements in the current $\bar{P}^*_{(k)}$ increases to 3, 4, 5 respectively.

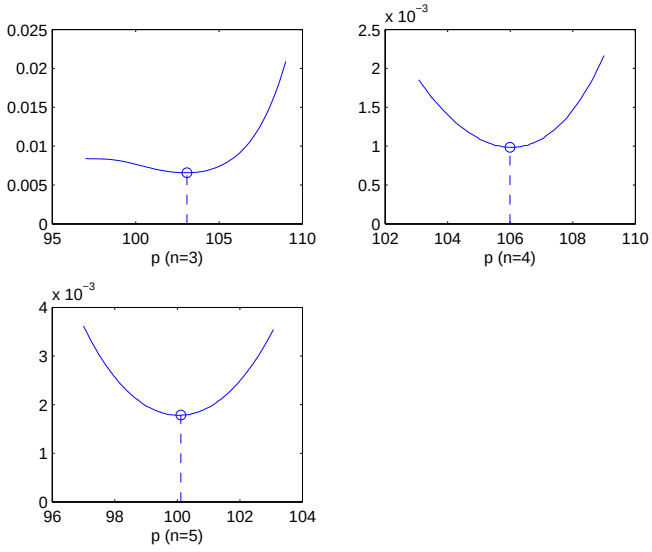

Figure 3.5: Objective function value vs. operating point p

Notice that the objective function we used for determining the new optimal operating point is not MSE. Instead, we use Equation (3.17). The reason to do so has been explained in the previous section. It is obvious that adding more operating point can yield a smaller value of MSE. However, it does not guarantee a smaller value of the objective function after adding new operating point. This is simply because after adding the new optimal operating point, the global model G in the objective function has been changed. Moreover, this global model is an approximation of the true model, therefore containing uncertainty. Thus, the objective function value after adding new operating point is not necessarily smaller than the one with less operating points.

Figure 3.6 shows the comparison between the actual process output and the identified global model output. The upper two subplots and the left bottom one show the performance of the proposed adaptive optimal design method when the number of elements in the current $\bar{P}^*_{(k)}$ equals to 3, 4, 5 respectively. The right bottom figure shows the mean value of prediction results by repeating experiments for 20 times where the 5 operating points are randomly selected.

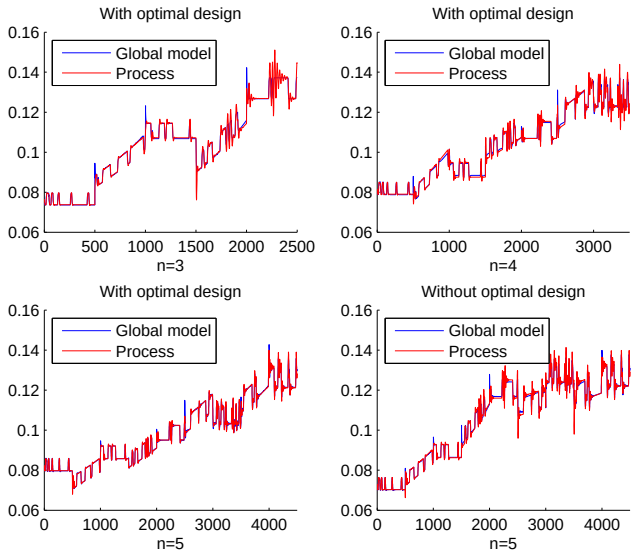

Figure 3.6: Comparison of outputs

The mean square errors for optimal operating point design are listed in Table 3.2 when the number of elements in the current operating set n is 3, 4 and 5 respectively. From Table 3.2, one can see that adding more operating points reduces the MSE, which is intuitive. The average MSE obtained from 20 experiments with randomly assigned operating points is 0.0111. Comparing the MSE between the two simulations when $n = 5$ for optimal operating point design and the one without optimal design, one can see that the MSE is reduced by 63.96%. Notice that even for $n = 3$, the MSE of the proposed adaptive optimal design method is smaller than the one without optimal design, despite the latter has five operating points.

Table 3.2: Mean square error for optimal operating point design

	n=3	n=4	n=5
MSE	0.0106	0.0085	0.0040

To get a full perspective, we plot the 3-D figure of outputs as a function of time and operating point in Figure 3.7. The error between the process output and model output is also shown as a function of time and operating point in Figure 3.8. One can see that the global model matches the process output well.

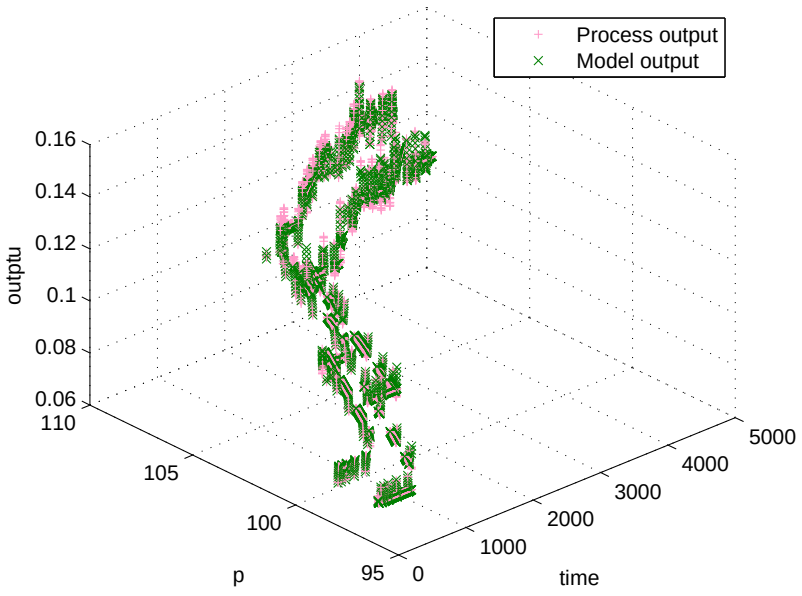

Figure 3.7: Measurement and predicted output vs. time and operating point

3.4.2 Solid oxide fuel cell (SOFC) model

A solid oxide fuel cell (SOFC) is considered in this example. For the SOFC modeling, a series of developments have been achieved considering the first principle model [8, 12, 24, 11]. The structure of SOFC is shown in Figure 3.9.

As shown in Figure 3.9, the fuel cell consists of the anode and the cathode on either side and an electrolyte in between. The electricity is generated by feeding hydrogen rich fuel and air into the fuel cell which results in a series electrochemical reactions. The fuel cell can be divided into four components: flow channels (including fuel flow channel and air flow channel), electrodes (including anode and cathode), electrolyte and interconnector. Among the transport dynamics of these components, the flow channel dynamics and the electrode dynamics have been investigated in details.

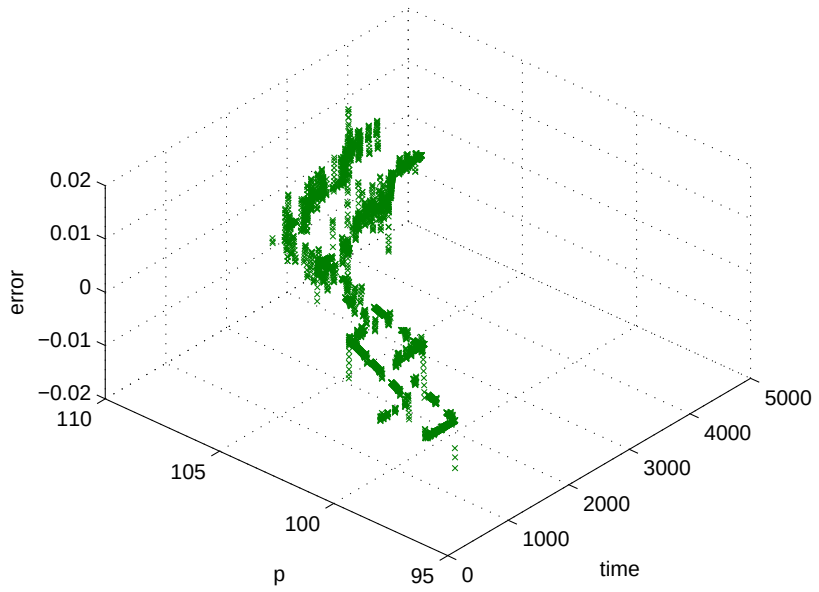

Figure 3.8: Error between measurement and predicted output vs. time and operating point

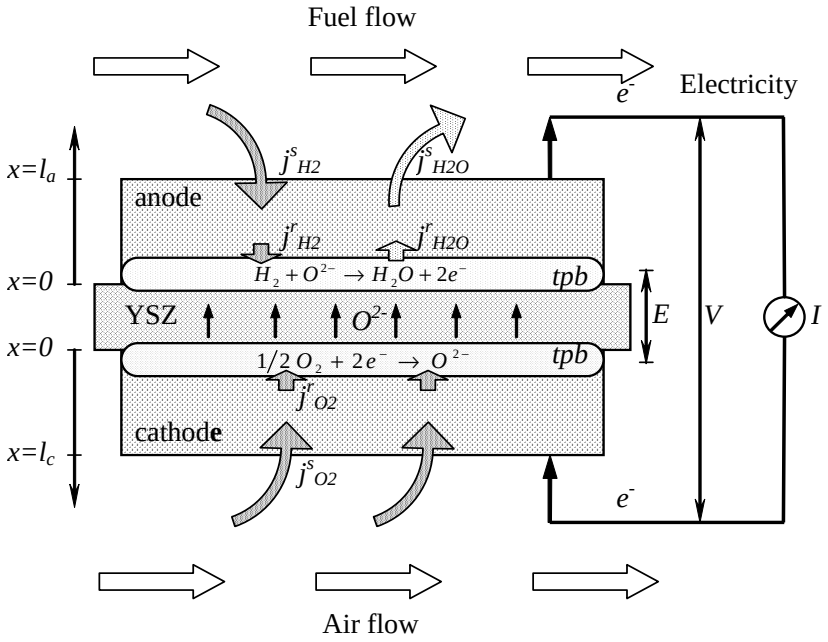

Figure 3.9: Structure of SOFC [24]

The key reaction occurs in the fuel cell is the reaction which converts the chemical energy contained in the fuel and oxidant to electrical energy as shown

below:

$$anode: \ H_2 + O^{2-} \rightarrow H_2O + 2e^- \tag{3.23}$$
$$cathode: \ \frac{1}{2}O_2 + 2e^- \rightarrow O^{2-}$$

Dynamic modeling of SOFC

Qi et al. (2005) [23] developed a cell-based dynamic model to investigate the nonlinear dynamic characteristics of SOFC. This nonlinear state space model is given by Table 3.3. The inputs, outputs and state variables are defined as shown in Table 3.4, Table 3.5 and Table 3.6 respectively [13]. The parameters in the voltage dynamics subsystem are given in Table 3.7.

Table 3.3: State space model for SOFC

State equations:
$\dot{x}_1 = \frac{1}{R_{ct}C_{ct}}E - \frac{1}{R_{ct}C_{ct}}x_1 - \frac{1}{C_{ct}}\frac{x_1}{u_1+R_o}$
$\dot{x}_2 = x_3$
$\dot{x}_3 = -h_1x_2 - h_2x_3 + h_1\frac{1}{2F}\frac{x_1}{u_1+R_o} + h_3\frac{A}{RT}(Ku_2 - x_4)$
$\dot{x}_4 = K^2u_2 - Kx_4$
$\dot{x}_5 = x_6$
$\dot{x}_6 = -o_1x_5 - o_2x_6 + o_1\frac{1}{4F}\frac{x_1}{u_1+R_o} + o_3\frac{A}{RT}(Ku_3 - x_7)$
$\dot{x}_7 = K^2u_3 - Kx_7$
$\dot{x}_8 = x_9$
$\dot{x}_9 = -w_1x_8 - w_2x_9 + w_1\frac{1}{2F}\frac{-x_1}{u_1+R_o} + w_3\frac{A}{RT}(Ku_4 - x_{10})$
$\dot{x}_{10} = K^2u_4 - Kx_{10}$
$\dot{x}_{11} = x_{12}$
$\dot{x}_{12} = -h_1x_{11} - h_2x_{12} - h_4\frac{RT}{A}\frac{1}{2F}\frac{x_1}{u_1+R_o}$ $-\frac{RT}{A}\frac{4}{L_a}\frac{1}{2F}[\frac{x_1}{u_1+R_o} - \frac{x_1}{(u_1+R_o)^2}(Ku_1 - x_{17})] + h_1u_2$
$\dot{x}_{13} = x_{14}$
$\dot{x}_{14} = -o_1x_{13} - o_2x_{14} - o_4\frac{RT}{A}\frac{1}{2F}\frac{x_1}{u_1+R_o}$ $-\frac{RT}{A}\frac{4}{L_c}\frac{1}{4F}[\frac{x_1}{u_1+R_o} - \frac{x_1}{(u_1+R_o)^2}(Ku_1 - x_{17})] + o_1u_3$
$\dot{x}_{15} = x_{16}$
$\dot{x}_{16} = -w_1x_{15} - w_2x_{16} - w_4\frac{RT}{A}\frac{1}{2F}\frac{-x_1}{u_1+R_o}$ $-\frac{RT}{A}\frac{4}{L_a}\frac{1}{2F}[-\frac{x_1}{u_1} + \frac{x_1}{(u_1+R_o)^2}(Ku_1 - x_{17})] + w_1u_4$
$\dot{x}_{17} = K^2u_1 - Kx_{17}$
Output equations:
$y_1 = x_1 - \frac{R_o}{u_1+R_o}x_1$
$y_2 = \frac{x_1}{u_1+R_o}$
$y_3 = x_2$
$y_4 = x_5$
$y_5 = x_8$

Table 3.4: Input variables for SOFC

Inputs	Description
u_1	External load
u_2	Bulk pressure of hydrogen
u_3	Bulk pressure of oxygen
u_4	Bulk pressure of water

Table 3.5: Output variables for SOFC

Inputs	Description
y_1	External voltage V_{out}
y_2	Current
y_3	Consumption rate of hydrogen
y_4	Consumption rate of oxygen
y_5	Production rate of water

Table 3.6: State variables for SOFC

State	Description
x_1	Voltage V_{ct}
x_2	Consumption rate of hydrogen
x_3	Derivative of consumption rate of hydrogen
x_4	Intermediate variable
x_5	Consumption rate of oxygen
x_6	Derivative of consumption rate of oxygen
x_7	Intermediate variable
x_8	Production rate of water
x_9	Derivative of production rate of water
x_{10}	Intermediate variable
x_{11}	Concentration of hydrogen at tpb
x_{12}	Derivative of concentration of hydrogen at tpb
x_{13}	Concentration of oxygen at tpb
x_{14}	Derivative of concentration of oxygen at tpb
x_{15}	Concentration of water at tpb
x_{16}	Derivative of concentration of water at tpb
x_{17}	Intermediate variable
Note that "tpb" stands for triple phase boundary	

In Table 3.4, the input external load u_1 is chosen as the operating point, which varies from 2 Ω to 6 Ω. The small perturbation Δu_1 along this operating trajectory is selected as input perturbation using generalized binary noise (GBN) [42]. Since SOFC behaves strong nonlinearity which is challenging by using LPV system, experiment design should be carefully investigated to prevent the output to "overreact". Following the process of adaptive operating

Table 3.7: Parameters for SOFC

Parameters	Descriptions	Nominal values used in simulation
R_{ct}	Charge transfer resistance	0.9 Ω
C_{ct}	Charge transfer capacitance	300×10^{-6} F
R_o	Ohmic resistance	0.1 Ω
h_1, h_2, h_3, h_4	Functions of diffusion coefficient of hydrogen D_{h_2}	1.041×10^{-4}
o_1, o_2, o_3, o_4	Functions of diffusion coefficient of oxygen D_{o_2}	2.451×10^{-5}
w_1, w_2, w_3, w_4	Functions of diffusion coefficient of water D_{H_2O}	1.041×10^{-4}
R	Gas constant	82.05×10^{-5} $J\ mol^{-1}\ K^{-1}$
T	Work temperature	1223 K
A	Fuel cell effective area	1 cm^2
F	Faradays constant	96487 $C\ mol^{-1}$
L_a	Thickness of anode diffusion layer	1 mm
L_c	Thickness of cathode diffusion layer	1 mm
K	Approximation factor	15

point design, four optimal operating points are determined:

$$\bar{P}^*_{(3)} = [2.00\ 3.00\ 4.00\ 6.00] \tag{3.24}$$

Figure 3.10 shows the objective functions when choosing the 1st and 2nd operating points. Figure 3.11, 3.12 and 3.13 show the process output, the outputs of local models and the global model identified through the adaptive optimal design procedure when the number of operating points n is 2, 3, 4 respectively. One can see that local linear models alone cannot capture the process output well. On the other hand, from the error between the process output and the global model, output is reduced when n increases.

The mean square error corresponding to the four optimal operating points as shown in Equation 3.24 is 1.70×10^{-4}. Comparing with the average MSE of 8.46×10^{-4} obtained from 20 experiments without optimal operating point design, the proposed design shows superiority in improving the modeling accuracy. Indeed, the MSE between the model output and the process output based on three operating points designed by the proposed method is 2.28×10^{-4}, which is smaller than the MSE based on four operating points without optimal design.

3.5 Conclusions

An adaptive optimal operating point design algorithm has been proposed for LPV identification in this chapter. The formulation of an online optimal op-

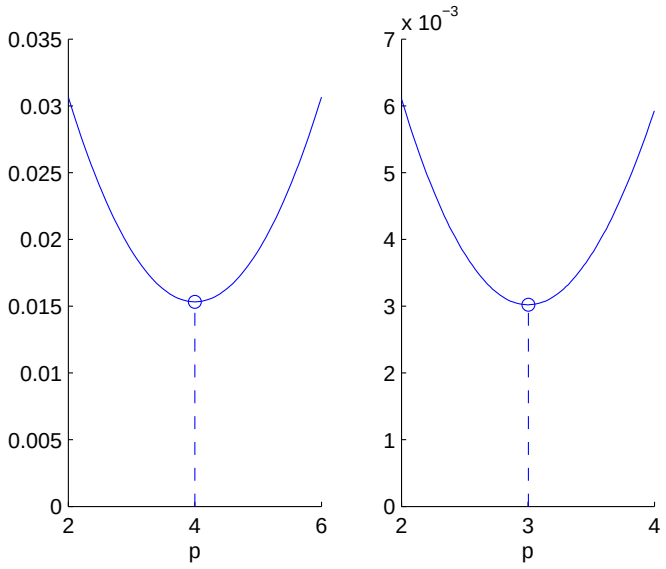

Figure 3.10: Objective function value vs. operating point p

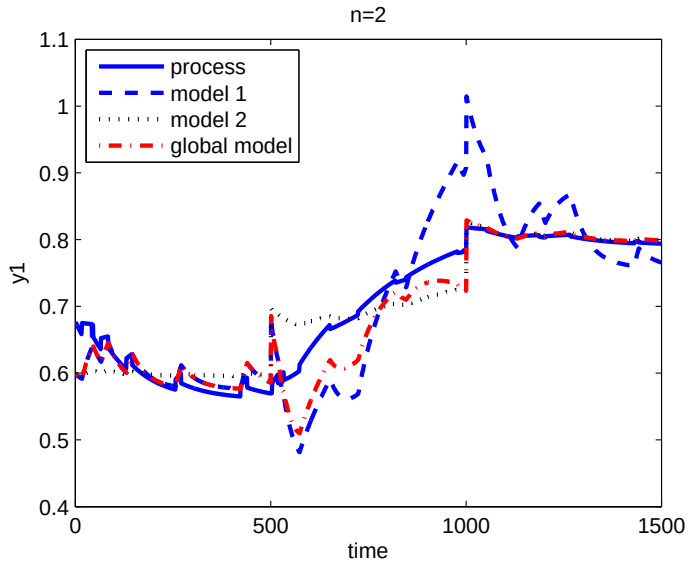

Figure 3.11: Process output and model outputs

erating point selection scheme is motivated by the fact that selecting different nominal operating points can yield significant different error between the model prediction and system output. Based on a hybrid identification method combining both local and global approaches, the optimal operating point design algorithm starts from the initial set of operating points. With this set of initial operating points, the local models are interpolated using the entire data set, obtained through experimentation along the operating trajectory, to get a global model. A candidate operating point within each transition period is obtained by minimizing an objective function. Within the transition region, the

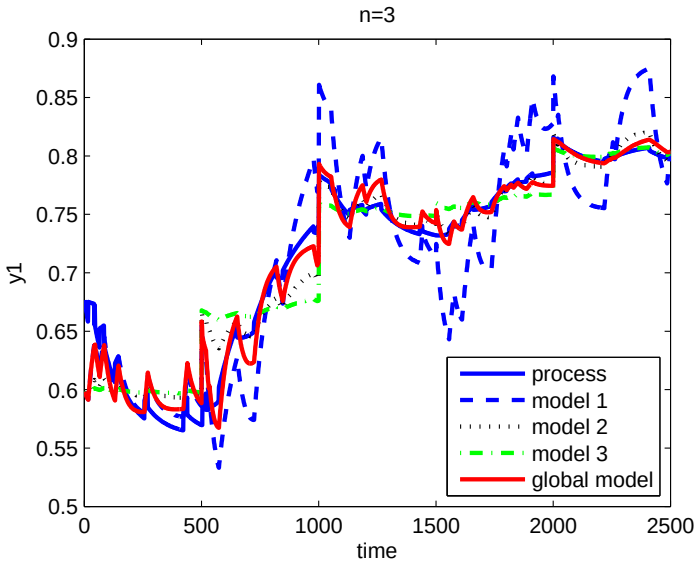

Figure 3.12: Process output and model outputs

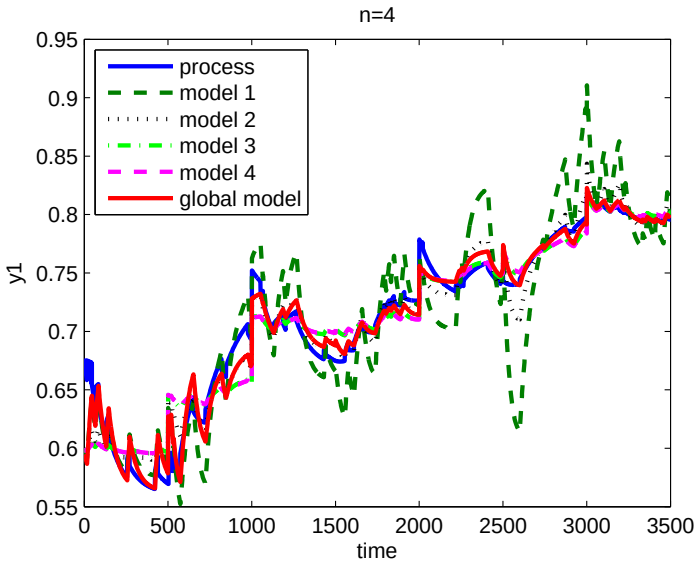

Figure 3.13: Process output and model outputs

candidate operating point with the largest objective function value is selected as the new operating point. The optimal operating point selection procedure is conducted iteratively until a satisfactory MSE is achieved. The contribution of this proposed algorithm is the enabling of optimal operation point design without a-priori knowledge about the true nonlinear system; hence it provides a practical and usable application of LPV model identification.

Chapter 4

Simultaneously Design of Operating Points and Input Perturbations for LPV Identification

A joint Linear Parameter Varying (LPV) model experiment design problem is solved by determining the operating points and input perturbation simultaneously. Comparing with operating points-only design, the simultaneous operating point and input design can further improve identification performance. The result is illustrated by the CSTR as well as a fuel cell example.

4.1 Introduction

Experiment design is a broad subject that tries to maximize the information contained in the experiment [9]. In dynamic systems, the experiment design can be optimized by determining the input, sampling rate, and types of sensors used. The optimal experiment design has also been applied to Linear Parameter Varying (LPV) systems as discussed in the last chapter; such techniques have recently received ample attention as an effective tool for nonlinear system identification.

A number of methods for LPV model identification have been developed. Most of these methods can be classified into two categories: local approaches and global approaches [35, 2], both of which have their own advantages and drawbacks. On top of these two categories, the hybrid approach developed by [39] and [42] combines the merits of both approaches; it is considered as a promising tool for modeling nonlinear process. In this method, linear models are obtained by linear identification at prechosen operating points of the nonlinear system. Afterward, the global model is obtained though interpolation by using the entire data set along the experiment trajectory. Following their

approach, the LPV model can be formulated as follows:

$$y(t) = \sum_{i=1}^{n} \alpha_i(p, \theta_i^{(2)}) G_i(\theta_i^{(1)}, p, q) u(t) + v(t) \tag{4.1}$$

where $u(t)$ and $y(t)$ are the input and output at time instant t respectively; α_i is the weighting function corresponding to the i^{th} local model G_i, which is the function of varying operating point p; $\theta_i^{(1)}$ is the parameter set contained in the i^{th} local model while $\theta_i^{(2)}$ is the parameter set contained in the i^{th} weighting function α_i; $v(t)$ is Gaussian noise with zero mean and bounded variance; q is a time shifted operator.

The hybrid LPV identification method provides a good alternative for identifying LPV models. It is assumed that the operating points are known before the identification is performed. Different operating points can yield different performances in identification. To determine the optimal operating points and maximize the accuracy of the identified LPV model, Khalate et al. (2010) [16] developed a procedure for experiment design. This approach determines the optimal operating points and minimizes the error between the *interpolated* weighting function and the *true* weighting function assuming the latter is known. However, some of these assumptions are difficult to realize in practice. One of the most important assumptions is that the first principle model is assumed to be available for the true process. This is typically an unrealistic assumption. A first principle model is difficult to obtain and is precisely the reason to have the data-based system identification.

In view of this problem, an adaptive operating point design (AOPD) algorithm is developed in this chapter to allow the determination of optimal operating point based on the identified LPV model. This design requires no prior knowledge about the nonlinear process model, which renders it more practical. To implement this design algorithm, we start from two nominal operating points along with the transition from one operating point to the other. The data set obtained at the local operating points is then used to identify the local models; afterward, the entire data set including the transition data is used to interpolate the local models therefore acquiring the global model. Operating points are selected such that the objective function is optimized. Here, the objective function is obtained as follows:

- Calculate the error between the interpolated global model as a function of operating point p and the model at a selected operating point between existing operating points;
- Varying the selected operating point along the transition region and integrate the 2-norm of the error obtained above;
- Select the operating point which has the largest integrated error to be the new optimal operating point.

The new operating point is added into the previous operating point set to form a new nominal operating point vector. This design procedure is repeated until the error between the process measurement and the model output is reduced to a certain tolerance.

As mentioned above, performance of the LPV model can be enhanced by optimally designing the operating points. However, for most nonlinear systems, more than one design factors should be considered and selected simultaneously to yield higher experimental design efficiency. In other words, a joint experiment design problem should be considered. For example, both operating points and input perturbations along the operating trajectory in the LPV models can be optimally determined. Targeting at solving this joint experiment design problem for LPV model identification, a simultaneous design for operating point and input perturbations is developed in this chapter.

The remainder of this chapter is organized as follows: Section 2 introduces the LPV adaptive input design; Section 3 illustrates the recursive method to estimate parameters both in local models and global model; Section 4 develops the simultaneous adaptive design procedure for operating points and input perturbations ; Section 5 gives the simulation results of the CSTR as well the solid oxide fuel cell (SOFC) example to demonstrate the efficiency of the proposed method. Sections 6 concludes the chapter.

4.2 Adaptive Input Design for LPV Model Identification

The optimal experiment design problem is defined as follows:

$$\varphi^* = arg \min_{\varphi \in \Phi} f(M(\hat{\theta}, \varphi)) \tag{4.2}$$

where φ is the experiment design, Φ is the space of the feasible experiment, M is the Fisher information matrix and $f = det(\cdot)^{-1}$, and $\hat{\theta}$ is the current parameter estimate. This φ can refer to any design variable such as sampling rate, input or operating point. In this section we mainly focus on input design. There are a number of ways to implement input design. An adaptive algorithm called receding horizon design [33, 14] is formulated as

$$U_k^* = [u_{k|k}^* \; u_{k+1|k}^* \; \cdots \; u_{k+h-1|k}^* \,] = \arg \min_{U_k \in \mathbb{U}} f(M(\hat{\theta}_k, U_k)) \tag{4.3}$$

where U_k^* is the optimal input vector containing $u_{k|k}^*,\ u_{k+1|k}^*,\ \cdots,\ u_{k+h-1|k}^*$ calculated at the k^{th} sampling instant, h is the optimization horizon, $\mathbb{U}$ is the feasible set which U_k^* can be chosen from, and $\hat{\theta}_k$ is the parameter estimate at sampling instant k. The Fisher information matrix M is defined as [40]

$$M = Z^T \Sigma^{-1} Z \tag{4.4}$$

where Z is sensitivity matrix given below,

$$Z = \begin{bmatrix} \frac{\partial y}{\partial \theta_1}|_{t_1} & \frac{\partial y}{\partial \theta_2}|_{t_1} & \cdots & \frac{\partial y}{\partial \theta_p}|_{t_1} \\ \frac{\partial y}{\partial \theta_1}|_{t_2} & \ddots & & \vdots \\ \vdots & & \ddots & \vdots \\ \frac{\partial y}{\partial \theta_1}|_{t_h} & \cdots & \cdots & \frac{\partial y}{\partial \theta_p}|_{t_h} \end{bmatrix} \tag{4.5}$$

where t_1 and t_h denote the starting and ending time of the experiment respectively, and Σ is the covariance matrix of output y. Each entry in the j^{th} row and i^{th} column denotes the sensitivity with respect to the i^{th} parameter θ_i at time instant t_j ($j = 1, \ldots, h$). This receding horizon design scheme allows the online design of the input and the updating of the parameters occur at the same time.

In the hybrid identification approach as shown in Equation (4.1), the ability of the LPV model to capture the nonlinearity of the process is highly related to the weighting function. Therefore, choosing a proper weighting function can be crucial in achieving high model accuracy. The weighting function should also follow parsimony principle; otherwise the identification can have overparameterization problem. Jin (2010) [15] developed a structure to describe the weight w_i of each local model G_i as shown below,

$$w_i(p) = \exp(\frac{-(p-\bar{p}_i)^2}{2\sigma_i^2}) \tag{4.6}$$

where p is the varying operating point, $\bar{p}_i$ is the i^{th} nominal operating point corresponding to the i^{th} local model, and σ_i is the validity width of the i^{th} local model. The normalized weighting function α_i in Equation (4.1) can be expressed as

$$\alpha_i = \frac{w_i}{\sum_{k=1}^{n} w_k} \tag{4.7}$$

This model of α_i, with an exponential structure, can smooth combinations of predictions from local models and capture the transition nonlinearity. Moreover, it only contains one parameter σ_i for each local model, which will reduce the number of parameters to be estimated. With the model of α_i as shown in Equation (4.6) and (4.7), we are able to calculate each entry $\frac{\partial \hat{y}_j}{\partial \sigma_i}|_{t_j}$ of the sensitivity matrix Z in Equation (4.5).

$$\begin{aligned} \frac{\partial \hat{y}_j}{\partial \sigma_i}|_{t_j} &= \frac{\exp(-\frac{(p-\bar{p}_i)^2}{2\sigma_i^2})}{\sum_{k=1}^{n} \exp(-\frac{(p-\bar{p}_k)^2}{2\sigma_k^2})} \frac{(p-\bar{p}_i)^2}{\sigma_i^3} \hat{y}_j^{(i)} \\ &= -\frac{\exp(-\frac{(p-\bar{p}_i)^2}{2\sigma_i^2})}{(\sum_{k=1}^{n} \exp(-\frac{(p-\bar{p}_k)^2}{2\sigma_k^2}))^2} \frac{(p-\bar{p}_i)^2}{\sigma_i^3} \\ &\quad \sum_{k=1}^{n} \exp(-\frac{(p-\bar{p}_k)^2}{2\sigma_k^2}) \hat{y}_j^{(k)} \end{aligned} \tag{4.8}$$

where σ_i is the validity width of the i^{th} local model, $\hat{y}_j^{(i)}$ denotes the predicted output of the i^{th} local model at time instant t_j ($j = 1, \ldots, h$), $\frac{\partial \hat{y}_j}{\partial \sigma_i}|_{t_j}$ is the sensitivity of the global predicted output with respect to the i^{th} parameter θ_i at time instant t_j ($j = 1, \ldots, h$), p is the varying operating point, and $\bar{p}_i$ denotes the i^{th} nominal operating point.

4.3 Estimation of Parameters in the Global LPV Model

As shown in Equation (4.1), the parameters contained in the LPV model composes of two parts, $\theta^{(1)}$ and $\theta^{(2)}$. To estimate the parameter $\theta^{(1)}$ in the local models, several algorithms have been developed [19, 18]. Among these approaches, the Prediction Error Method (PEM) is the most widely-used approach. Let the local model G_i be a Output Error (OE) model as follows.

$$G_i = \frac{b_1^{(i)} + b_2^{(i)} q^{-1} + \ldots + b_{nb}^{(i)} q^{-nb+1}}{1 + f_1^{(i)} q^{-1} + \ldots + f_{nf}^{(i)} q^{-nf}} \tag{4.9}$$

where $\theta_i^{(1)} = [b_1^{(i)}\ b_2^{(i)} \ldots b_{nb}^{(i)}\ f_1^{(i)} \ldots f_{nf}^{(i)}]^T$, q is the time shifted operator.

In order to enable the online estimation of parameter set $\theta^{(2)}$ in the weighting function along with the input design, we implement recursive prediction-error method (RPEM) in this nonlinear identification problem. The quadratic prediction-error criterion $V_j(\theta, Z^j)$ at time instant $t = j$ has the following form

$$\begin{aligned} V_j(\theta, Z^j) &= \frac{1}{j} \sum_{t=1}^{j} \frac{1}{2} \varepsilon^2(t, \theta) \\ &= \frac{1}{j} \sum_{t=1}^{j} \frac{1}{2} (y_t - \hat{y}_t)^2 \end{aligned} \tag{4.10}$$

where θ is the parameter to be estimated, Z^j is the input and output data at time instant $t = j$, $Z^j = [u_1, \ldots, u_j, y_1, \ldots, y_j]$, ε is the prediction error, and the $\hat{y}$ is the predicted output. This numerical search algorithm aims at finding a θ such that $V_j(\theta, Z^j)$ is minimized. The recursive solution is

$$\hat{\theta}_j = \hat{\theta}_{j-1} - \mu R_j^{-1} V_j^{'} \tag{4.11}$$

where $\hat{\theta}_j$ is the parameter estimate at time $t = j$, R_j is a $n_\theta \times n_\theta$ matrix that modifies the search direction where n_θ is the dimension of θ, μ is the search step size, and $V_j^{'}$ is the gradient of the criterion function V_j at time $t = j$. Different choice of R_j results in different method. One common method is the Levenberg-Marquardt algorithm [17, 21] in which the following equation is used to approximate the Hessian matrix.

$$R_j = \frac{1}{j} \sum_{t=1}^{j} \psi(t, \hat{\theta}_t) \psi^T(t, \hat{\theta}_t) + \lambda I \tag{4.12}$$

where $\psi(t, \hat{\theta}_t)$ is the sensitivity with respect to $\hat{\theta}$ at time t described in Equation (4.13)

$$\psi(t, \hat{\theta}_t) = \frac{\partial \hat{y}_t}{\partial \hat{\theta}_t} \tag{4.13}$$

and λ is tuning parameter which controls the search direction. $V_j^{'}$ can be calculated as

$$V_j^{'} = \frac{dV_j}{d\theta} = -\frac{1}{j}\sum_{t=1}^{j}(y_t - \hat{y}_t)\psi(t, \hat{\theta}_t) \tag{4.14}$$

4.4 Simultaneous Adaptive Design for Operating Points and Input Perturbations

The online design scheme can cause estimation problems when using the hybrid identification approach of Xu et al. (2009) [39] and Zhu and Xu (2008) [42]. In their approach, the global model is obtained only after the local models are identified, while the global model is simply interpolated from the local models. This may create a conflict between implementing input and identifying the global model. As shown in Equation (4.5) the structure of output y, with unknown parameters, should be available to calculate the sensitivity in order to obtain the optimal input perturbations. For LPV models, the global model structure will not be available until all the local models are acquired. However, when performing online input perturbations design, some local models are still unknown.

To solve the problem mentioned above, we develop an experiment design procedure in which the operating points and input perturbations are adaptively determined. The framework of the algorithm is shown in Figure 4.1 with the procedure stated below:

As shown in Figure 4.1, the simultaneous design follows the procedure below:

Step 1: Start from two nominal operating points which are usually the minimum and the maximum value within the operating range.

Step 2: Perform experiment at the current operating points and in the transition to get local data $\mathbb{D}_i$ and transition data $\mathbb{D}_{i,i+1}$.

Step 3: Identify local models $\hat{G}_i$ using local data set $\mathbb{D}_i$.

Step 4: Perform design of online input perturbations along the whole operating trajectory and estimate parameters set $\theta_i^{(2)}$ contained in the weighting factor set α_i. At the same time, the parameters set $\theta_i^{(1)}$ in the local models is re-identified. Therefore, the global is obtained.

Step 5: Compare and calculate the sum of mean square prediction error $MSE = \frac{1}{N}(y - \hat{y})^T(y - \hat{y})$.

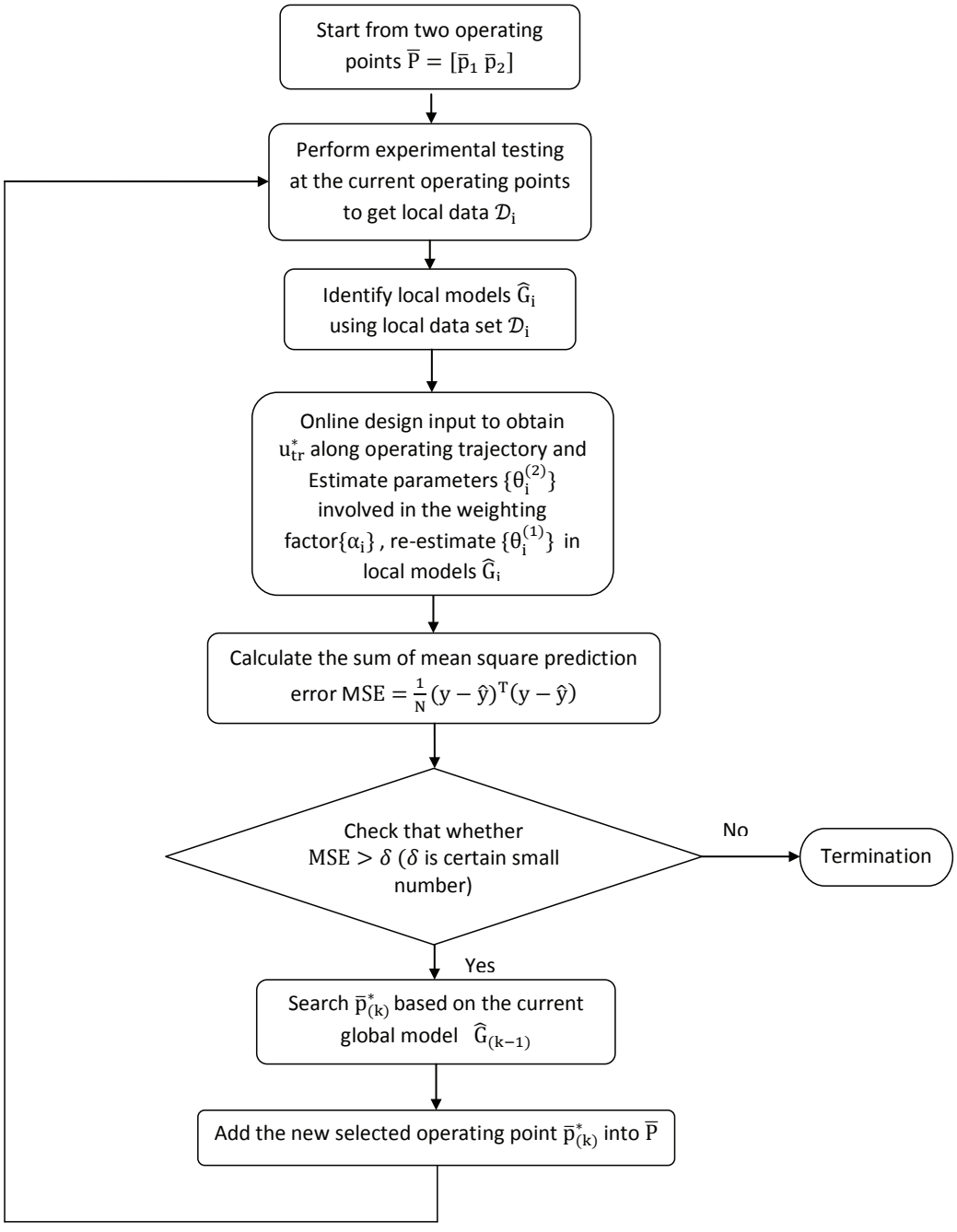

Figure 4.1: The framework for simultaneous adaptive operating point and input perturbations design procedure

Step 6: Check whether the mean squares error is larger than certain tolerance δ, i.e. $MSE > \delta$.

Step 7: If not, terminate the design procedure with the current optimal operating point vector $\bar{P}_{(k-1)}$; if yes, search the optimal operating point $\bar{p}^*_{(k)}$ based on the current global model $\hat{G}_{(k-1)}$, where k is the kth run of the experiment.

Step 8: Append the new $\bar{p}^*_{(k)}$ into the current operating point vector $\bar{P}_{(k)}$. Go to step 2.

Note that in Step 4, the parameter set $\theta^{(1)}$ contained in local model G_i is re-estimated together with parameter set $\theta^{(2)}$ in the weighting function. The reason for this simultaneous estimation is that estimation for $\theta^{(1)}$, conducted before the on-line design is implemented, uses only the data at the operating points. Re-estimation for $\theta^{(1)}$ using the data along the whole trajectory will provide better global property of the model. Analogous to Equation (4.8), the sensitivity with respect to $\theta^{(1)}$ needs to be calculated. For example, if $\theta_i^{(1)} = [b_i \ f_i]^T$ and the local model G_i has a 1st order OE structure as shown in Equation (4.9), the sensitivity corresponding to the i^{th} local model at time t can be calculated as

$$\psi_i(t, \hat{\theta}_t^{(1)}) = \begin{bmatrix} \frac{1}{1+f_t^{(i)}q^{-1}}u(t-1) \\ -\frac{b_t^{(i)}q^{-1}}{(1+f_t^{(i)}q^{-1})^2}u(t-1) \end{bmatrix} \tag{4.15}$$

The order of local model depends on the system nonlinearity. The more nonlinear the system is, the higher order of the local models should be.

4.5 Simulation

4.5.1 Continuous stirred tank reactor (CSTR) model

The continuous stirred tank reactor (CSTR) is considered here again. The dynamics of the CSTR model has been explained in Chapter 3 by Equation (3.20) and Equation (3.21)

Table 4.1 [15] shows the description and nominal value for each parameter in Equation (3.20) and (3.21).

The production concentration of component A, C_A, and the temperature of the reactor, T, as shown in Table 4.1 are chosen as the two states, while C_A is selected as output. The coolant flow rate q_c is selected as operating point which varies within the range of [97 109]. The inlet coolant temperature, T_{c0}, is the input.

Following the design procedure outlined in Figure 4.1, three optimal operating points are determined. The five operating points, including the minimum and maximum values of operating range, are determined as

$$\bar{P}^*_{(3)} = [97,\ 100.11,\ 103.00,\ 105.75,\ 109] \tag{4.16}$$

Table 4.1: Parameters and their nominal values in CSTR model

Variables or parameters	Descriptions or nominal values
production concentration of component A, C_A	1st state
temperature of the reactor, T	2nd state
coolant flow rate, q_c	input
feed concentration of component A, C_{A0}	1 mol/L
feed temperature, T_0	350.0 K
specific heats, C_p, C_{pc}	1 $cal/(gk)$
liquid density, ρ, ρ_c	1×10^3 g/L
heat of reaction, $- \triangle H$	-2×10^5 cal/mol
activation energy term, E/R	1×10^4 K
reaction rate constant, k_0	7.2×10^{10} min^{-1}
heat transfer term, hA	7×10^5 $cal/(min\ K)$
reactor volume, V	100 L
inlet coolant temperature, T_{c0}	350.0 K
process flow rate, q	100 L/min

Figure 4.2 shows the objective function values with different number of operating points. The optimal operating points are selected when the objective functions achieve their local minimums. Notice that because the nonlinearity of the objective function, global minimum cannot always be guaranteed.

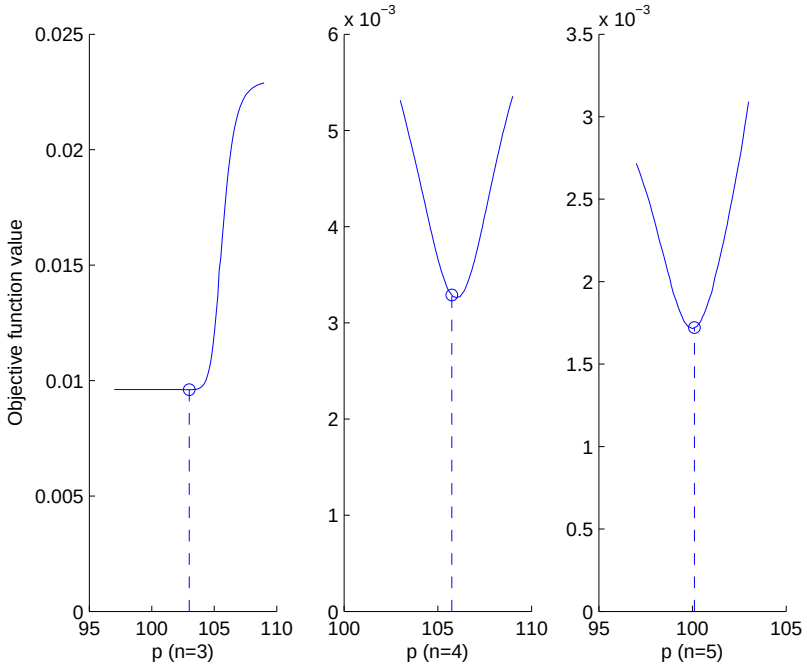

Figure 4.2: Objective function value vs. operating point p

Figure 4.3 shows the outputs of the process and the prediction of the global model obtained by using the simultaneous design. One can see that for this CSTR example, larger operating point has more prediction error. Overall, the proposed method gives good prediction ability.

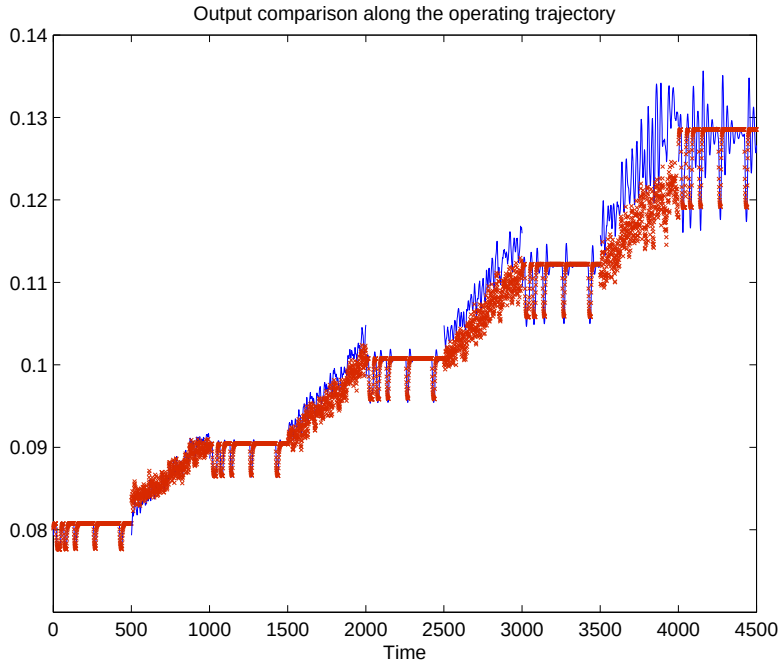

Figure 4.3: Comparison of outputs from the process and the global model when $n = 5$ ("$-$": process output; "$\times$": model output)

Figure 4.4 shows when $n = 5$ the weighting functions, which are defined in Equation (4.6) and (4.7), are normally distributed with the optimal operating points as their mean. This means that when manipulating the operating point near each selected optimal operating point, the global model will rely more on the local model determined by the corresponding operating point.

To illustrate the advantage of simultaneous adaptive design, we compare the prediction errors of the proposed joint design and the one with operating point-only design. The result is shown in Table 4.2. Although the error reduction is not obvious at the local areas, one can still see that the prediction error with the simultaneous joint design can be reduced up to 56% comparing to the optimal operating points-only design.

4.5.2 Solid oxide fuel cell (SOFC) model

The commonly-used SOFC developed by Siemens-Westinghouse has two tubes: the outer tube and the inner tube. The outer tube is the cell while the inner tube is the air injection and guidance tube. For the model developed by [24], a finite volume of the cell is studied where the properties such as temperature,

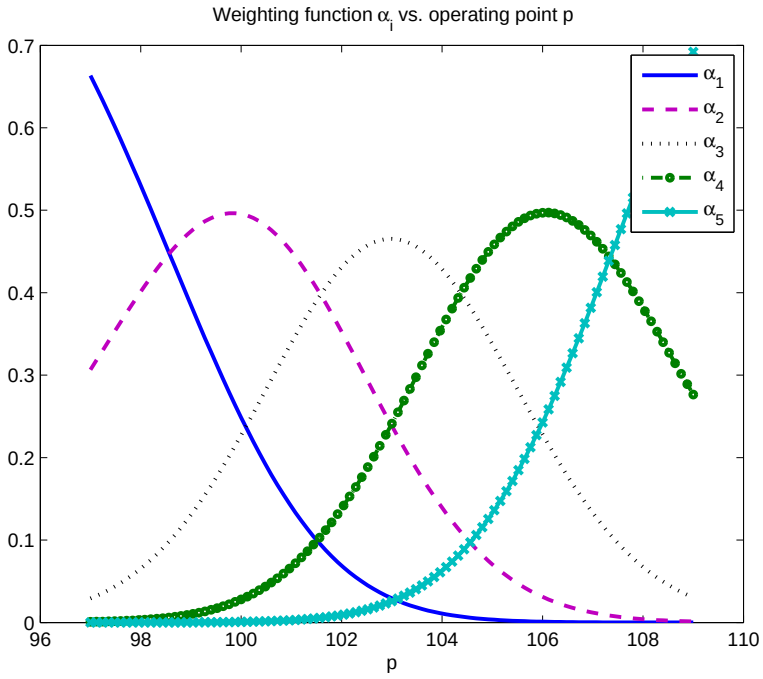

Figure 4.4: Weighting function α_i vs. varying operating point p

Table 4.2: Error comparison between operating points design and the joint design

	Operating point-only design	Simultaneous joint design
Error at local models	0.0037	0.0038
Error at transition	0.075	0.031
Error along the whole trajectory	0.0787	0.0348

pressure can be assumed uniform along the axial direction. According to the structure of the cell, Qi et al. (2006) [24] divided each slice of the cell into five volumes with the descriptions listed in Table 4.3.

Table 4.3: Descriptions for Control Volumes

Control Volume	Descriptions
CV1	Cell tube slice
CV2	Fuel flow in the anode side flow channel
CV3	Air flow in the cathode side air low channel
CV4	Injection tube
CV5	Air flow in side the injection tube

Modeling for the SOFC is equivalent to modeling of the five control volumes. Modeling for CV1 dynamics includes electricity conversion dynamics

and heat transfer dynamics; modeling for CV2 includes reforming and shift reaction, mass transfer dynamics, heat transfer dynamics and momentum balance; modeling for CV3 consists of mass transfer dynamics, heat transfer dynamics and momentum balance; in CV4 and CV5 there is no reaction or mass transfer but only heat exchanges occur. Considering the structure and dynamics discussed above, a state space model containing 28 states is derived. This state space model is given by Table 4.4 as shown below [24], where the inputs, outputs and state variables as well as their values are defined in Table 4.5, Table 4.6 and Table 4.7 respectively [24].

Table 4.4: State space model for SOFC

State equations:

$$
\begin{aligned}
\dot{x}_1 = \; & \tfrac{1}{R_{ct}C_{ct}}E - \tfrac{1}{R_{ct}C_{ct}}x_1 - \tfrac{1}{C_{ct}}\tfrac{x_1}{u_1+R_o} \\
\dot{x}_2 = \; & x_3 \\
\dot{x}_3 = \; & -h_1x_2 - h_2x_3 + h_1\tfrac{1}{2F}\tfrac{x_1}{u_1+R_o} \\
& +h_3\tfrac{A}{dV_a}(\dot{x}_{22} + \tfrac{x_{22}}{x_{17}}\dot{x}_{17}) \\
\dot{x}_4 = \; & x_5 \\
\dot{x}_5 = \; & -o_1x_4 - o_2x_5 + o_1\tfrac{1}{4F}\tfrac{x_1}{u_1+R_o} \\
& +o_3\tfrac{A}{dV_c}(\dot{x}_{26} + \tfrac{x_{26}}{x_{18}}\dot{x}_{18}) \\
\dot{x}_6 = \; & x_7 \\
\dot{x}_7 = \; & -w_1x_6 - w_2x_7 + w_1\tfrac{1}{2F}(\tfrac{-x_1}{u_1+R_o}) \\
& +w_3\tfrac{A}{dV_a}(\dot{x}_{21} + \tfrac{x_{21}}{x_{17}}\dot{x_{17}}) \\
\dot{x}_8 = \; & x_9 \\
\dot{x}_9 = \; & -h_1x_8 - h_2x_9 - h_4\tfrac{Rx_{15}}{A}\tfrac{1}{2F}\tfrac{x_1}{u_1+R_o} + h_1\tfrac{R}{dV_a}x_{22}x_{17} \\
& -\tfrac{Rx_{15}}{A}\tfrac{4}{L_a}\tfrac{1}{2F}[\tfrac{\dot{x}_1}{u_1+R_o} - \tfrac{x_1}{(u_1+R_o)^2}(Ku_1 - x_{14})] \\
\dot{x}_{10} = \; & x_{11} \\
\dot{x}_{11} = \; & -o_1x_{10} - o_2x_{11} - o_4\tfrac{Rx_{15}}{A}\tfrac{1}{4F}\tfrac{x_1}{u_1+R_o} + o_1\tfrac{R}{dV_c}x_{26}x_{18} \\
& -\tfrac{Rx_{15}}{A}\tfrac{4}{L_c}\tfrac{1}{4F}[\tfrac{\dot{x}_1}{u_1+R_o} - \tfrac{x_1}{(u_1+R_o)^2}(Ku_1 - x_{14})] \\
\dot{x}_{12} = \; & x_{13} \\
\dot{x}_{13} = \; & -w_1x_{12} - w_2x_{13} - w_4\tfrac{Rx_{15}}{A}\tfrac{1}{2F}\tfrac{-x_1}{u_1+R_o} \\
& w_1\tfrac{R}{dV_a}x_{21}x_{17} - \tfrac{Rx_{15}}{A}\tfrac{4}{L_a}\tfrac{1}{2F} \\
& \times[-\tfrac{\dot{x}_1}{u_1+R_o} + \tfrac{\dot{x}_1}{(u_1+R_o)^2}(Ku_1 - x_{14})] \\
\dot{x}_{14} = \; & K^2u_1 - Kx_{14} \\
\dot{x}_{15} = \; & \tfrac{1}{m_{cell}C_{p,cell}}[x_2H_{H_2} + x_4H_{O_2} + x_6H_{H_2O} \\
& -\tfrac{u_1}{(u_1+Ro)^2}x_1^2 - f_a(x_{27}\tfrac{\sum^2 4_20x_i}{dV_a})^{1/2}A(x_{15} - x_{17}) \\
& -f_c(x_{28}\tfrac{x_{25}+x_{26}}{dV_c})^{1/2}A_2(x_{15} - x_{18}) \\
& -\tfrac{\sigma}{R_{rad}}A_2(x_{15}^4 - x_{16}^4) - AK_r(\tfrac{x_{20}Rx_{17}}{dV_a})^{\alpha} \\
& \times(\tfrac{x_{21}Rx_{17}}{dV_a})^{\beta}exp(-\tfrac{E_r}{Rx_{17}})\Delta H_r] \\
\dot{x}_{16} = \; & \tfrac{1}{m_{tube}C_{p,tube}}[\tfrac{\sigma}{R_{rad}}A_2(x_{15}^4 - x_{16}^4) \\
& -f_c(x_{28}\tfrac{x_{25}+x_{26}}{dV_c})^{1/2}A_1(x_{16} - x_{18}) \\
& -f_t(u_{16}\tfrac{u_{14}}{Rx_{19}})^{1/2}A_o(x_{16} - x_{19})]
\end{aligned}
$$

Continued on next page

Table 4.4 – continued from previous page

$$
\begin{aligned}
\dot{x}_{17} = \; & \tfrac{1}{\sum_{20}^{24}(x_i C_{v,i})}[A_a \tfrac{u_2}{Ru_3} u_4 \textstyle\sum_5^9 (u_i H_i^{in}) \\
& -A_a x_{27} \tfrac{\sum_{20}^{24}(x_i H_i)}{dV_a} - f_a (x_{27} \tfrac{\sum_{20}^{24} x_i}{dV_a})^{1/2} \\
& A(x_{17} - 15) - x_2 H_{H_2} - x_6 H_{H_2O} \\
& +AK_r (\tfrac{x_{20} Rx_{17}}{dV_a})^{\alpha} (\tfrac{x_{21} Rx_{17}}{dV_a})^{\beta} exp(-\tfrac{E_r}{Rx_{17}}) \Delta H_r \\
& -x_{17} \textstyle\sum^{24} 20(\dot{x}_i C_{v,i})] \\
\dot{x}_{18} = \; & \tfrac{1}{\sum_{25}^{26}(x_j C_{v,j})}[A_c \tfrac{u_{10}}{Ru_{11}} u_{12} H_{air}^{in} - A_c x_{28} \tfrac{\sum_{25}^{26} x_j}{dV_c} H_{air} \\
& -x_4 H_{O_2} - f_c (x_{28} \tfrac{\sum_{24}^{26} x_j}{dV_c})^{1/2} (A_2 (x_{18} - x_{15}) \\
& +A_1 (x_{18} - x_{16})) - x_{18} \textstyle\sum_{25}^{26} (\dot{x}_j C_{v,j})] \\
\dot{x}_{19} = \; & \tfrac{1}{(u_{14} dV_t)/(Ru_{15}) C_{v,air}}[A_t \tfrac{u_{14}}{Ru_{15}} u_{16} (H_{air}^{in} - H_{air}) \\
& -f_t (u_{16} \tfrac{u_{14}}{Rx_{19}})^{1/2} A_0 (x_{19} - x_{16})] \\
\dot{x}_{20} = \; & A_a \tfrac{u_2}{Ru_3} u_4 u_5 - A_a x_{27} \tfrac{x_{20}}{dV_a} \\
& -AK_r (\tfrac{x_{20} Rx_{17}}{dV_a})^{\alpha} (\tfrac{x_{21} Rx_{17}}{dV_a})^{\beta} exp(-\tfrac{E_r}{Rx_{17}}) \\
\dot{x}_{21} = \; & A_a \tfrac{u_2}{Ru_3} u_4 u_6 - A_a x_{27} \tfrac{x_{21}}{dV_a} \\
& -AK_r (\tfrac{x_{20} Rx_{17}}{dV_a})^{\alpha} (\tfrac{x_{21} Rx_{17}}{dV_a})^{\beta} exp(-\tfrac{E_r}{Rx_{17}}) \\
& -AK_s [exp(\tfrac{4276}{/} x_{17} - 3.961) \tfrac{x_{23} Rx_{17}}{dV_a} \tfrac{x_{21} Rx_{17}}{dV_a} \\
& -\tfrac{x_{24} Rx_{17}}{dV_a} \tfrac{x_{22} Rx_{17}}{dV_a}] - x_6 \\
\dot{x}_{22} = \; & A_a \tfrac{u_2}{Ru_3} u_4 u_7 - A_a x_{27} \tfrac{x_{22}}{dV_a} \\
& +3AK_r (\tfrac{x_{20} Rx_{17}}{dV_a})^{\alpha} (\tfrac{x_{21} Rx_{17}}{dV_a})^{\beta} exp(-\tfrac{E_r}{Rx_{17}}) \\
& +AK_s [exp(\tfrac{4276}{/} x_{17} - 3.961) \tfrac{x_{23} Rx_{17}}{dV_a} \tfrac{x_{21} Rx_{17}}{dV_a} \\
& -\tfrac{x_{24} Rx_{17}}{dV_a} \tfrac{x_{22} Rx_{17}}{dV_a}] - x_2 \\
\dot{x}_{23} = \; & A_a \tfrac{u_2}{Ru_3} u_4 u_8 - A_a x_{27} \tfrac{x_{23}}{dV_a} \\
& +AK_r (\tfrac{x_{20} Rx_{17}}{dV_a})^{\alpha} (\tfrac{x_{21} Rx_{17}}{dV_a})^{\beta} exp(-\tfrac{E_r}{Rx_{17}}) \\
& -AK_s [exp(\tfrac{4276}{/} x_{17} - 3.961) \tfrac{x_{23} Rx_{17}}{dV_a} \tfrac{x_{21} Rx_{17}}{dV_a} \\
& -\tfrac{x_{24} Rx_{17}}{dV_a} \tfrac{x_{22} Rx_{17}}{dV_a}] \\
\dot{x}_{24} = \; & A_a \tfrac{u_2}{Ru_3} u_4 u_9 - A_a x_{27} \tfrac{x_{24}}{dV_a} \\
& +AK_s [exp(\tfrac{4276}{/} x_{17} - 3.961) \tfrac{x_{23} Rx_{17}}{dV_a} \tfrac{x_{21} Rx_{17}}{dV_a} \\
& -\tfrac{x_{24} Rx_{17}}{dV_a} \tfrac{x_{22} Rx_{17}}{dV_a}] \\
\dot{x}_{25} = \; & A_c \tfrac{u_{10}}{Ru_{11}} u_{12} (1 - u_{13}) - A_c x_{28} \tfrac{x_{25}}{dV_c} \\
\dot{x}_{26} = \; & A_c \tfrac{u_{10}}{Ru_{11}} u_{12} u_{13} - A_c x_{28} \tfrac{x_{26}}{dV_c} - x_4 \\
\dot{x}_{27} = \; & \tfrac{1}{\sum_{20}^{24}(x_i M_i)}[A_a \tfrac{u_2}{Ru_3} \textstyle\sum_5^9 (u_i M_i) u_4^2 \\
& -A_a \tfrac{\sum_{20}^{24}(x_i M_i)}{dV_a} x_{27}^2 - x_2 M_{H_2} x_{27} \\
& +A_a \Delta P_a - A\tau_{w,a} - x_{27} \textstyle\sum_{20}^{24} (\dot{x}_i M_i)] \\
\dot{x}_{28} = \; & \tfrac{1}{\sum_{25}^{26}(x_i M_i)}[A_c \tfrac{u_{10}}{Ru_{11}} ((1 - u_{13}) M_{N_2} + u_{13} M_{O_2}) u_{12}^2 - A_c \tfrac{\sum 26_{25}(x_j M_j)}{dV_c} x_{28}^2 \\
& -A_c \tfrac{\sum_{25}^{26}(x_j M_j)}{dV_c} x_{28}^2 \\
& -x_4 M_{O_2} x_{28} + A_c \Delta P_c - (A_1 + A_2) \tau_{w,c} \\
& -x_{28} \textstyle\sum_{25}^{26} (\dot{x}_i M_i)
\end{aligned}
$$

Output equations:

$$
y_1 = \; x_1 - \tfrac{R_o}{u_1 + R_o} x_1
$$

Continued on next page

Table 4.4 – continued from previous page

$$
\begin{aligned}
y_2 &= \frac{x_1}{u_1+R_o} \\
y_3 &= \frac{\sum_{20}^{24} x_i R x_1 7}{dV_a} \\
y_4 &= x_{17} \\
y_5 &= x_{27} \\
y_6 &= \frac{x_{20}}{\sum_{20}^{24} x_i} \\
y_7 &= \frac{x_{21}}{\sum_{20}^{24} x_i} \\
y_8 &= \frac{x_{22}}{\sum_{20}^{24} x_i} \\
y_9 &= \frac{x_{23}}{\sum_{20}^{24} x_i} \\
y_{10} &= \frac{x_{24}}{\sum_{20}^{24} x_i} \\
y_{11} &= \frac{\sum_{25}^{26} x_j R x_{18}}{dV_c} \\
y_{12} &= x_{18} \\
y_{13} &= x_{28} \\
y_{14} &= \frac{x_{26}}{\sum_{25}^{26} x_j} \\
y_{15} &= u_{14} \frac{x_{19}}{u_{15}} \\
y_{16} &= x_{19} \\
y_{17} &= u_{16}
\end{aligned}
$$

Table 4.5: Input variables for SOFC

Inputs	Descriptions	Values
R_{load}	External load resistance	2∼6 [Ω]
P_{fuel}^{in}	Fuel flow inlet pressure	1 [atm]
T_{fuel}^{in}	Fuel flow inlet temperature	823 [K]
u_{fuel}^{in}	Fuel flow inlet velocity	0.927 [m/s]
$\chi_{CH_4}^{in}$	Inlet mole fraction of CH_4	0.173
$\chi_{H_2O}^{in}$	Inlet mole fraction of H_2O	0.284
$\chi_{H_2}^{in}$	Inlet mole fraction of H_2	0.258
χ_{CO}^{in}	Inlet mole fraction of CO	0.057
$\chi_{CO_2}^{in}$	Inlet mole fraction of CO_2	0.228
P_{air}^{in}	Cathode side air flow inlet pressure	1 [atm]
T_{air}^{in}	Cathode side air flow inlet temperature	1104 [K]
u_{air}^{in}	Cathode side air flow inlet velocity	7.79 [m/s]
χ_{air}^{in}	Inlet mole fraction of O_2	0.21
P_{inj}^{in}	Injection air flow inlet pressure	1 [atm]
T_{inj}^{in}	Injection air flow inlet temperature	1104 [K]
u_{inj}^{in}	Injection air flow inlet velocity	12.08 [m/s]

The default values of parameters in the state space model are listed in Table 4.8.

Table 4.6: Output variables for SOFC

Outputs	Descriptions
V_{out}	Fuel cell voltage $[V]$
i	Fuel cell current $[A]$
P_{fuel}	Fuel flow pressure $[atm]$
T_{fuel}	Fuel flow temperature $[K]$
u_{fuel}	Fuel flow velocity $[m/s]$
χ_{CH_4}	Mole fraction of CH_4
χ_{H_2O}	Mole fraction of H_2O
χ_{H_2}	Mole fraction of H_2
χ_{CO}	Mole fraction of CO
χ_{CO_2}	Mole fraction of CO_2
P_{air}	Cathode side air flow pressure $[atm]$
T_{air}	Cathode side air flow temperature $[K]$
u_{air}	Cathode side air flow velocity $[m/s]$
χ_{air}	Mole fraction of O_2
P_{inj}	Injection air flow pressure $[atm]$
T_{inj}	Injection air flow temperature $[K]$
u_{inj}	Injection air flow velocity $[m/s]$

Results

With a large number of states coupled with each other and highly nonlinearity of the processes, the experiment design and parameter estimation is challenging. As stated in the previous section, for highly nonlinear system, an LPV model requires higher order of local models. For this fuel cell model, at least 3rd-order OE model is adopted. In this example, the first input u_1 in Table 4.5 is selected as operating point which has a range from 2 Ω to 6 Ω. Experiment design seeks the optimal input perturbation along the operating trajectory.

Based on the simultaneous design algorithm described by Figure 4.1, the following four operating points are obtained:

$$\bar{P}^*_{(2)} = [2,\ 3.00,\ 4.00,\ 6] \tag{4.17}$$

Among the 17 outputs, the fuel cell temperature T_{fuel}, cathode side air flow velocity u_{air} and injection air flow velocity u_{inj} are selected to monitor and control. Figure 4.5, 4.7 and 4.9 show the process outputs and model predictions along the experimental trajectory for T_{fuel}, u_{air} and u_{inj} respectively. The three predicted outputs at four local models are also shown in Figure 4.6, 4.8 and 4.10.

Notice that since the temperature is a slow process, time delay is incorporated into the local models. From Figure 4.5, one can see that the predicted model output can match the real output well. However, for lower operating point (smaller resistance load) the slow dynamic cannot be sufficiently captured. This is shown in Figure 4.6.

Table 4.7: State variables for SOFC

States	Descriptions	Initial values
V_{ct}	Voltage V_{ct} $[V]$	0.84243
$J^s_{H_2}$	Consumption rate of hydrogen $[\mu mol/s]$	1.0887×10^{-6}
$\dot{J}^s_{H_2}$	Derivative of consumption rate of hydrogen $[\mu mol/s^2]$	-2.3809×10^{-17}
$J^s_{O_2}$	Consumption rate of oxygen $[\mu mol/s]$	5.4433×10^{-7}
$\dot{J}^s_{H_2}$	Derivative of consumption rate of oxygen $[\mu mol/s^2]$	-1.2938×10^{-17}
$J^s_{H_2O}$	Production rate of water $[\mu mol/s]$	-1.0887×10^{-6}
$\dot{J}^s_{H_2O}$	Derivative of production rate of water $[\mu mol/s^2]$	2.0487×10^{-17}
$p^{tpb}_{H_2}$	Concentration of hydrogen at tpb $[atm]$	2.5091×10^{-1}
$\dot{p}^{tpb}_{H_2}$	Derivative of concentration of hydrogen at tpb $[atm/s]$	-7.3746×10^{-14}
$p^{tpb}_{O_2}$	Concentration of oxygen at tpb $[atm]$	1.5583×10^{-1}
$\dot{p}^{tpb}_{O_2}$	Derivative of concentration of oxygen at tpb $[atm/s]$	-6.3027×10^{-13}
$p^{tpb}_{H_2O}$	Concentration of water at tpb $[atm]$	2.8338×10^{-1}
$\dot{p}^{tpb}_{H_2O}$	Derivative of concentration of water at tpb $[atm/s]$	-3.0365×10^{-13}
v_R	Intermediate variable	4.01×10^{1}
T_{cell}	Fuel cell temperature $[K]$	1.0808×10^{3}
T_{tube}	Fuel tube temperature $[K]$	1.0930×10^{3}
T_{fuel}	Fuel flow temperature $[K]$	8.2491×10^{2}
T_{air}	Cathode side air flow temperature $[K]$	1.1036×10^{3}
T_{inj}	Injection air flow temperature $[K]$	1.1039×10^{3}
N_{CH_4}	Mole fraction of CH_4	3.7793×10^{-7}
N_{H_2O}	Mole fraction of H_2O	6.2663×10^{-7}
N_{H_2}	Mole fraction of H_2	5.5964×10^{-7}
N_{CO}	Mole fraction of CO	1.2937×10^{-7}
N_{CO_2}	Mole fraction of CO_2	4.9439×10^{-7}
N_{N_2}	Mole fraction of N_2	1.5458×10^{-6}
N_{O_2}	Mole fraction of O_2	4.1081×10^{-7}
u_{fuel}	Fuel flow velocity $[m/s]$	9.4325×10^{-1}
u_{air}	Cathode side air flow velocity $[m/s]$	7.7901
Note that "tpb" stands for triple phase boundary		

The discrepancy within the local model areas in Figure 4.7 and 4.8 indicates that the u_1-u_{air} input-output relationship exists high nonlinearity so that an OE model cannot completely follow the dynamics of the nonlinear system. However, the model output at transition period shows nice agreement with the real output. Similar results are obtained in Figure 4.9 and 4.10. This may be due to the similar physical characteristic shared by the two output variables u_{air} and u_{inj}.

Overall, for the three outputs the comparisons of model predictions and real outputs reach acceptable agreement both in the local areas and transition periods.

Figure 4.11 shows the weighting factor as a function of operating point p.

Table 4.8: Parameters for SOFC

Parameters	Descriptions	Nominal values used in simulation
Electrochemical parameters		
E_a	Activity energy of anode reaction	$1.1 \times 10^5\ J/mol$
E_c	Activity energy of cathode reaction	$1.2 \times 10^5\ J/mol$
F	Faraday constant	$96487\ C\ mol^{-1}$
Electrical parameters		
R_{ct}	Charge transfer resistance	$0.9\ \Omega$
C_{ct}	Charge transfer capacitance	$300 \times 10^{-6}\ F$
R_o	Ohmic resistance	$0.01\ \Omega$
Mechanical parameters		
A	Fuel cell effective area	$1\ cm^2$
L_a	Thickness of anode diffusion layer	$0.1\ mm$
L_c	Thickness of cathode diffusion layer	$2.21\ mm$
L_e	Thickness of electrolyte diffusion layer	$0.04\ mm$
r_3	Radius of outer cell tube	$11\ mm$
r_2	Radius of inner cell tube	$8.66\ mm$
r_1	Radius of outer inject tube	$6\ mm$
r_0	Radius of inner inject tube	$5\ mm$
A_a	Fuel channel cross area	$r_3^2 \times (4 - \pi)\ m^2$
A_c	Air channel cross area	$\pi \times (r_2^2 - r_1^2)\ m^2$
A_t	Injection channel cross area	$\pi \times r_0^2\ m^2$
dV_a	Fuel channel element volume	$A_a \times A/(2 \times \pi \times r_3)\ m^3$
dV_c	Air channel element volume	$A_c \times A/(2 \times \pi \times r_3)\ m^3$
dV_t	Injection channel element volume	$A_t \times A/(2 \times \pi \times r_3)\ m^3$
Flow mechanics parameters		
D_a	Hydraulic diameter of fuel side flow	$0.273 \times 2 \times r_3\ m$
D_c	Hydraulic diameter of air side flow	$2 \times (r_2 - r_1)\ m$
D_t	Hydraulic diameter of inject tube	$2 \times r_0\ m$
Thermal dynamics parameters		
ε_{cell}	Emissivity of cell inner surface	0.9
ε_{tube}	Emissivity of inject tube outer surface	0.4
F_{c-t}	View factor: cell to injection tube	0.69
ρ_{cell}	Density of entire cell	$5.67 \times 10^{-8}\ kg/m^3$
$C_{p,cell}$	Entire specific heat of cell	$740\ J/(kg \cdot K)$
ρ_{tube}	Density of injection tube	$3900\ kg/m^3$
$C_{p,tube}$	Specific heat of injection tube	$1217.7\ J/(kg \cdot K)$
Other parameters		
K	Approximation factor	10
T_{tube}	Temperature of injection tube	$1123\ K$

From Figure 4.11 one can see that each local model has varying weights in different operating regions. Moreover, the weight always reaches a relatively

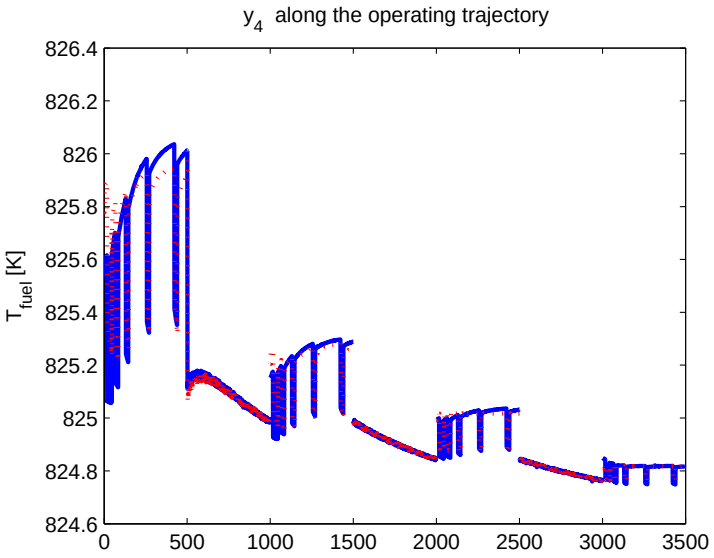

Figure 4.5: Output T_{fuel} from the process and the global model when $n = 4$ ("-": process output; "...": model output)

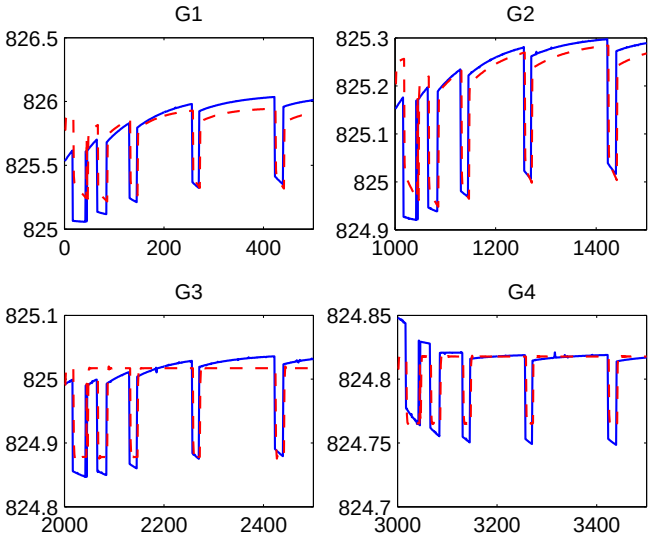

Figure 4.6: Local model output T_{fuel} ("—": process output; "- -": model output)

large value near the operating point based on which the local model is built.

Table 4.9 is obtained by comparing the mean square error of the proposed simultaneous design with the optimal operating point-only design which uses a generalized binary noise (GBN) as input perturbations [42]. From Table 4.9 one can see that by simultaneous design the mean square error can be reduced significantly.

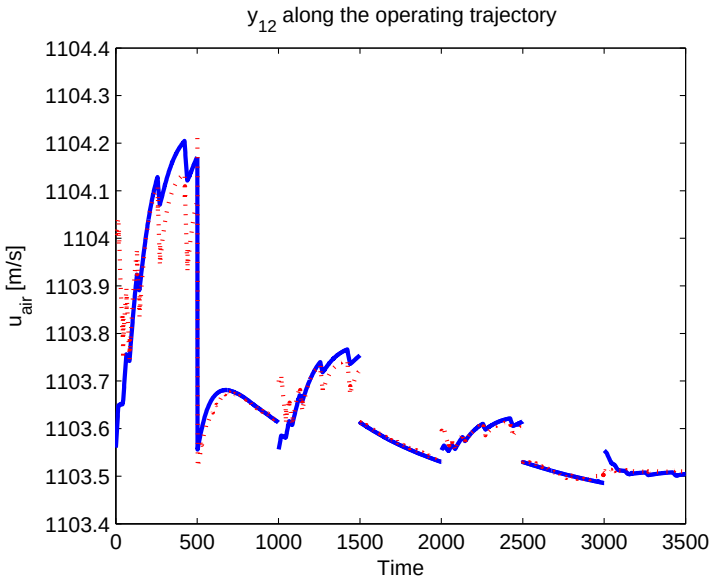

Figure 4.7: Output u_{air} from the process and the global model when $n = 4$ ("-": process output; "...": model output)

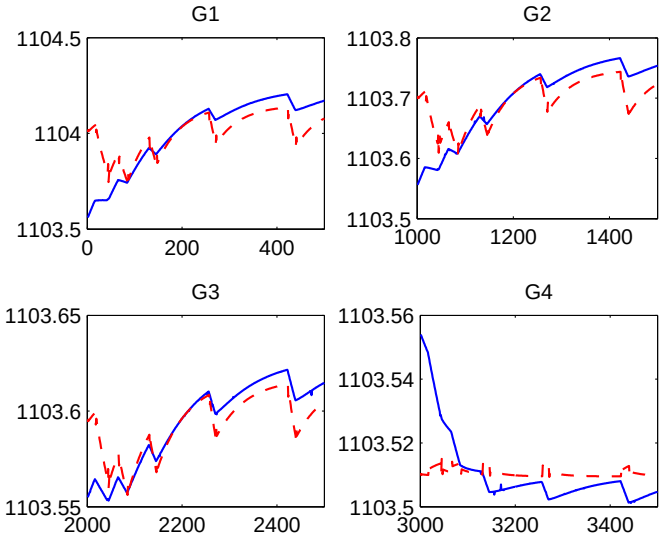

Figure 4.8: Local model output u_{air} ("—": process output; "- -": model output)

4.6 Conclusion

A joint experiment design problem in LPV model is considered in this chapter. Based on a hybrid LPV identification method, the proposed method incorporates optimal experiment design and recursive estimation to simultaneously design the operating points and the input perturbations. In the experiment

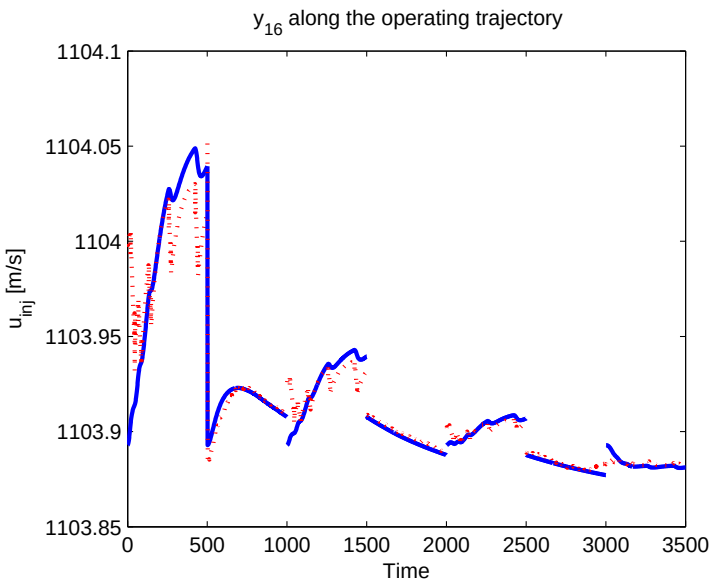

Figure 4.9: Output u_{inj} from the process and the global model when $n = 4$ ("-": process output; "...": model output)

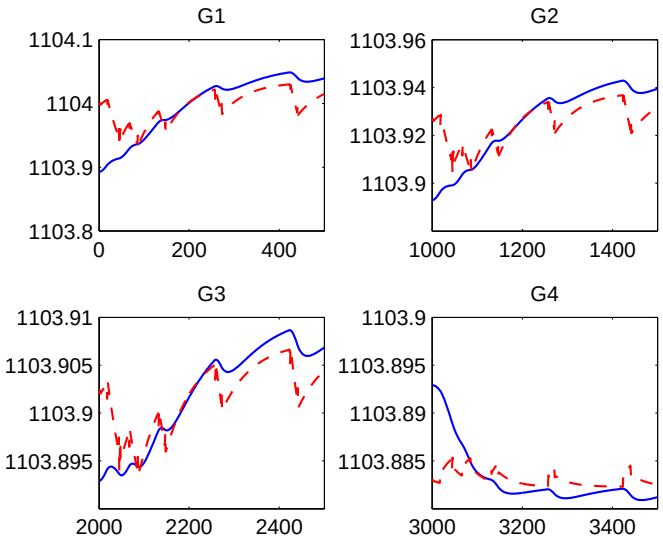

Figure 4.10: Local model output u_{inj} ("—": process output; "- -": model output)

design procedure, local models are identified to obtain the initial local model parameters, while these parameters are re-identified simultaneously with the parameters in the weighting function by online experiment along the whole operating trajectory. The superiority of this simultaneous design over the operating point-only design has been demonstrated by simulation examples. The contribution of this chapter is to show that the accuracy of the LPV model,

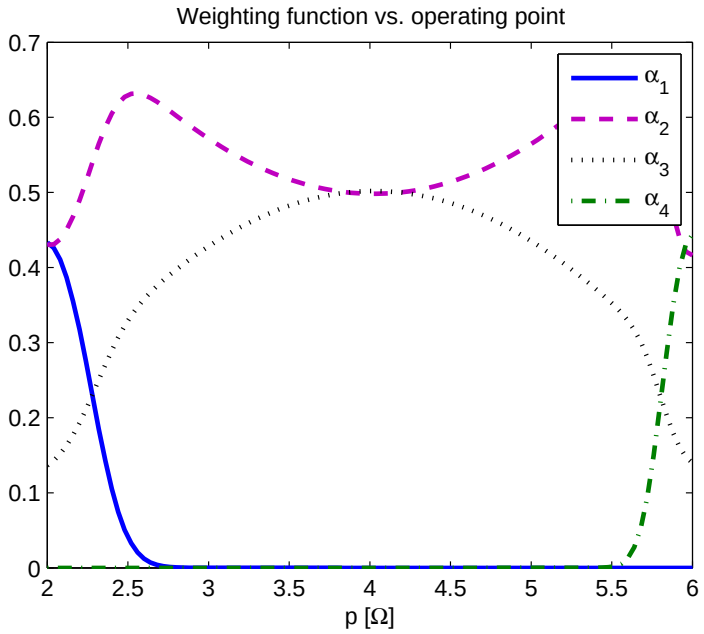

Figure 4.11: Weighting function α_i vs. varying operating point p

Table 4.9: Error comparison between operating points design and the joint design

	Only operating points design	Simultaneous joint design
Mean square error at transition	0.0012	0.0001

which is used to approximate nonlinear process, can be improved by solving this joint experiment design problem.

Chapter 5

Conclusions and Future Work

5.1 Summary

This thesis is concerned with problems related to three aspects of experimental design for nonlinear systems. The ultimate goal of optimal experiment design is to improve the model accuracy by optimally selecting the experimental conditions. However, the efficiency of optimal experiment design is often challenged by the following three issues: poor initial guess of the nominal model; operating point selection; and joint experimental design concerning operating points and input design simultaneously.

First, the background and preliminaries are presented in Chapter 1. One commonly-used implementation of adaptive experimental design is the receding-horizon design. In this method, optimal experiment design and parameter estimation can be conducted iteratively. LPV modeling for nonlinear systems is another key technique utilized in operating points-only design and simultaneous design. Among different approaches to LPV model identification, the hybrid identification attracts most attention and is used in this thesis as a foundation of the proposed LPV experiment design algorithms.

With the motivation to solve the initial condition problem regarding the nonlinear system identification, a constrained receding-horizon design (CRHD) is developed in Chapter 2 [43]. Based on sensitivity analysis and the Fisher information matrix (FIM), the objective function is formulated to reduce the parameter covariance. However, if the initial guess of the model is inappropriately selected, the efficiency of experiment design will be severely compromised. By taking steady-state a-priori knowledge into account, the constraints on the parameters can be derived and incorporated into the receding-horizon experiment design. Illustration examples and mathematical derivations prove that the parameter covariance can be reduced by using the optimal input obtained from the constrained receding-horizon design. On the other hand, it is also proven mathematically that by using constrained receding-horizon design (CRHD) the convergence can be faster than the one without constraints. For practical application, it also considers the uncertainty in constraints. The effi-

ciency and effectiveness of constrained receding-horizon design (CRHD) have been demonstrated using a electrical circuit system and a continuously-stirred tank reactor (CSTR) example.

The objective of Chapter 3 and 4 is to develop experiment design for LPV identification to improve the model accuracy. Chapter 3 begins with an introduction of LPV model identification approaches including local approach and global approach. The reason we choose the hybrid identification approach is that it combines the advantages of both local approach and global approach, which are the simplicity in structure and the ability to capture global system nonlinearity. The optimal operating points design starts from the initial operating points. By interpolating the local models using the entire data set, the global model is obtained. With the global model, the objective function can be calculated. The candidate with the largest objective function value will be selected as the new operating point. This procedure is performed iteratively until the error is within certain small tolerance. As mentioned before, the proposed operating points design requires no a-priori knowledge about the true nonlinear system, which renders its utility. A brief introduction to SOFC system dynamics is also given before revealing the superiority of the proposed method by simulation.

Chapter 3 only takes one design factor (experimental condition) into consideration, which is the operating point. However, in most cases, only one design factor cannot guarantee the experimental efficiency. Usually more than one experimental factors need to be optimally selected at the same time. For LPV model identification, input perturbations need to be designed in addition to the operating points. A simultaneous operating points and input perturbation design is developed in Chapter 4, incorporating optimal experiment design and recursive estimation. One of the main differences between the algorithm in Chapter 3 and the one in Chapter 4 is that parameters contained in local model are re-identified simultaneously with the parameters in the weighting function by online experimental data. Two examples are used to demonstrate that the simultaneous design algorithm outperforms the one with operating point-only design.

5.2 Recommendations for Future Work

Throughout the entire thesis, we have been working on the solutions to the three issues regarding optimal experiment design. Based on the current research, we summarize some potential areas that are worthy of future investigations:

- The prediction horizon and the control horizon (the number of input steps being implemented) of the receding-horizon experiment design are fixed before the experiment design. By choosing different prediction and control horizons, it was noticed that these two factors can affect the efficiency of the parameter estimation as well as experimental design.

Since tuning the horizon can be easily applied in practice, this aspect of experiment design will be of interest and useful for process identification in the future.

- The work has only utilized the equality constraint in the constrained receding-horizon design (CRHD). Considering that this constraint can contain uncertainty, the constraint is released after some iterations of estimation to avoid the bias induced by constraint uncertainty. However, inequality constraints can also be utilized in the constrained receding-horizon design (CRHD). Mathematical development needs to be performed before new recursion of the inequality constrained receding-horizon design is developed.

- Through two propositions as well as illustrating examples we show that both the convergence and estimation covariance can be improved using the constrained receding-horizon design (CRHD). However, how to quantify the initial guesses which can yield convergence can be difficult. The research on quantifying the efficiency of the proposed constrained receding-horizon design (CRHD) is worth investigating.

- For the operating points and input perturbation design in Chapter 3 and 4, the entire experimental data set obtained at the operating trajectory is needed. This may require testing at a large number of operating points which may not be available in practice. This is also a common disadvantage shared within any LPV global or hybrid identification approach. Therefore, it can be desirable to develop a new LPV identification framework to render an experiment design with testing at fewer operating points.

Bibliography

[1] Operating point analysis using the gui. *http://www.mathworks.com/access/helpdesk/help/toolbox/slcontrol/ug/bqkvccz-1.html*, 2009.

[2] A. Baneerjee and Y. Arkun. Model predictive control of plant transitions using a new identification technique for interpolating nonlinear models. *Journal of Process Control*, 8:441–457, 1998.

[3] C. Bohn and H. Unbehauen. Sensitivity models for nonlinear filters with application to recursive parameter estimation for nonlinear state space models. *IEEE proceedings, control theory and application*, 148:137–145, 2001.

[4] Yunfei Chu and Juergen Hahn. Parameter set selection for estimation of nonlinear dynamic systems. *AIChE Journal*, 53(11):2858 – 2870, 2007.

[5] John L. Crassidis and John L. Junkins. *Optimal Estimation of Dynamic Systems*. Chapman & Hall/CRC Press, 2004.

[6] A F Emery and Aleksey V Nenarokomov. Optimal experiment design. *Measurement Science and Technology*, 9:864 – 876, 1998.

[7] M. Eslami. *Theory of Sensitivity in Dynamic Systems: An Introduction*. Berlin; New York : Springer-Verlag, 1994.

[8] R. S. Gemmen and C. D. Johnson. Effect of load transients on sofc operation–current reversal on loss of load. *Journal of Power Sources*, 144:152–164, 2005.

[9] Graham C. Goodwin and Robert L. Payne. *Dynamic System Identification : Experiment Design and Data Analysis*. New York : Academic Press, 1977.

[10] John D. Hedengren. A nonlinear model library for dynamics and control. *Computer Aids for Chemical Engineering (CACHE) News*, 2008.

[11] B. Huang, Y. Qi, and M. Murshed. Solid oxide fuel cell: Perspective of dynamics modeling and control. In *IFAC International Symposium on Dynamics and Control of Process Systems*, 2010.

[12] P. Iora, P. Aguiar, C. S. Adjiman, and N. P. Brandon. Comparison of two it dir-sofc models: impact of variable thermodynamic, physical and flow properties. steady-state and dynamic analysis. *Chemical Engineering Science*, 60:2963–2975, 2005.

[13] B. Jayasankar, B. Huang, and A. Ben-Zvi. Receding horizon experiment design with application in sofc parameter estimation. *International Symposium on Dynamics and Control of Process Systems, Leuven, Belgium*, 2010.

[14] B.R. Jayasankar. Identifiability study and receding-horizon experiment design for solid oxide fuel cell. Master's thesis, University of Alberta, 2009.

[15] X. Jin. Multiple arx model based identication for switching/nonlinear systems with em algorithm. Master's thesis, University of Alberta, 2010.

[16] A. A. Khalate, X. Bombois, R. Toth, and R. Babuska. Optimal experimental design for LPV identification using a local approach. *15th IFAC Symposium on System Identification. Saint-Malo, France*, 2009.

[17] K. Levenberg. A method for the solution of certain nonlinear problems in least squares. *The Quarterly of Applied Mathematics*, 2:164–168, 1944.

[18] L. Ljung. *System Identification: Theory for the User*. Prentice-Hall: Upper Saddle River, 1999.

[19] L. Ljung. Estimating linear time-invariant models of nonlinear time-varying systems. *European Journal of Control*, 7:203–219, 2001.

[20] L. Ljung. Experiments with identification of continuous time models. *Proceedings of the 15th IFAC symposium on system identification*, pages 90–95, 2009.

[21] D. W. Marquardt. An algorithm for least squares estimation of nonlinear parameters. *Journal of the Society for Industrial and Applied Mathematics*, 11:431–441, 1963.

[22] L. Pronzato and E. Walter. Robust experiment design via stochastic approximation. *Mathematical Biosciences*, 75:103–120, 1985.

[23] Y. Qi, B. Huang, and K. T. Chuang. Dynamic modeling of solid oxide fuel cell: The effect of diffusion and inherent impedance. *Journal of Power Sources*, 150:32–47, 2005.

[24] Y. Qi, B. Huang, and J. Luo. Dynamic modeling of a finite volumn of solid oxide fuel cell: The effect of transport dynamics. *Chemical Engineering Science*, 61:6057–6076, 2006.

[25] Konrad Reif, Stefan Gnther, Engin Yaz, and Rolf Unbehauen. Stochastic stability of the discrete-time extended kalman filter. *IEEE Transactions on Automatic Control*, 44:714–728, 1999.

[26] C. R. Rojas, J.S. Welsh, G.C. Goodwin, and A. Feuer. Robust optimal experiment design for system identification. *Automatica*, 43:993–1008, 2007.

[27] W.J. Rugh and J.S. Shamma. A survey of research on gain-scheduling. *Automatica*, pages 1401–1425, 2000.

[28] R. Senthil, K. Janarthanan, and J. Prakash. Nonlinear state estimation using fuzzy kalman filter. *Ind. Eng. Chem. Res.*, 45:8678–8688, 2006.

[29] D. Simon. Kalman filtering with inequality constraints for turbofan engine health estimation. *IEE Proceedings - Control Theory and Applications*, 153(3):371–378, 2006.

[30] D. Simon. Kalman filtering with state constraints: a survey of linear and nonlinear algorithms. *IET Control Theory and Applications*, 2009.

[31] D. Simon and T. Chia. Kalman filtering with state equality constraints. *IEEE Transactions on Aerospace and Electronic Systems*, 38:128–136, 2002.

[32] Yongkyu Song and Jessy W. Grizzle. The extended kalman filter as a local asymptotic observer for discrete-time nonlinear systems. *Journal of Mathematical Systems, Estimation, and Control*, 75:103–120, 1995.

[33] J. D. Stigter, D. Vries, and K. J. Keesman. On adaptive optimal input design: a bioreactor case study. *AIChE Journal*, 52:3290–3296, 2006.

[34] R. Toth. *Modeling and Identification of Linear Parameter-Varying Systems*. Springer-Verlag, 2010.

[35] R. Toth, P. Heuberger, and P. Van der Hof. Asymptotically optimial orthonormal basis functions for LPV system identification. *Automatica*, 45:1359–1370, 2009.

[36] E. Walter and L. Pronzato. How to design experiments that are robust to parameter uncertainty. *IFAC/IFORS Symp. on Identification and System Parameter Estimation*, 1:921–926, 1985.

[37] E. Walter and L. Pronzato. Optimal experiment design for nonlinear models subject to large prior uncertainties. *American Journal of Physiology - Regulatory, Integrative and Comparative Physiology*, 253:530–534, 1987.

[38] J.S. Welsh and C. R. Rojas. A scenario based approach to robust experiment design. In *Proceedings of the 15th IFAC symposium on system identification*, 2009.

[39] Z. Xu, J. Zhao, J. Qian, and Y. Zhu. Nonlinear mpc using an identified LPV model. *Ind. Eng. Chem. Res.*, 48:3043–3051, 2009.

[40] K. Zhen Yao, Benjamin M. Shaw, Bo Kou, Kim B. McAuley, and D. W. Bacon. Modeling ethylene/butene copolymerization with multi-site catalysts: Parameter estimability and experimental design. *Polymer Reaction Engineering*, 11(3):563–588, 2003.

[41] Martin B. Zarrop. *Optimal Experiment Design for Dynamic System Identification*. Berlin; New York : Springer-Verlag, 1979.

[42] Y. Zhu and Z. Xu. A method of LPV identification for control. In *The International Federation of Automatic Control. Seoul, Korea*, 2008.

[43] Yijia Zhu and Biao Huang. Constrained receding-horizon experiment design and parameter estimation in the presence of poor initial conditions, aiche-10-12613.r1. *AIChE Journal*, 2010.

Chapter 6

Appendix

6.1 Lemma 1 (Observability condition)

Suppose that a nonlinear system described by (6.1) and (6.2) where w_t and v_t are state noise and output noise respectively has the constraint function $g(\theta) = 0$,

$$\dot{x}_t = f(\theta, x_t, u_t) + Nw_t \tag{6.1}$$

$$y_t = h(x_t) + Rv_t \tag{6.2}$$

which satisfies the observability rank condition on a compact subset $K \subset R^n$ (n is the dimension of state). If the estimates of the EKF are sufficiently close to the true state, then the linearized system along the estimated trajectory of the EKF is uniformly observable; i.e., there exist γ_1, γ_2, $1 < \gamma_1 \leq \gamma_2 < \infty$ and $\delta_1 > 0$ such that

$$\gamma_1 I \leq O_e^T(X_{n-1}^-, X_{n-2}^+) O_e(X_{n-1}^-, X_{n-2}^+) \leq \gamma_2 I \tag{6.3}$$

for all $x_l^- \in K$ such that $|x_l^- - x_l| \leq \delta_1$, $l = 0, \ldots, n-1$, and all $x_j^+ \in K$ such that $|x_j^+ - x_j| \leq \delta_1$, $j = 0, \ldots, n-2$, and for each $x_0 \in K$, where $x_{l+1} = f(x_l)$, $l = 0, \ldots, n-2$, $X_{n-1}^- \triangleq (x_0^-, \cdots, x_{n-1}^-)$, $X_{n-2}^+ \triangleq (x_0^+, \cdots, x_{n-2}^+)$. "$-$" and "$+$" denote "a priori" and "posterior" respectively.

6.2 Assumption 2

1. $A(x) \triangleq \frac{\partial f}{\partial x}(x)$ is invertible at each $x \in R^n$.
2. The following norms are bounded:

$$\|A\| \triangleq \sup_{x \in R^n} \|A(x)\| \quad , \quad \|A^{-1}\| \triangleq \sup_{x \in R^n} \|[A(x)]^{-1}\|, \tag{6.4}$$

$$\|H\| \triangleq \sup_{x \in R^n} \|R^{-1} \frac{\partial h}{\partial x}\| \quad , \quad |||D^2 f||| \triangleq \sup_{x \in R^n} |||D^2 f(x)|||, \tag{6.5}$$

$$|||D^2 h||| \triangleq \sup_{x \in R^n} |||D^2 h(x)||| \tag{6.6}$$

3. Let $g(x, y) \triangleq h(x) - h(y) - \frac{\partial h}{\partial x}(x)(x - y)$, and suppose that there exists $g < \infty$ such that $|g(x, y)| \leq g|||D^2 h|||x - y|^2$ for all x, $y \in R^n$.

6.3 Lemma 3 (Asymptotic observer)

Consider the system in (6.1) and (6.2) and the EKF framework for the associated noise system. Suppose that Assumption 2 holds. Then, if $|e_k|$, $|||D^2 f|||$, *and* $|||D^2 f|||$ *are such that for some* $\gamma > 0$,

$$\varphi(q^{\frac{1}{2}} V^{\frac{1}{2}}(0, e_0), |||D^2 f|||, |||D^2 h|||) \leq -\gamma \tag{6.7}$$

where $e_k = x_k - x_k^-$; p, q *are the corresponding boundaries for error covariance, i.e.,*

$$\begin{aligned} \|P_k^{+^{-1}}\| &\leq p_1 && (6.8)\\ \|P_k^{-^{-1}}\| &\leq \|P_k^{+^{-1}}\| + \|H\|^2 \leq p_1 + \|H\|^2 \triangleq p && (6.9)\\ \|P_k^+\| &\leq \|P_k^-\| \leq q && (6.10)\\ q\|H\|\|R^{-1}\|^2 &\triangleq \delta && (6.11) \end{aligned}$$

and the following equations are set as follows.

$$\begin{aligned} V(k, e_k) &= e_k^T \bar{P}_k^{-1} e_k && (6.12)\\ \phi(|e_k|, X, Y) &\triangleq \delta g Y \|A\| + \frac{1}{2} X (pq + \delta g Y |e_k|)^2 && (6.13)\\ \varphi(|e_k|, X, Y) &\triangleq -\frac{1}{rq^2} + p|e_k|\phi(|e_k|, X, Y)\{2pq\|A\| + \phi(|e_k|, X, Y)|e_k|\} && (6.14) \end{aligned}$$

Then the EKF for the noisy system is a local, uniform asymptotic observer for the system in (6.1) and (6.2).

6.4 Lemma 4

Let $\mathcal{O}$ *be a convex compact subset of* R^n, $\tilde{\mathcal{O}}$ *the complement of* $\mathcal{O}$, *and* $\epsilon > 0$ *a positive constant. Define* $d(x, \tilde{\mathcal{O}}) = \inf\{|x - y| : y \in \tilde{\mathcal{O}}\}$, *and* $\mathcal{O}_\epsilon = \{x \in \mathcal{O} : d(x, \tilde{\mathcal{O}}) \geq \epsilon\}$. *Also, assume that*

$$\begin{aligned} \alpha_1 &= \|N\|^2(1 + \|A\|^2 + \|A\|^4 + \cdots + \|A\|^{2(n-2)}) && (6.15)\\ \alpha_2 &= \lambda_{min}(NN^T) && (6.16)\\ a &= \max(1, \|A\|) && (6.17)\\ \beta_k &= (1 + \|P_0^-\|\|Dh\|^2) a^k \prod_{l=1}^{k} \{1 + \|Dh\|^2 && (6.18)\\ &\quad \times [\|A\|^{2l}\|P_0^-\| + \|N\|^2(\|A\|^{2(l-1)} + \|A\|^{2(l-2)} + \cdots + 1)]\} \end{aligned}$$

Consider the system in (6.1) and (6.2) as well as its associated EKF. Suppose that the system satisfies the observability rank condition on a convex compact set $\mathcal{O}$, *and that* $[\frac{\partial f}{\partial x}]^{-1}$ *exists at each* $x \in \mathcal{O}$. *Let* $\delta_1 > 0$ *be a constant which satisfies the inequality in (6.3) for some* $0 < \gamma_1 \leq \gamma_2$. *Let* $p = (\gamma_2 + \frac{1}{\alpha_2})$, $q = a^2(\alpha_1 + \frac{1}{\gamma_1}) + \|N\|^2$. *Let* $\delta_2 > 0$ *be such that*

$$\varphi((pq)^{1/2}\delta_2, |||D^2 f|||, |||D^2 h|||) \leq -\gamma \tag{6.19}$$

for some $\gamma > 0$, where φ is defined in (6.14). Let M be such an integer that when iteration number $k < M$,

$$[1 + (q\|A\|^2 + \|N\|^2)\|Dh\|^2]\|A\|(1 + q\|Dh\|^2) \times (1 - \frac{\gamma}{p})^{k/2}(pq)^{1/2} > 1 \quad (6.20)$$

while when $k \geq M$,

$$[1 + (q\|A\|^2 + \|N\|^2)\|Dh\|^2]\|A\|(1 + q\|Dh\|^2) \times (1 - \frac{\gamma}{p})^{k/2}(pq)^{1/2} < 1 \quad (6.21)$$

Suppose further that $x_k \in \mathcal{O}_\epsilon$, $k \geq 0$, for some $\epsilon > 0$, and that $|e_0| \leq \frac{\delta}{\beta_n + M - 1}$ with $\delta = \min(\epsilon/2, \delta_1, \delta_2)$. Then we have the following result:
1. $|x_k^- - x_k| \leq \delta$ and $|x_k^+ - x_k| \leq \delta$, $\forall k \geq 0$.
2. The linearized system around x_k^- and x_k^+, i.e., $z_{k+1} = \frac{\partial f}{\partial x}(x_k^+)z_k$, $y_k = \frac{\partial h}{\partial x}(x_k^-)z_k$, satisfies the observability condition in (6.3) for $k \geq n - 1$. Thus there exist $q < \infty$, $p < \infty$ such that $\|P_k^-\| \leq q$, and $\|P_k^{+-1}\| \leq p$, $\forall k \geq n - 1$.
3. The error is bounded by δ and converges to zero, i.e., for $k \leq n-1$, $|e_k| \leq \delta$, and for $k > n - 1$, $|e_k| \leq \min(\delta, (1 - \frac{\gamma}{p})^{(k-n+1)/2}(pq)^{1/2}\delta)$.

Note that: (a) In order to satisfy the observability condition, it is necessary to keep the estimates x_k^- and x_k^+ near x_k for $0 \leq k \leq n + M - 1$, thus requiring a good initial guess. (b) We also need to have a converging period $(n - 1 \leq k \leq n + M - 1)$ for the EKF in order to build up the observability condition; after this, the recursions proceed automatically.

6.5 Proposition 5

Let $\hat{M}$ be the value of M when there is no constraint and $\tilde{M}$ be the value of M when there is constraint. Then the following inequality holds:

$$\tilde{M} \leq \hat{M} \quad (6.22)$$

Proof: *The condition for existence of M is that there exist γ_1 and γ_2 such that the following inequality holds*

$$\gamma_1 I \leq O_e^T(X_{n-1}^-, X_{n-2}^+)O_e(X_{n-1}^-, X_{n-2}^+) \leq \gamma_2 I \quad (6.23)$$

where $X_{n-1}^- \triangleq (x_0^-, \cdots, x_{n-1}^-)$, $X_{n-2}^+ \triangleq (x_0^+, \cdots, x_{n-2}^+)$. n is the dimension of the state. "$-$" and "$+$" denote "a priori" (predicted state) and "posterior" (updated state) respectively. The observability matrix O_e in (6.23) can be derived by using Lie derivative.

$$O_e(x_0^-, x_1^-, x_2^-, x_0^+, x_1^+) = \begin{bmatrix} \frac{\partial h}{\partial x}(x_0^-) \\ \frac{\partial h}{\partial x}(x_1^-)\frac{\partial f}{\partial x}(x_0^+) \\ \frac{\partial h}{\partial x}(x_2^-)\frac{\partial f}{\partial x}(x_1^+)\frac{\partial f}{\partial x}(x_0^+) \end{bmatrix} \quad (6.24)$$

$$= \begin{bmatrix} \frac{\partial h}{\partial x}(x_0^-) \\ \frac{\partial h}{\partial x}(x_1^-)A(x_0^+) \\ \frac{\partial h}{\partial x}(x_2^-)A(x_1^+)A(x_0^+) \end{bmatrix} \quad (6.25)$$

where h is the function defined in (2.5) and $A = \frac{\partial f}{\partial x}$ is the linearized system function. For (6.23) to hold, the boundaries γ_1 and γ_2 on $J_e(X^-_{n-1}, X^+_{n-2}) \triangleq O^T_e(X^-_{n-1}, X^+_{n-2})O_e(X^-_{n-1}, X^+_{n-2})$ (cf. (6.3) in Appendix for detail) should exist.

Define that the "a priori" estimate x^- is within the range $\underline{x}^- \leq x^- \leq \bar{x}^-$, the posteriori estimate x^+ is within the range $\underline{x}^+ \leq x^+ \leq \bar{x}^+$. The boundaries of J_e (if exist) in (6.23) can be defined by,

$$\hat{\gamma}_1 = \min_{\substack{\underline{x}^- \leq x^- \leq \bar{x}^- \\ \underline{x}^+ \leq x^+ \leq \bar{x}^+}} \lambda_{min}\{J_e\} \tag{6.26}$$

$$\hat{\gamma}_2 = \max_{\substack{\underline{x}^- \leq x^- \leq \bar{x}^- \\ \underline{x}^+ \leq x^+ \leq \bar{x}^+}} \lambda_{max}\{J_e\} \tag{6.27}$$

where λ is the eigenvalue of J_e.

With the constraint being imposed, the new boundaries with the constraints can be defined by

$$\tilde{\gamma}_1 = \min_{\substack{\underline{x}^- \leq x^- \leq \bar{x}^- \\ \underline{x}^+ \leq x^+ \leq \bar{x}^+ \\ g(\theta)=0}} \lambda_{min}\{J_e\} \tag{6.28}$$

$$\tilde{\gamma}_2 = \max_{\substack{\underline{x}^- \leq x^- \leq \bar{x}^- \\ \underline{x}^+ \leq x^+ \leq \bar{x}^+ \\ g(\theta)=0}} \lambda_{max}\{J_e\} \tag{6.29}$$

Clearly, the boundaries of J_e with constraints will be tighter than the ones without constraint, i.e.,

$$\hat{\gamma}_1 \leq \tilde{\gamma}_1 \leq \tilde{\gamma}_2 \leq \hat{\gamma}_2 \tag{6.30}$$

Let M be such an integer that when iteration number $K < M$ (cf. (6.20)[32]), the following inequality holds,

$$[1 + (q\|A\|^2 + \|N\|^2)\|Dh\|^2]\|A\|(1 + q\|Dh\|^2) \times (1 - \frac{\gamma}{p})^{K/2}(pq)^{1/2} > 1 \tag{6.31}$$

and for $K \geq M$ (cf. (6.21)[32]), inequality 6.32 holds,

$$[1 + (q\|A\|^2 + \|N\|^2)\|Dh\|^2]\|A\|(1 + q\|Dh\|^2) \times (1 - \frac{\gamma}{p})^{K/2}(pq)^{1/2} < 1 \tag{6.32}$$

where the covariance boundaries p and q are defined as follows (cf. Lemma 3[32]).

$$\|P_k^{+-1}\| \leq p_1 \tag{6.33}$$

$$\|P_k^{--1}\| \leq \|P_k^{+-1}\| + \|H\|^2 \leq p_1 + \|H\|^2 \triangleq p \tag{6.34}$$

$$\|P_k^+\| \leq \|P_k^-\| \leq q \tag{6.35}$$

Here P_k^- and P_k^+ denote covariance of "a priori" (predicted) and "posterior" (updated) state estimate respectively; N is the noise matrix in system equation (6.1); $\|A\|$ is defined as $\|A\| \triangleq \sup_{x \in R^n} \|A(x)\|$ (cf. Assumption 2 [32]); h is the output function in (6.2), while Dh is the derivative of $h(x)$; γ is defined through $\varphi(q^{\frac{1}{2}}V^{\frac{1}{2}}(0, e_0), |||D^2 f|||, |||D^2 h|||) \leq -\gamma$ (cf. Lemma 3).

According to Equation (6.32), to ensure convergence after M iterations, the following inequality must hold:

$$[1 + (q\|A\|^2 + \|N\|^2)\|Dh\|^2]\|A\|(1 + q\|Dh\|^2) \times (1 - \frac{\gamma}{p})^{M/2}(pq)^{1/2} < 1 \quad (6.36)$$

Let the covariance boundaries p and q satisfy the following equations (cf. Lemma 4[32]):

$$p = (\gamma_2 + \frac{1}{\alpha_2}) \quad (6.37)$$

$$q = a^2(\alpha_1 + \frac{1}{\gamma_1}) + \|N\|^2 \quad (6.38)$$

where α_1, α_2, and a are defined by the following equations (cf. Lemma 4[32]),

$$\begin{aligned} \alpha_1 &= \|N\|^2(1 + \|A\|^2 + \|A\|^4 + \cdots + \|A\|^{2(n-2)}) && (6.39)\\ \alpha_2 &= \lambda_{min}(NN^T) && (6.40)\\ a &= \max(1, \|A\|) && (6.41) \end{aligned}$$

Denote $\hat{p}$, $\hat{q}$ as the covariance boundaries corresponding to $\hat{\gamma}_1$ and $\hat{\gamma}_2$ when no constraints are imposed, while $\tilde{p}$, $\tilde{q}$ be the covariance boundaries corresponding to $\tilde{\gamma}_1$ and $\tilde{\gamma}_2$ when constraints are imposed. From (6.30), (6.37) and (6.38), we have

$$\begin{aligned} \tilde{p} &\leq \hat{p} && (6.42)\\ \tilde{q} &\leq \hat{q} && (6.43) \end{aligned}$$

Thus,

$$\begin{aligned} 1 + (\tilde{q}\|A\|^2 + \|N\|^2)\|Dh\|^2 &\leq 1 + (\hat{q}\|A\|^2 + \|N\|^2)\|Dh\|^2 && (6.44)\\ 1 + \tilde{q}\|Dh\|^2 &\leq 1 + \hat{q}\|Dh\|^2 && (6.45)\\ (\tilde{p}\tilde{q})^{1/2} &\leq (\hat{p}\hat{q})^{1/2} && (6.46) \end{aligned}$$

Notice that here in (6.36), $\|A\|$, $\|N\|$ and $\|Dh\|$ are fixed once the system is given. Define μ as

$$\mu = [1 + (q\|A\|^2 + \|N\|^2)\|Dh\|^2]\|A\|(1 + q\|Dh\|^2)(pq)^{1/2} \quad (6.47)$$

Using (6.44), (6.45), (6.46) and (6.47), we have

$$\tilde{\mu} \leq \hat{\mu} \quad (6.48)$$

where $\tilde{\mu}$ is defined when $\tilde{p}$ and $\tilde{q}$ are used in (6.47); $\hat{\mu}$ is defined when $\hat{p}$ and $\hat{q}$ are used in (6.47).

Considering (6.36) and the definition of μ in (6.47), one can obtain the following inequalities,

$$\begin{aligned} (1 - \frac{\gamma}{\tilde{p}})^{\tilde{M}/2}\tilde{\mu} &< 1 && (6.49)\\ (1 - \frac{\gamma}{\hat{p}})^{\hat{M}/2}\hat{\mu} &< 1 && (6.50) \end{aligned}$$

In addition, we have $(1-\frac{\gamma}{p}) < 1$ *and* $\mu \geq 1$ *which can be inferred from Lemma 4 [32]. Take logarithm from both sides of (6.49) and (6.50), it follows clearly that*

$$\tilde{M} > 2\log_{(1-\frac{\gamma}{\tilde{p}})} \frac{1}{\tilde{\mu}} \tag{6.51}$$

$$\hat{M} > 2\log_{(1-\frac{\gamma}{\hat{p}})} \frac{1}{\hat{\mu}} \tag{6.52}$$

From (6.42) and (6.48), we have

$$(1-\frac{\gamma}{\tilde{p}}) \leq (1-\frac{\gamma}{\hat{p}}) \tag{6.53}$$

$$\frac{1}{\tilde{\mu}} \geq \frac{1}{\hat{\mu}} \tag{6.54}$$

From the monotony of logarithm with the base less than 1, one can get the following inequality,

$$\log_{(1-\frac{\gamma}{\tilde{p}})} \frac{1}{\tilde{\mu}} \leq \log_{(1-\frac{\gamma}{\hat{p}})} \frac{1}{\hat{\mu}} \leq \log_{(1-\frac{\gamma}{\hat{p}})} \frac{1}{\hat{\mu}} \tag{6.55}$$

This leads to

$$\tilde{M} \leq \hat{M} \tag{6.56}$$

where the equality holds only when equalities hold in (6.30).